63- 4-5

RADC-TDR-63-269

Date: April 30, 1963

FAILURE MECHANISMS IN CERAMIC DIELECTRICS

Don A. Berlincourt

Electronic Research Division
Clevite Corporation
Cleveland, Ohio

Final Report

Contract No. AF 30(602)-2594

Prepared for
Rome Air Development Center
Research and Technology Division
Air Force Systems Command
United States Air Force
Griffiss Air Force Base
New York

ASTIA NOTICE

Qualified requestors may obtain copies of this report from the Armed Services Technical Information Agency, Arlington Hall Station, Arlington 12, Virginia. ASTIA Services for the Department of Defense Contractors are available through the "Field of Interest Register" on a "need-to-know" certified by the cognizant military agency of their project or contract.

PATENT NOTICE

When Government drawings, specifications, or other data are used for any purpose other than in connection with a definitely related Government procurement operation, the United States Government thereby incurs no responsibility nor any obligation whatsoever and the fact that the Government may have formulated, furnished, or in any way supplied the said drawings, specifications or other data is not to be regarded by implication or otherwise as in any manner licensing the holder or any other person or corporation, or conveying any rights or permission to manufacture, use, or sell any patented invention that may in any way be related thereto.

RADC-TDR-63-269

Date: April 30, 1963

Copy No. 37

FAILURE MECHANISMS IN CERAMIC DIELECTRICS

Don A. Berlincourt

Electronic Research Division
Clevite Corporation
Cleveland, Ohio

Final Report
Contract No. AF 30(602)-2594
Project No. 5519, Task No. 45155

Prepared for
Rome Air Development Center
Research and Technology Division
Air Force Systems Command
United States Air Force
Griffiss Air Force Base
New York

FOREWORD

This report was prepared for Rome Air Development Center, Air Force Systems Command, United States Air Force under Contract No. AF 30(602)-2594, Project No. 5519, Task No. 45155.

Robert Gerson directed this research work in the period preceding September 1, 1962, when he assumed a new position as Professor of Physics at University of Missouri School of Mines and Metallurgy. The research work has since been directed by Don A. Berlincourt, who has had the assistance of F. J. Scholz, J. M. Peterson, and W. M. Szczecinski. The reader is referred also to the three quarterly technical notes of this series, RADC-TDR-62-267, RADC-TDR-62-406 and RADC-TDR-62-633.

Title of Report: RADC-TDR-63-269

PUBLICATION REVIEW

This report has been reviewed and is approved.

Approved: S/Milton Haus
(for) DAVID F. BARBER
Chief, Applied Research Laboratory
Directorate of Engineering

Approved: S/Joseph Maresky
(for) WILLIAM P. BETHKE
Director of Engineering

FOR THE COMMANDER: S/Irving J. Gabelman
IRVING J. GABELMAN
Director of Advanced Studies

ABSTRACT

With the objective of developing an empirical approach to factors influencing failure in ceramics of high dielectric constant (greater than ~ 200), a number of perovskite (ABO_3) dielectrics were prepared and studied. Small substitutions of Nb^{5+} for the B^{4+} ion (Ti^{4+}, Zr^{4+}) and of Sc^{3+} for the A^{2+} ion (Pb^{2+}, Ba^{2+}, Sr^{2+}) were made. Nb^{5+} and Sc^{3+} thus act respectively as electron donor and acceptor. It was demonstrated that the zirconates, as a class, are far superior to the titanates with respect to long term degradation, which is probably best ascribed to electrolysis of oxygen. This can proceed more rapidly with the titanates, since Ti^{4+} is much more readily reduced than is Zr^{4+}. In general, also, the zirconates have higher volume resistivities than the titanates, but there is no clear-cut difference in dielectric strength. Degradation in dielectrics with p-type conduction, which was found to be the usual case, is generally inhibited by donor doping.

Approved:

Hans Jaffe
Director of Electronic Research
Clevite Corporation

TABLE OF CONTENTS

I. INTRODUCTION

The objective of work under this contract was to develop an empirical approach to the factors influencing failure in ceramics of high dielectric constant (greater than ~ 200). One may in general classify failure of ceramic dielectrics as due either to dielectric degradation or dielectric breakdown. Sudden formation of a breakdown path is therefore one type of failure. The other type, dielectric degradation, is a more gradual process involving an increase in conductivity and/or decrease in permittivity of the dielectric. This does not in general occur along distinct paths, and is considered to be isotropic transverse to the direction of the electric field but not in the direction parallel to the field. Most capacitors are operated at voltage levels such that the electric fields are well below the dielectric strength of the dielectric material. With polycrystalline dielectrics, however, there may be local field concentrations due to porosity or grain boundaries. Since degradation may be a volume effect due to a great many localized breakdown paths, the problem of dielectric strength cannot be neglected. It is clear that the mechanisms of failure in polycrystalline materials are complex, since the ceramic contains the single crystal case, with the additional influences of the disordered regions about grain boundaries.

Dielectric materials chosen for this study are perovskites of high dielectric constant. In the sense that "high" is used here, with $\epsilon/\epsilon_o \gtrsim 200$, all materials must be fairly close in free energy to a ferroelectric state. Ferroelectricity itself complicates the problem further, since domain walls as well as grain boundaries add further mechanisms for concentration of

electrical or mechanical stress. Mechanical stress results from domain reorientation and piezoelectric effects, with strains due to domain reorientation exceeding 0.5% in some lead titanate zirconate piezoelectric ceramics. Piezoelectric strains, linear functions of electric field, are about an order of magnitude less at 20 kv/cm. Electric stress concentrations are emphasized by ferroelectric domains due to pronounced anisotropy of permittivity (about twenty to one for $BaTiO_3$). Antiferroelectric ceramics are not subject to severe mechanical stress unless driven by an applied electric field into a ferroelectric state. Electric stress concentration due to antiferroelectric domains (not subject to orientation by electric field) is less severe than in ferroelectric ceramics. Cubic or paraelectric ceramics are dielectrically isotropic and are also not subject to severe mechanical stress unless driven by the applied electric field into a ferroelectric state.

All commercial ceramic capacitors constructed from high permittivity ceramics are based on barium titanate, a ferroelectric of perovskite structure. This choice has been heavily influenced by economics, however, and it was not established that materials based on barium titanate are best for high reliability. Dielectric compositions studied in this work are based on $BaTiO_3$ (ferroelectric), $PbTiO_3$ (ferroelectric), $PbZrO_3$ (antiferroelectric), $BaZrO_3$ (paraelectric), and $SrTiO_3$ (paraelectric), with the state at room temperature shown in parenthesis. These compositions can be mixed in all proportions without formation of nonperovskite phases. It is possible to have mixtures of perovskite phases, as for instance $PbZr_{.95}Ti_{.05}O_3$, which is mixed ferroelectric-antiferroelectric in the virgin state. By adjustment of composition one may obtain ferroelectric, antiferroelectric, or paraelectric phases, and the transition temperature between these phases may also be adjusted.

In work aimed at developing an understanding of failure of ceramic dielectrics it is necessary to study ceramics of low porosity. This is not exactly equivalent to a very close approach to theoretical density, since the density may also be lowered by vacancies. While porosity always degrades dielectric properties, leading to such effects as moisture absorption and inhomogenous electric field distribution, lattice vacancies may in some instances produce desirable effects. Porosity in itself may certainly be one of the primary causes of failure in ceramic dielectrics, but in this work an attempt was made to eliminate porosity as a prima facie cause of failure so that other failure mechanisms could be brought to light.

To accomplish this ceramic compositions tested must be prepared with low porosity, and for each composition the optimum time-temperature firing cycle must be determined. It is evident that preparation of a very large number of different compositions would have resulted in over-expenditure of effort on ceramic preparation and routine electrical testing, and a sacrifice in time available for experiments aimed at determination of failure mechanisms. About twenty-five compositions were selected for attempted preparation as low porosity ceramics, including a range of ferroelectric, antiferroelectric, and paraelectric materials. Nearly all compositions prepared contain lead as one of the constituents, although in some cases it is present in minor amounts. There are two major reasons for this choice. First, the Pb^{2+} ion is highly polar, making a strong contribution to the dielectric constant and to ferroelectric properties. Second, it is possible to control the lead vapor pressure during firing by the use of various "grogs." Due to volatility of the lead, the ceramic is forced to develop a lead vapor pressure approximately equal to that

of the "grog." The vacancy concentration, both cation and anion, is in turn affected by the vapor pressure. The vacancy concentration may also be influenced, though to a much smaller extent, by firing in oxygen rather than air. Oxygen firing also usually allows more complete densification, but it is not necessary if other factors are optimum.

With perovskite materials (ABO_3) the A-position (Pb^{2+}, Ba^{2+}, Sr^{2+} in this work) is filled by a positive ion of large ionic radius, the B-position (Ti^{4+}, Zr^{4+} in this work) by a positive ion whose radius is 30 to 40% smaller. Off-valency additives (Nb^{5+}, Sc^{3+} in this work) may be chosen to fit into either position.

A-position		B-position		off-valency additives	
Pb^{2+}	1.32 Å	Zr^{4+}	0.77	Nb^{5+}	0.70
Ba^{2+}	1.38	Ti^{4+}	0.60	Sc^{3+}	0.83
Sr^{2+}	1.18			La^{3+}	1.09
				Ta^{5+}	0.69
				Nd^{3+}	1.03

From the table above, it is clear that Nb^{5+}, Sc^{3+}, and Ta^{5+} fit into the B-position and La^{3+}, Nd^{3+} fit into the A-position. A three-valent ion in the A-position and a five-valent ion in the B-position produce much the same effects. Both act as electron donors, and both cause vacancies in the A-position. When additions of this type are made it is especially desirable to have at least some Pb^{2+} in the A-position, as its volatility facilitates chemical equilibrium. In work reported here only Nb^{5+} was used as an electron donor, and it was added in the proportion $PbO:Nb_2O_5$. This fits into a perovskite

lattice with one A-position vacancy for every two atoms of Nb^{5+}. Thus an addition of 2 atom %Nb^{5+} leads to an A-position vacancy for every 100 unit cells. This seems to be a fairly low vacancy concentration, but any vacancy will on the average see another vacancy only about $100^{1/3}$ or 4. 6 lattice cells away. A lower valency substituent, such as Sc^{3+} in the B-position, acts as an acceptor. This is added in the proportion $2PbO:Sc_2O_3$, and the acceptor fits into the perovskite lattice with one oxygen vacancy for every two atoms of Sc^{3+}.

Thus the off-valency substituents used in this work, Nb^{5+} and Sc^{3+}, act respectively as electron donor and acceptor. The donor (Nb^{5+}) has profound effects on the dielectric properties of the base material, the acceptor less so. The donor tends to increase drastically the volume resistivity of most perovskite ceramic dielectrics, indicating that these normally have p-type conductivity. The acceptor has less profound effects, but it tends to decrease slightly the volume resistivity of ceramics with p-type conduction, and to increase the volume resistivity of ceramics with n-type conduction. In general the volume resistivities of undoped zirconates are higher than for the undoped titanates, presumably because Ti^{4+} is more easily reduced to Ti^{3+} than is Zr^{4+} to Zr^{0}.

In summary the objective of this work, which was to develop an empirical approach to factors influencing failure in ceramics of high dielectric constant, was attacked in the following steps:

1. Attempt to correlate dielectric strength and resistance to dielectric degradation with composition. This includes

comparisons of titanates and zirconates and n-versus p-type doping.

2. Attempt to correlate dielectric strength and resistance to degradation with grain size.
3. Attempt to correlate dielectric strength and resistance to degradation with volume resistivity.
4. Attempt to correlate dielectric strength with resistance to degradation.

A statistical list of types of failure in capacitors used in electronic circuits is not available. Capacitors are generally operated at voltage levels such that the material is subjected to electric fields well below the dielectric strength, and temperature and electric field levels are such that dielectric degradation is very slow. It is likely that the majority of failures in ceramic capacitors is actually due to factors not dependent upon the ceramic material. Typical examples may be broken leads, poor electrodes, poor solder joints on the electrode, etc. Failures of this type are not within the scope of this project.

Since the electric field is generally, in practice, limited to levels substantially below the dielectric strength, the main emphasis in this work was placed on dielectric degradation. Dielectric degradation is primarily electrochemical, best ascribed to electrolysis of oxygen, and results in reduced volume resistivity and permittivity (hence reduced time constant, $\rho\epsilon$). The rate of degradation of commercial capacitors operating at rated electric stress is slow enough to make laboratory testing inconvenient. The usual approach under these circumstances is to accelerate the test either by increasing the electric stress or by raising the temperature or by a combination of these. These deviations from

normal conditions may, however, introduce new deterioration mechanisms, and in this work this factor was considered.

II. CERAMIC PREPARATION

The raw materials used in preparing the ceramic specimens were as follows:

Barium oxide (BaO) - reagent grade

Lead oxide (PbO) - sublimed litharge

Titanium oxide (TiO_2 - pigment grade

Strontium carbonate ($SrCO_3$) - reagent grade

Niobium oxide (Nb_2O_5) - 99.5%, Kennametal

Scandium oxide (Sc_2O_3) - 99%, Vitro Chemical Co.

The chemicals were weighed and then milled for six to eight hours with distilled water in a plastic jar. For a 100-gram batch of powder about 140-150 cc of water and about 150 grams of lead titanate zirconate stones were used for milling. The material was then poured into Pyrex dishes and dried for about 15 hours at 75-80°C. The resulting cake was broken up, mortared, loaded into closed alumina tubes, and then reacted in the solid state in an electric furnace (see Table I for reaction temperatures) for two to three hours. At this point in the process the material had been transformed almost completely to the desired composition. After cooling the material was again broken up, hand mortared, and milled as before. About 2% cp glycerol (based on powder weight) was added during milling; this then served as a binder during pressing of the ceramic. The mixture was again dried and the powder, which was usually quite fine at this point, was screened through a #20 sieve.

Pressing was accomplished using a 2 cm diameter steel die and a pressure of 4,000 to 7,000 psi. About one to two percent water (based on powder weight) was added prior to pressing. After pressing the binder was burned out in a muffle furnace, starting at 100°C to remove moisture and prevent cracking, then working up to 450 - 500°C over a two- to three-hour period.

Firing was accomplished in a low alumina crucible fitted with a tight-fitting alumina cover. The test discs were stacked on a spiral of platinum wire, with powder of the same composition as the discs dusted between them to prevent sticking. For determination of weight gained or lost during firing, the second disc from the top was carefully weighed before firing. Lead atmosphere was maintained during firing by including a three gram pellet of PbO on a piece of platinum foil and a three gram pellet of $PbZrO_3$ in the crucible.

Table I. Summary of Ceramic Compositions and Firings Made

$Pb_{0.05}Ba_{0.80}Sr_{0.15}TiO_3$

Theoretical density, g/cc: 5.99

Reaction temperature, °C: 1150

Firing	Temperature (°C)	Hold Time, Hours	% of Theoretical Density	% Weight Change
A I	1400	1	92	----
A II	1410	1	90	-0.5
A III	1405	1/2	96	-0.2
A IV	1415	1/2	97	-0.6
B I	1420	1/2	90	-3.4
B II	1415	1/2	85	-3.2
B III	1415	1/2	91	-3.0
B IV	1550	3/4	93	-4.1

$(Pb_{0.05}Ba_{0.80}Sr_{0.15}TiO_3)_{0.99} + (PbNb_2O_6)_{0.01}$

Theoretical density, g/cc: 5.95

Reaction temperature, °C: 1115

Firing	Temperature (°C)	Hold Time, Hours	% of Theoretical Density	% Weight Change
A I	1410	1	72	+1.0
A II	1460	1/2	75	+0.5
A III	1490	1/2	84	-0.5
B I	1500	1/2	68	-2.1
B II	1500	2-1/2	66	-2.2
B III	1500	1/2	64	-2.0
B IV	1475	1/2	70	----
B V	1550	3/4	79	-1.2

Table I. Summary of Ceramic Compositions and Firings Made (Cont'd)

$Pb_{0.05}Ba_{0.50}Sr_{0.45}TiO_3$

Theoretical density, g/cc: 5.71

Reaction temperature, °C: 1150

Firing	Temperature (°C)	Hold Time, Hours	% of Theoretical Density	% Weight Change
A I	1400	1	69	----
A II	1470	1/2	98	-0.3
A III	1490	1/2	98	-0.2
B I	1500	1/2	97	-2.0
B II	1490	1/2	95	-1.8

$(Pb_{0.05}Ba_{0.50}Sr_{0.45}TiO_3)_{0.99} + (PbNb_2O_6)_{0.01}$

Theoretical density, g/cc: 5.67

Reaction temperature, °C: 1115

Firing	Temperature (°C)	Hold Time, Hours	% of Theoretical Density	% Weight Change
A I	1470	1/2	67	+1.7
A II	1490	1/2	66	+0.9
B I	1520	1	68	-0.2
B II	1500	2-1/2	64	+0.6
B III	1520	1/2	78	-1.8
B IV	1550	3/4	89	-2.8

Table I. Summary of Ceramic Compositions and Firings Made (Cont'd)

$(Pb_{0.05}Ba_{0.50}Sr_{0.45}TiO_3)_{0.99} + (Pb_2Sc_2O_5)_{0.01}$

Theoretical density, g/cc: 5.68

Reaction temperature, °C: 1115

Firing	Temperature (°C)	Hold Time, Hours	% of Theoretical Density	% Weight Change
A I	1470	1/2	55	-0.4
A II	1505	1/2	91	-1.3
B I	1520	1	70	-0.4
B II	1500	2-1/2	68	-1.0
B III	1520	1/2	73	-2.2

$Pb_{0.30}Sr_{0.70}TiO_3$

Theoretical density, g/cc: 5.97

Reaction temperature, °C: 1115

Firing	Temperature (°C)	Hold Time, Hours	% of Theoretical Density	% Weight Change
A I	1405	1/2	97	+4.4
A II	1415	1/2	97	+0.4
A III	1415	1/2	98	-0.2
B I	1420	1/2	96	+0.3
B II	1415	1/2	96	+3.2

Table I. Summary of Ceramic Compositions and Firings Made (Cont'd)

$(Pb_{0.30}Sr_{0.70}TiO_3)_{0.99} + (PbNb_2O_6)_{0.01}$

Theoretical density, g/cc: 5.93

Reaction temperature, °C: 1090

Firing	Temperature (°C)	Hold Time, Hours	% of Theoretical Density	% Weight Change
A I	1410	1/2	87	+6.5
A II	1460	1/2	99	+0.4
A III	1465	1/2	99	-0.4
B I	1465	1/2	98	0.0
B II	1475	1/2	--	+4.6

$(Pb_{0.30}Sr_{0.70}TiO_3)_{0.99} + (Pb_2Sc_2O_5)_{0.01}$

Theoretical density, g/cc: 5.98

Reaction temperature, °C: 1090

Firing	Temperature (°C)	Hold Time, Hours	% of Theoretical Density	% Weight Change
A I	1405	1/2	87	+0.6
A II	1460	1/2	92	-0.8
A III	1500	1/2	93	-0.6
A IV	1520	1	85	-5.0
B I	1520	1	97	-1.7
B II	1500	1/2	92	+1.6

Table I. Summary of Ceramic Compositions and Firings Made (Cont'd)

$Pb_{0.5}Sr_{0.5}TiO_3$

Theoretical density, g/cc: 6.53

Reaction temperature, °C: 1115

Firing	Temperature (°C)	Hold Time, Hours	% of Theoretical Density	% Weight Change
A I	1405	1/2	93	+1.9
A II	1425	1/2	92	-0.4
A III	1375	1/2	96	+0.2
B I	1380	1/2	96	+0.6

$(Pb_{0.50}Sr_{0.50}TiO_3)_{.99} + (PbNb_2O_6)_{0.01}$

Theoretical density, g/cc: 6.49

Reaction temperature, °C: 1090

Firing	Temperature (°C)	Hold Time, Hours	% of Theoretical Density	% Weight Change
A I	1410	1/2	98	+2.2
A II	1425	1/2	98	+4.6
A II - R	1200	3	98	+1.8
A III	1420	1/2	99	+1.1
B I	1420	1/2	99	+0.1
B II	1420	1/2	96	+3.5

Table I. Summary of Ceramic Compositions and Firings Made (Cont'd)

$PbZrO_3$

Theoretical density, g/cc: 8.10

Reaction temperature, °C: 850

Firing	Temperature (°C)	Hold Time, Hours	% of Theoretical Density	% Weight Change
A I	1350	1/2	97	-1.7
A II	1375	1/2	97	-0.7
B I	1375	1/2	96	-3.0

$(PbZrO_3)_{0.98} + (PbNb_2O_6)_{0.02}$

Theoretical density, g/cc: 8.00

Reaction temperature, °C: 925

Firing	Temperature (°C)	Hold Time, Hours	% of Theoretical Density	% Weight Change
A I	1350	1/2	96	-2.9
A II	1375	1/2	97	-3.6
B I	1375	1/2	97	-0.3

Table I. Summary of Ceramic Compositions and Firings Made (Cont'd)

$Pb_{0.50}Sr_{0.50}ZrO_3$

Theoretical density, g/cc: 6.78

Reaction temperature, °C: 1120

Firing	Temperature (°C)	Hold Time, Hours	% of Theoretical Density	% Weight Change
A I	1490	1/2	97	-3.1
A II	1500	1/2	98	-2.0
B I	1500	1/2	95	-1.6
B II	1500	1/2	92	-2.9
B III	1475	1/2	94	+3.9

$(Pb_{0.50}Sr_{0.50}ZrO_3)_{0.99} + (PbNb_2O_6)_{0.01}$

Theoretical density, g/cc: 6.74

Reaction temperature, °C: 1120

Firing	Temperature (°C)	Hold Time, Hours	% of Theoretical Density	% Weight Change
A I	1490	1/2	95	-1.8
A II	1500	1/2	97	-0.7
B I	1500	1/2	93	-0.6
B II	1500	1/2	79	-3.1
B III	1490	1/2	92	-3.0

Table I. Summary of Ceramic Compositions and Firings Made (Cont'd)

$Pb_{0.75}Sr_{0.25}ZrO_3$

Theoretical density, g/cc: 7.36

Reaction temperature, °C: 1090

Firing	Temperature (°C)	Hold Time, Hours	% of Theoretical Density	% Weight Change
A I	1430	1/2	97	-2.3
A II	1450	1/2	99	-0.6
A III	1450	1/2	94	-5.3
B I	1450	1/2	90	-3.6
B II	1460	1/2	92	-2.0

$Pb_{0.60}Ba_{0.40}ZrO_3$

Theoretical density, g/cc: 7.29

Reaction temperature, °C: 1025

Firing	Temperature (°C)	Hold Time, Hours	% of Theoretical Density	% Weight Change
A I	1480	1/2	95	-2.9
A II	1500	1/2	96	-1.6
A III	1500	1/2	93	-5.9
B I	1500	1/2	77	-10.8
B II	1500	1/2	73	-9.5
B III	1500	1/2	93	-1.2

Table I. Summary of Ceramic Compositions and Firings Made (Cont'd)

$(Pb_{0.60}Ba_{0.40}ZrO_3)_{0.99} + (PbNb_2O_6)_{0.01}$

Theoretical density, g/cc: 7.25

Reaction temperature, °C: 1120

Firing	Temperature (°C)	Hold Time, Hours	% of Theoretical Density	% Weight Change
A I	1480	1/2	97	-0.7
A II	1500	1/2	95	-2.4
B I	1465	1/2	74	-2.9
B II	1500	1/2	87	-2.4
B III	1480	3/4	86	-1.8
B IV	1500	1/2	82	-2.3
B V	1520	1/2	88	-2.6

$Pb_{0.75}Ba_{0.25}ZrO_3$

Theoretical density, g/cc: 7.56

Reaction temperature, °C: 1025

Firing	Temperature (°C)	Hold Time, Hours	% of Theoretical Density	% Weight Change
A I	1430	1/2	96	-0.7
A II	1450	1/2	97	-0.8
A III	1460	1/2	93	-3.7
B I	1460	1/2	93	-1.1

Table I. Summary of Ceramic Compositions and Firings Made (Cont'd)

$Ba_{0.85}Sr_{0.15}TiO_3$

Theoretical density, g/cc: 5.89

Reaction temperature, °C: 1150

Firing	Temperature (°C)	Hold Time, Hours	% of Theoretical Density	% Weight Change
I	1600 G	1	90	-2.3

$(Ba_{0.85}Sr_{0.15}TiO_3)_{0.99} + (BaNb_2O_6)_{0.01}$

Theoretical density, g/cc: 5.89

Reaction temperature, °C: 1150

Firing	Temperature (°C)	Hold Time, Hours	% of Theoretical Density	% Weight Change
I	1600 G	1	95	-2.4

$Ba_{0.55}Sr_{0.45}TiO_3$

Theoretical density, g/cc: 5.57

Reaction temperature, °C: 1150

Firing	Temperature (°C)	Hold Time, Hours	% of Theoretical Density	% Weight Change
I	1600 G	1	96	-1.3

$(Ba_{0.55}Sr_{0.45}TiO_3)_{0.99} + (BaNb_2O_6)_{0.01}$

Theoretical density, g/cc: 5.57

Reaction temperature, °C: 1130

Firing	Temperature (°C)	Hold Time, Hours	% of Theoretical Density	% Weight Change
I	1600 G	1	98	-1.5

Table I. Summary of Ceramic Compositions and Firings Made (Cont'd)

$(Ba_{0.55}Sr_{0.45}TiO_3)_{0.99} + (Ba_2Sc_2O_5)_{0.01}$

Theoretical density, g/cc: 5.57

Reaction temperature, °C: 1130

Firing	Temperature (°C)	Hold Time, Hours	% of Theoretical Density	% Weight Change
I	1600 G	1	82	-2.1
II	1675 G	1	92	-2.2

$Pb_{0.15}Ba_{0.70}Sr_{0.15}TiO_3$

Theoretical density, g/cc: 6.18

Reaction temperature, °C: 1100

Firing	Temperature (°C)	Hold Time, Hours	% of Theoretical Density	% Weight Change
I	1500	1	90	----
II	1475	1	92	-0.6
III	1460	1	92	-0.5
IV	1460	1	93	-0.7

$(Pb_{0.15}Ba_{0.70}Sr_{0.15}TiO_3)_{0.99} + (PbNb_2O_6)_{0.01}$

Theoretical density, g/cc: 6.18

Reaction temperature, °C: 1100

Firing	Temperature (°C)	Hold Time, Hours	% of Theoretical Density	% Weight Change
I	1500	1	98	+2.2
II	1475	1	94	+1.1
III	1500	1	97	-1.1

Table I. Summary of Ceramic Compositions and Firings Made (Cont'd)

$(PbTiO_3)_{0.57} + (BaZrO_3)_{0.43}$

Theoretical density, g/cc: 7.21

Reaction temperature, °C: 1000

Firing	Temperature (°C)	Hold Time, Hours	% of Theoretical Density	% Weight Change
I	1300	1	87	+6.0
II	1350	1	89	+3.0
III	1385	1	82	-0.9

$\left[(PbTiO_3)_{0.57} + (BaZrO_3)_{0.43}\right]_{0.99} + (PbNb_2O_6)_{0.01}$

Theoretical density, g/cc: 7.21

Reaction temperature, °C: 1000

Firing	Temperature (°C)	Hold Time, Hours	% of Theoretical Density	% Weight Change
I	1300	1	89	+3.1
II	1350	1	89	+3.9
III	1385	1	86	-0.3

Table I. Summary of Ceramic Compositions and Firings Made (Cont'd)

$(PbZrO_3)_{0.98} + (Pb_2Sc_2O_5)_{0.02}$

Theoretical density, g/cc: 8.10

Reaction temperature, °C: 850

Firing	Temperature (°C)	Hold Time, Hours	% of Theoretical Density	% Weight Change
I	1270	3/4	73	-4.7
II	1340	3/4	82	-7.1
III	1340	3/4	84	-5.8

Code:

A, B, are batch mixes.

I, II, etc. are firing numbers.

R means repeat firing of previously fired discs.

G means gas furnace. In all other cases an electric furnace was used.

The test specimens were fired in a Harper electric furnace equipped with a Wheelco controller. An optical pyrometer was used to check temperature. Firing data are listed in Table I. Table I also lists the theoretical densities and actual measured densities for the various compositions. Theoretical or crystal densities were determined from x-ray measurements of lattice dimensions. It may be noted that considerable difficulty was experienced in obtaining high density ceramics of several compositions, and in these cases several firings were made with changes in hold time and peak temperature. Weight changes as a result of firing are noted also in Table I, and in most cases these were of the order 1% or less. Increases were due to pick-up of lead during firing, decreases due to lead loss.

With several of the barium strontium titanate compositions containing 5 atom % Pb^{2+} in the perovskite A-position, the sintering temperature was above the 1500°C limit of an electric globar-type furnace. Two methods were used in circumventing this difficulty. First a series of compositions containing 15 atom % Pb^{2+} was prepared in the hope that this would lower the sintering temperature below 1500°C (see Table I). Second, similar compositions were prepared containing no lead, and these were sintered at temperatures above 1600°C in a gas furnace.

III. LOW-SIGNAL ELECTRICAL MEASUREMENTS

The permittivity at one mcps and the dc volume resistivity of the materials of Table I were measured as functions of temperature, the former in the range -200 to 300°C, the latter in the range of 25 to 300°C. Since it is extremely difficult to measure accurately values of volume

resistivity greater than about 10^{13} ohm cm, the actual temperature ranges of the volume resistivity measurements were different for different compositions. In some cases also the permittivity was measured over limited temperature ranges, but care was taken to cover the range in which permittivity varied markedly.

Permittivity and tan δ measurements were made with a General Radio 716 CS capacitance bridge at 1 mcps unless otherwise noted. The test specimens were electroded with fired-on DuPont silver frit and placed in an electric oven heated to 300°C. The measurements were made with temperature slowly decreasing to 25°C. The test specimens were than placed inside a dewar containing liquid nitrogen (-196°C) and permittivity and tan δ were measured as the temperature was allowed to rise slowly to room temperature.

The volume resistivity was measured as a function of temperature with temperature slowly dropping from 300°C. These measurements were made with a Bruel and Kjaer megohmeter with an electric field in the range 10 to 100 volts/mm. Virgin test specimens were used, i.e. specimens not previously subjected to high electric stress (> 100 v/mm).

A. Permittivity-Temperature Curves

Figure 1 shows the temperature dependence of permittivity for $Pb_{.05}Ba_{.80}Sr_{.15}TiO_3$, $(Pb_{.05}Ba_{.80}Sr_{.15}TiO_3)_{.99}(PbNb_2O_6)_{.01}$, $Pb_{.05}Ba_{.50}Sr_{.45}TiO_3$, and $(Pb_{.05}Ba_{.50}Sr_{.45}TiO_3)_{.99}(Pb_2Sc_2O_5)_{.01}$. These materials may be considered barium strontium titanate with Curie points above and below room temperature. Thus the composition with high barium content must undergo a phase transition (paraelectric to ferroelectric on cooling after firing, while that with lower barium content does not. Attempts to

FIGURE 1.

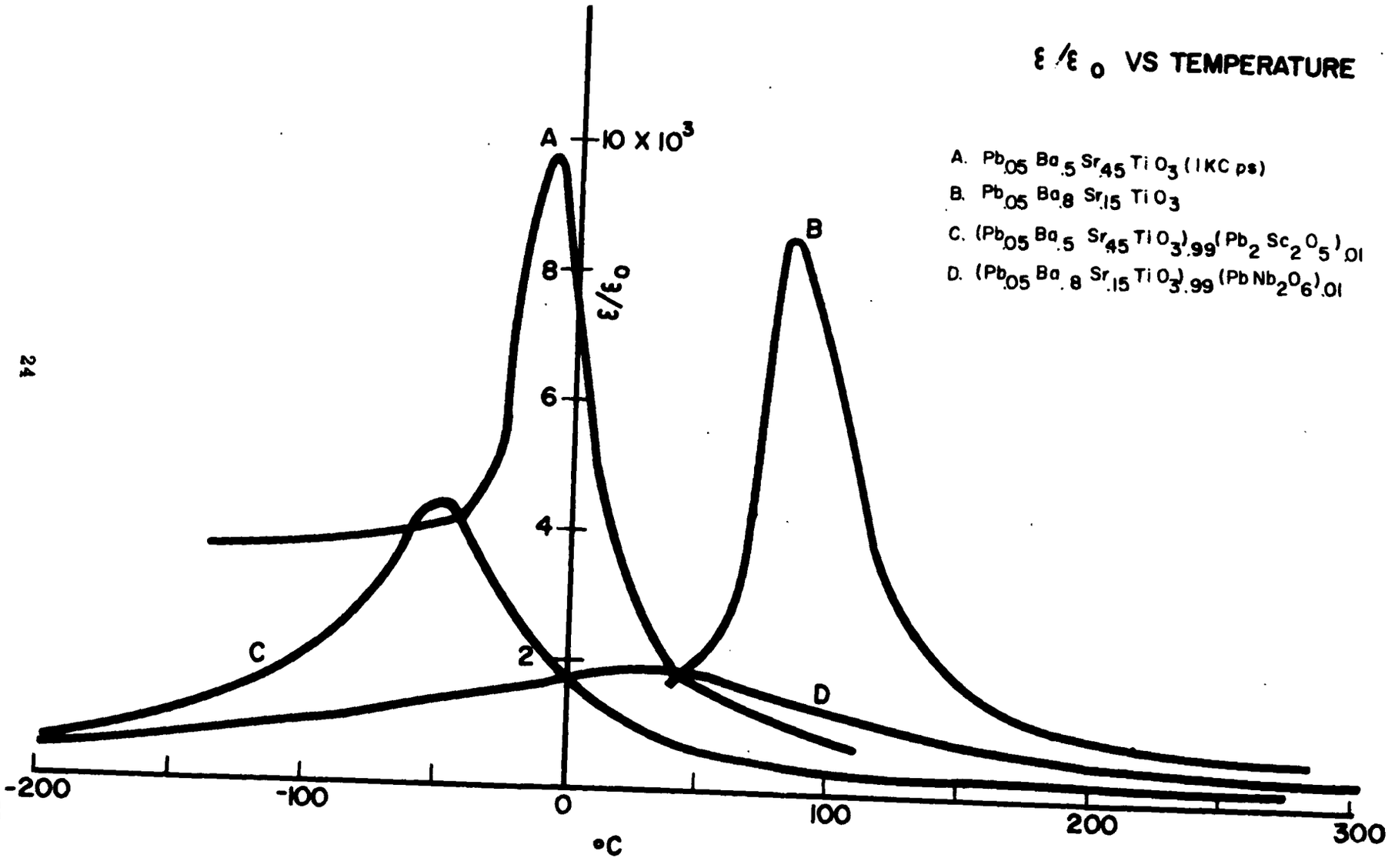
ε/ε0 VS TEMPERATURE
A. Pb.05 Ba.5 Sr.45 TiO3 (1KC ps)
B. Pb.05 Ba.8 Sr.15 TiO3
C. (Pb.05 Ba.5 Sr.45 TiO3).99 (Pb2 Sc2 O5).01
D. (Pb.05 Ba.8 Sr.15 TiO3).99 (Pb Nb2 O6).01
A
10 X 10^3
8
6
4
2
ε/ε0
B
C
D
-200
-100
0
100
200
300
°C

fire ceramics with both donor (Nb^{5+}) and acceptor (Sc^{3+}) additives were made, but those with the donor additive would not sinter at temperatures attainable in the electric furnace. It was therefore necessary to fire the composition with Nb^{5+} in a gas furnace. Curie points occurred about as expected, and it is interesting to note that Sc^{3+} lowered drastically the permittivity and Curie point (compare A and C). Nb^{5+} lowered the permittivity and Curie point even more drastically (compare B and D).

Figures 2 and 3 show the temperature variation of permittivity for $Pb_{.3}Sr_{.7}TiO_3$, $Pb_{.5}Sr_{.5}TiO_3$, $(Pb_{.3}Sr_{.7}TiO_3)_{.99}(PbNb_2O_6)_{.01}$, $(Pb_{.5}Sr_{.5}TiO_3)_{.99}(PbNb_2O_6)_{.01}$, and $(Pb_{.3}Sr_{.7}TiO_3)_{.99}(Pb_2Sc_2O_5)_{.01}$. These are materials which have paraelectric-ferroelectric Curie points above and below room temperature. Here the donor additive (Nb^{5+}) raises the permittivity, while the acceptor additive (Sc^{3+}) lowers the permittivity and drastically depresses the Curie peak. It is apparent that Sc^{3+} acts to inhibit ferroelectricity, and the phase at temperatures below the peak of permittivity is not distinguishable from that above by x-ray line splittings (both simple cubic). The donor additive (Nb^{5+}) acts to make the Curie peak more pronounced, and lowers the Curie point slightly (by about 10 Centigrade degrees).

Figure 4 shows permittivity as function of temperature for $PbZrO_3$ and $(PbZrO_3)_{.98}(PbNb_2O_6)_{.02}$. The donor additive lowers the Curie point, increases the Curie peak, and raises the general level of the dielectric constant. It is noted that 4 atom % Nb^{4+} is here sufficient to bring about a ferroelectric (rhombohedral) state below the Curie point.[1][2] Plain $PbZrO_3$ is, of course, antiferroelectric (orthorhombic) below the Curie point.

---

[1] B. Jaffe, W. R. Cook, Jr., O. Mattiat, A. Lungo, and D. R. Curran, WADC Tech. Rep. 57-569, Contract AF 33(616)-3609 (1957).

[2] N. N. Krainik, Zhur. Tekh. Fiz. 28, 525 (1958).

FIGURE 2.

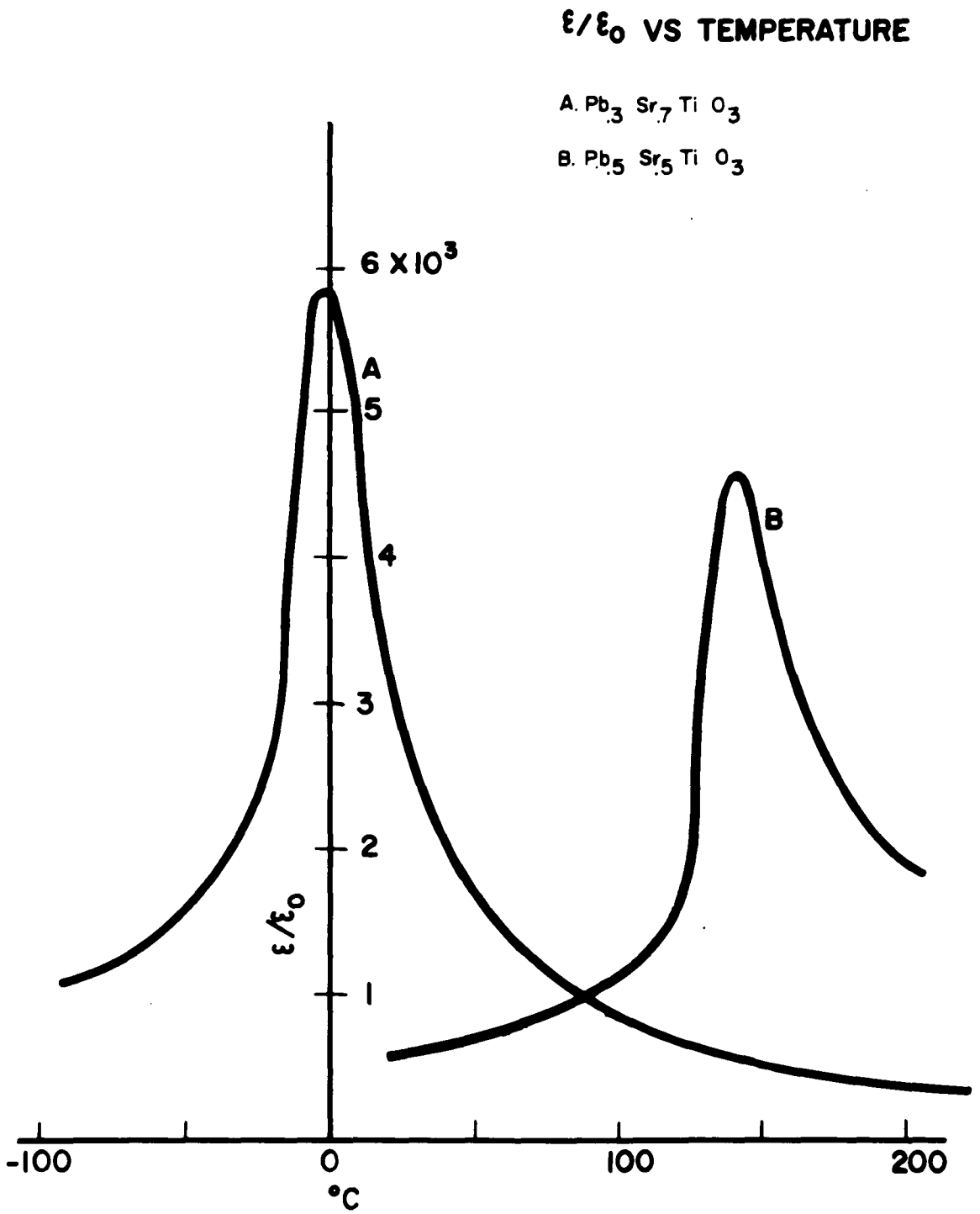

ERD 5698

FIGURE 3.

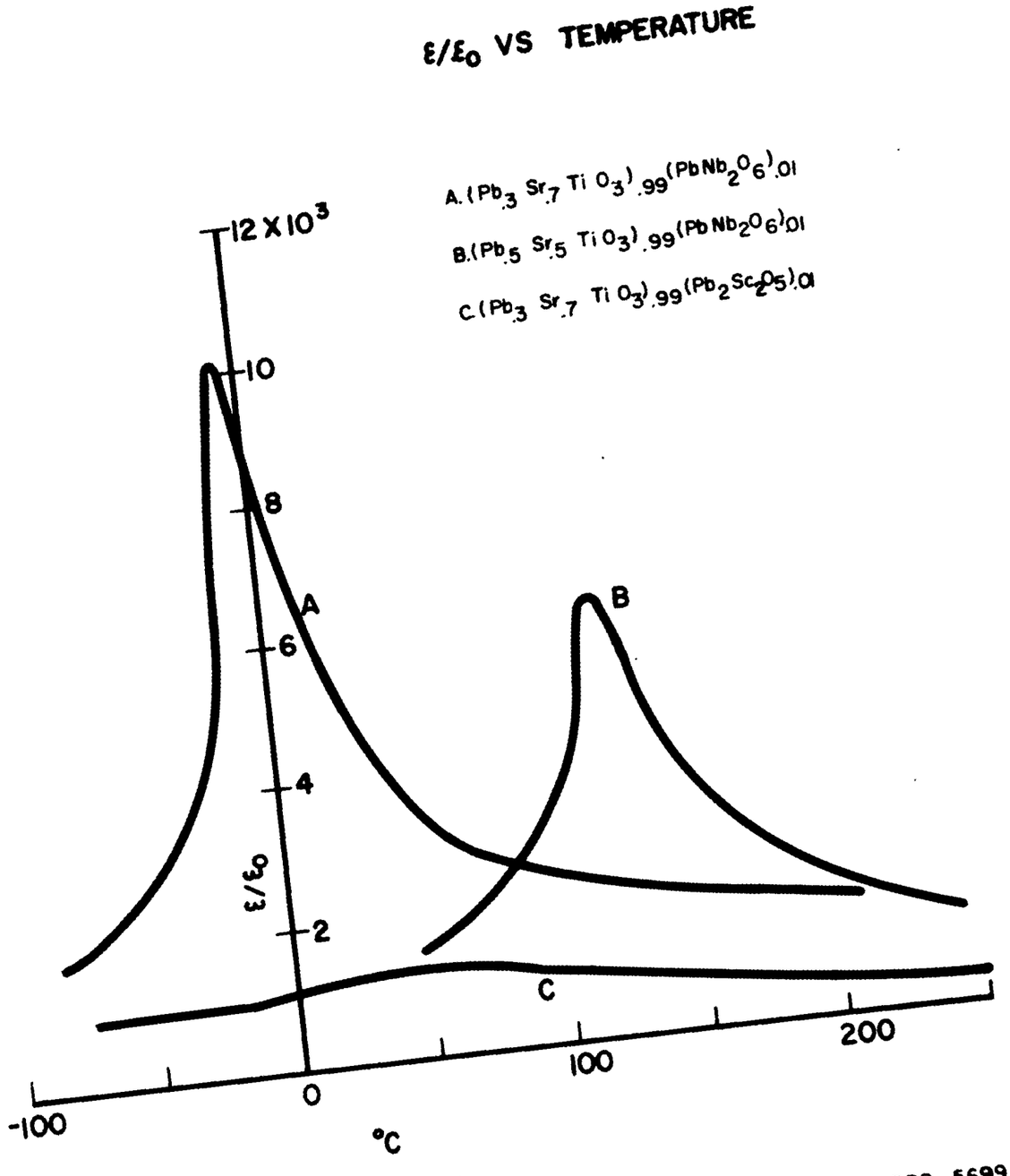

ERD 5699

FIGURE 4.

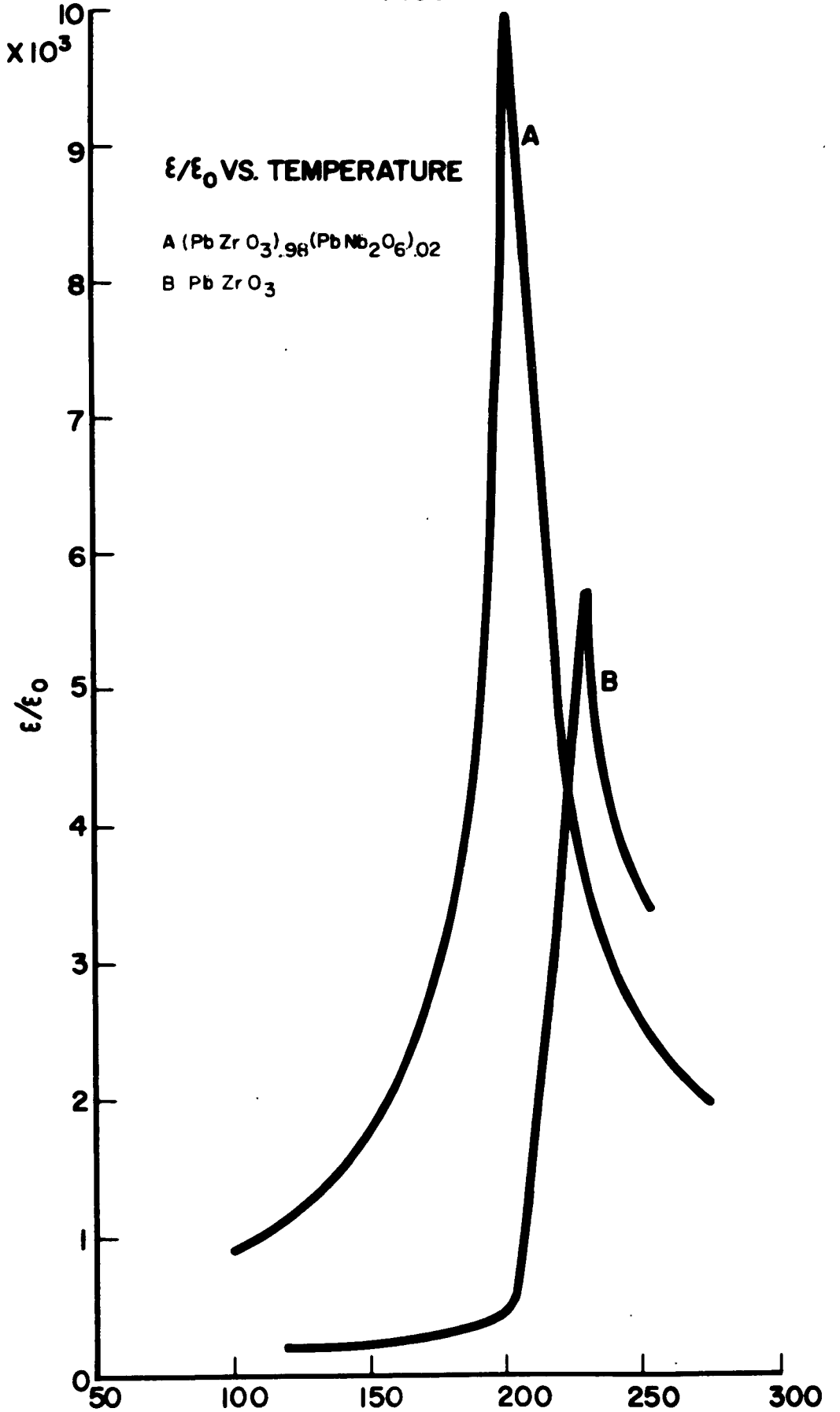

ERD 5700

Figure 5 shows the temperature variation of permittivity for $(PbZrO_3)_{.98}(Pb_2Sc_2O_5)_{.02}$. Comparison with Figure 4 shows that the acceptor additive (Sc^{3+}) depresses the Curie peak with no change in the Curie point. The lower peak permittivity indicates that Sc^{3+} in place of Zr^{4+} encourages antiferroelectricity, i.e., with Sc^{3+} the difference in free energy between the ferroelectric and antiferroelectric states is increased.

Figure 6 shows permittivity as function of temperature for $Pb_{.75}Sr_{.25}ZrO_3$, $Pb_{.5}Sr_{.5}ZrO_3$, and $(Pb_{.5}Sr_{.5}ZrO_3)_{.99}(PbNb_2O_6)_{.01}$. These are low permittivity compositions which are apparently paraelectric (cubic), but may be antiferroelectric. At any rate, no line splitting or superstructure could be detected in x-ray diffraction patterns.

Figure 7 shows permittivity as function of temperature for $Pb_{.75}Ba_{.25}ZrO_3$, $Pb_{.6}Ba_{.4}ZrO_3$, and $(Pb_{.6}Ba_{.4}ZrO_3)_{.99}(PbNb_2O_6)_{.01}$. These compositions are ferroelectric below their respective Curie points. It is interesting to note that the Curie peaks are broadened considerably as the Curie point is lowered by Ba^{2+}. The Nb^{5+} additive further lowers the Curie point.

Figures 8 and 9 show permittivity as function of temperature for 1) $Ba_{.55}Sr_{.45}TiO_3$, 2) $(Ba_{.55}Sr_{.45}TiO_3)_{.99}(Ba_2Sc_2O_5)_{.01}$, 3) $Ba_{.55}Sr_{.45}TiO_3)_{.99}(BaNb_2O_6)_{.01}$, and 4) $Ba_{.85}Sr_{.15}TiO_3$. Compositions 1), 2), and 3) have ferroelectric-paraelectric Curie points well below room temperature, and the Curie point of composition 4) is close to room temperature. Comparison of the curves for compositions 1), 2), and 3) indicates that both Sc^{3+} and Nb^{5+} depress the Curie peak and lower the Curie point.

FIGURE 5.

$\varepsilon/\varepsilon_0$ VS. TEMPERATURE FOR

$(PbZrO_3)_{0.98} + (Pb_2Sc_2O_5)_{0.02}$

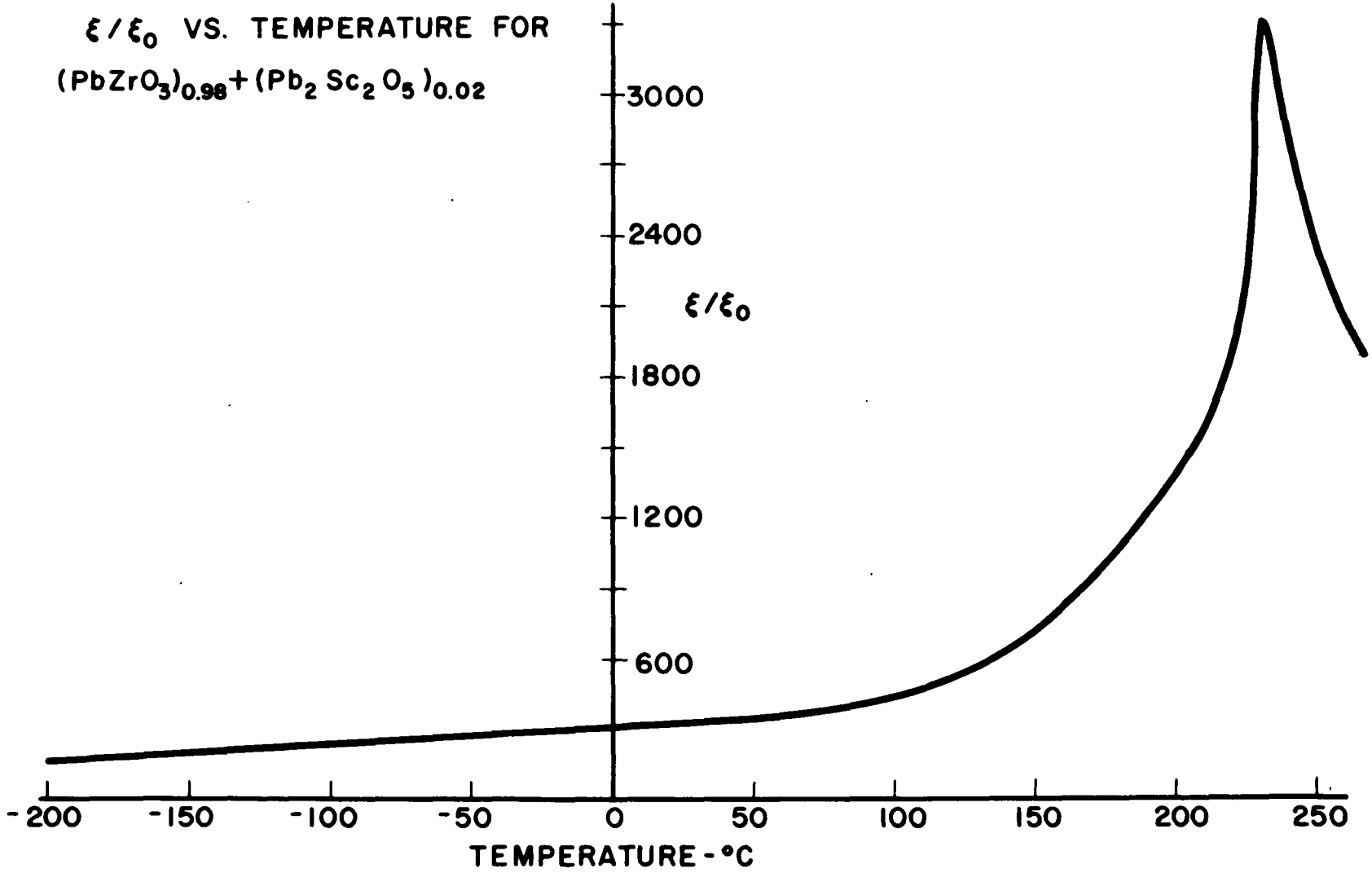

FIGURE 6.

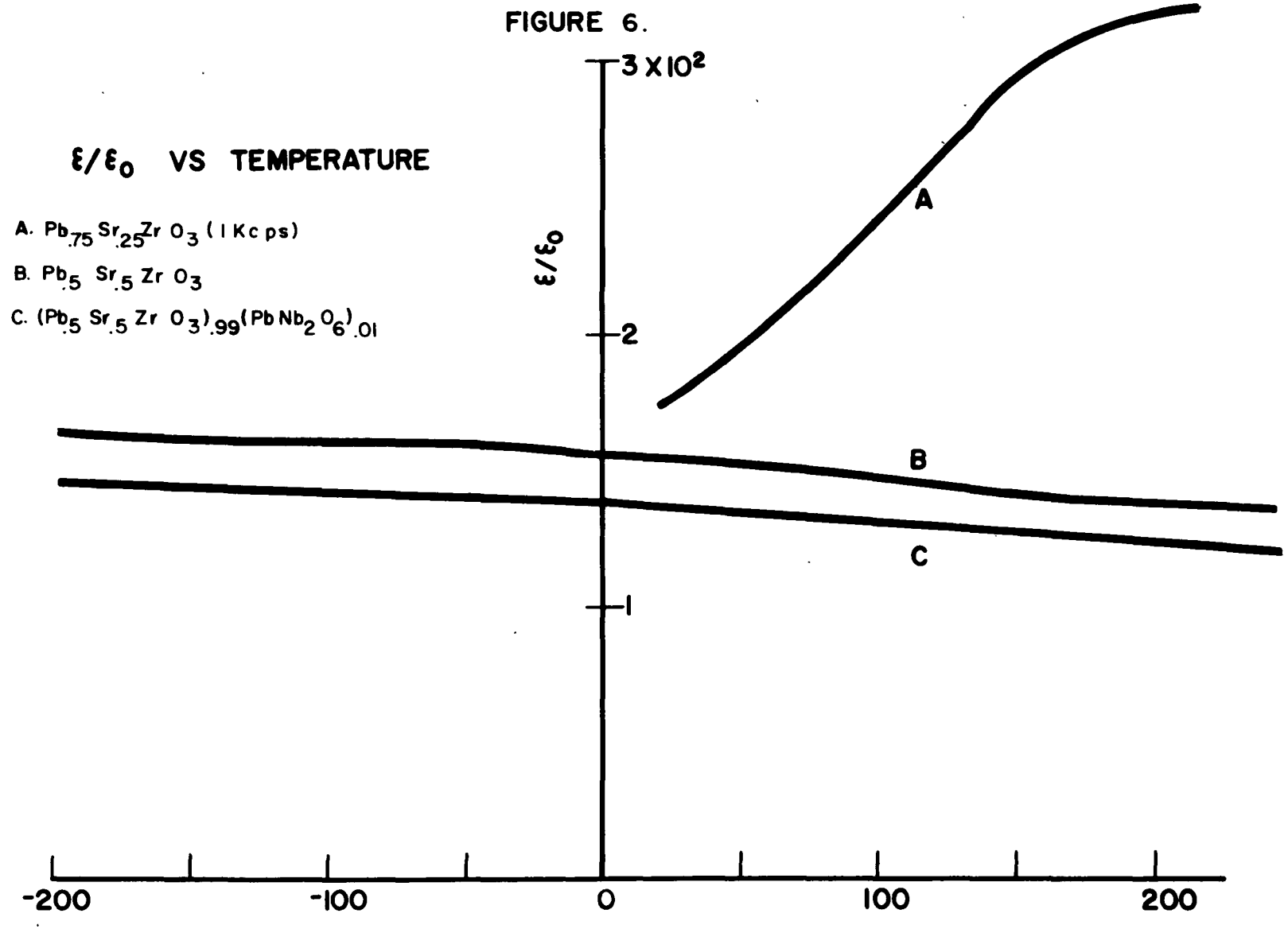
ε/ε0 VS TEMPERATURE
A. Pb.75 Sr.25 Zr O3 (1 Kc ps)
B. Pb.5 Sr.5 Zr O3
C. (Pb.5 Sr.5 Zr O3).99(Pb Nb2 O6).01
3 X 10²
2
1
ε/ε0
A
B
C
-200
-100
0
100
200

FIGURE 7.

$\varepsilon / \varepsilon_o$ VS. TEMPERATURE

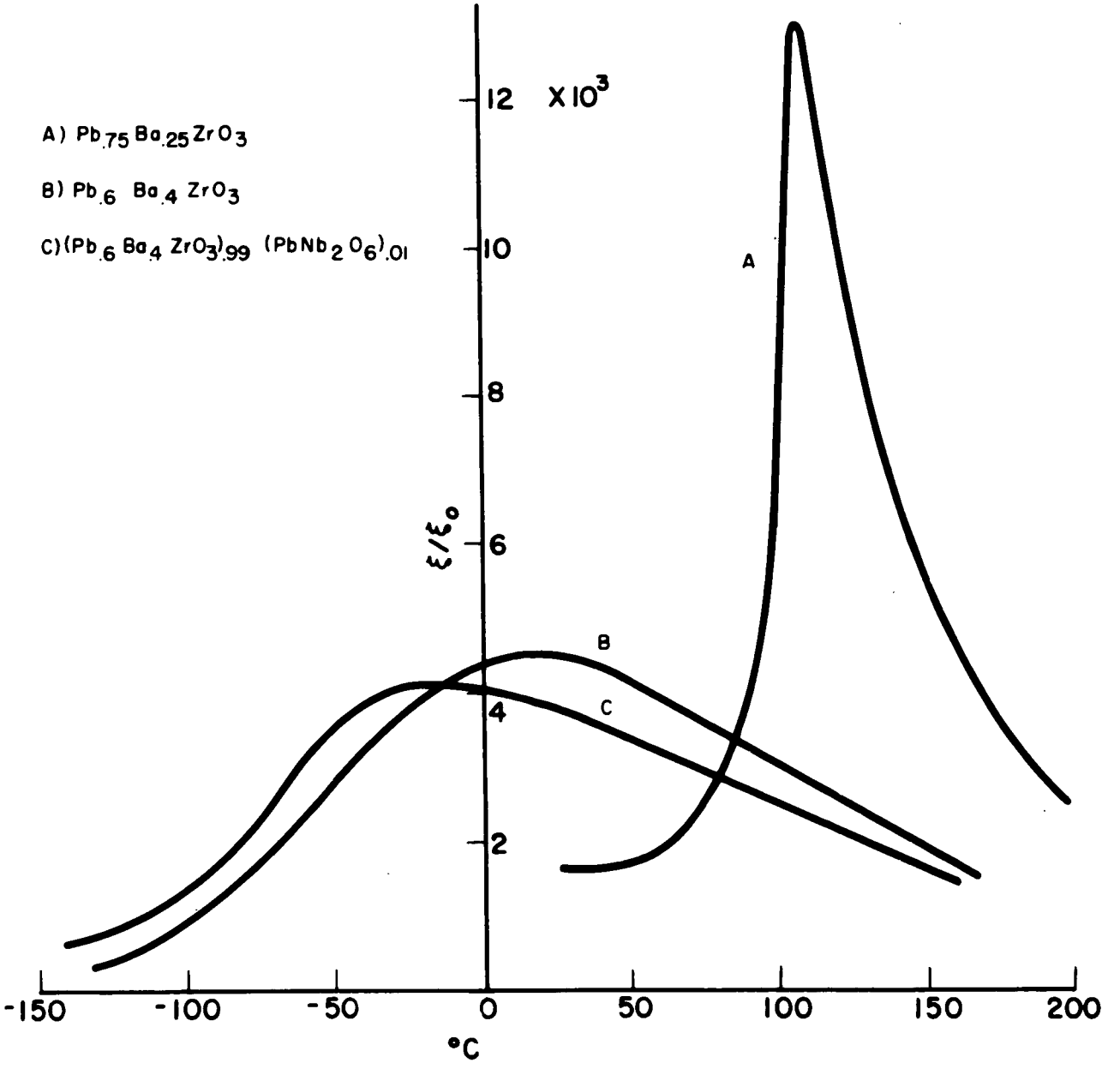

ERD 5702

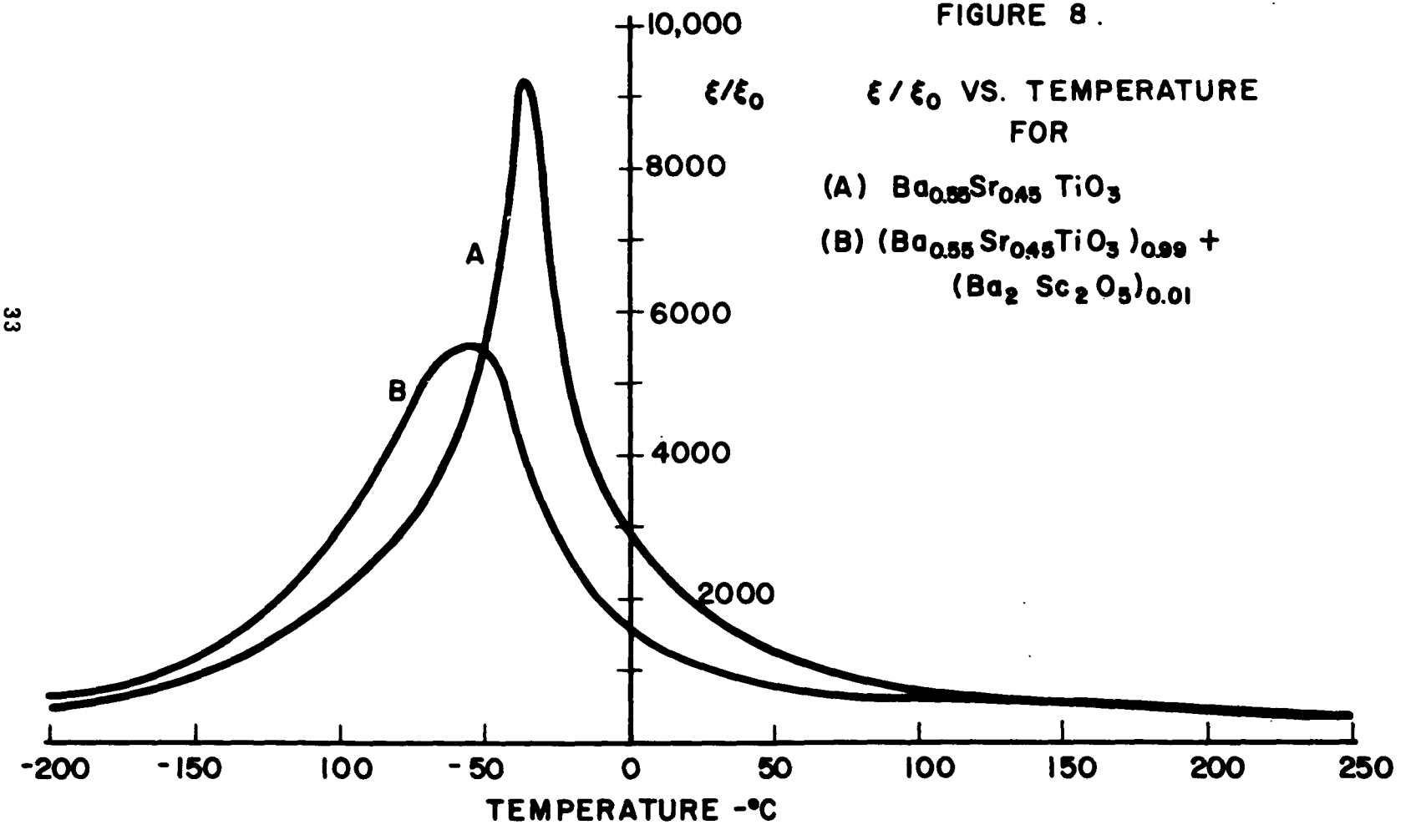

FIGURE 8.

$\varepsilon / \varepsilon_0$ VS. TEMPERATURE FOR

(A) $Ba_{0.55}Sr_{0.45}TiO_3$

(B) $(Ba_{0.55}Sr_{0.45}TiO_3)_{0.99} + (Ba_2Sc_2O_5)_{0.01}$

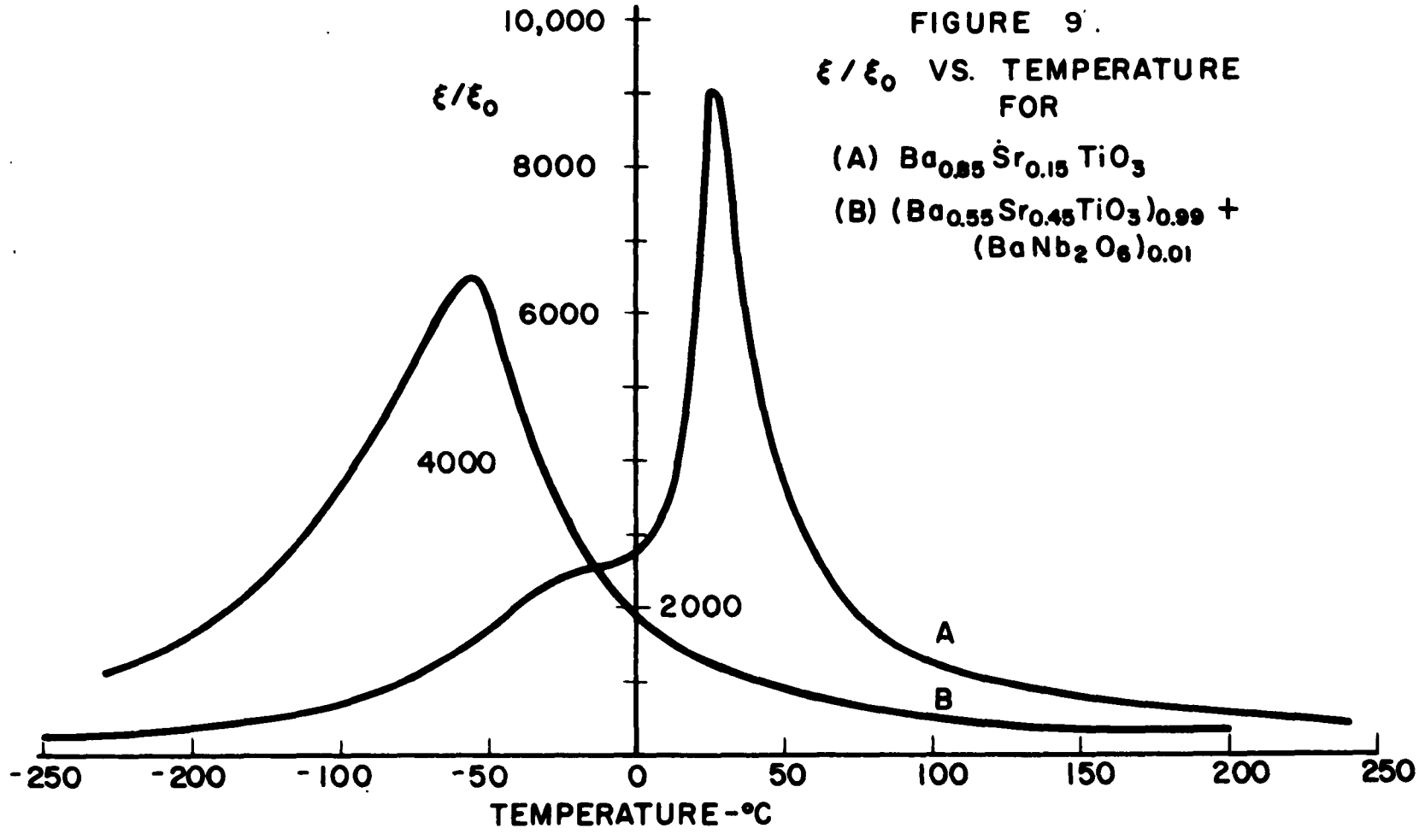

FIGURE 9.

$\varepsilon / \varepsilon_0$ VS. TEMPERATURE FOR

(A) $Ba_{0.85} Sr_{0.15} TiO_3$

(B) $(Ba_{0.55} Sr_{0.45} TiO_3)_{0.99} + (Ba Nb_2 O_6)_{0.01}$

Figure 10 shows permittivity as function of temperature for four compositions. The donor additive (Nb^{5+}) lowers the Curie point and peak permittivity of $Pb_{.15}Ba_{.7}Sr_{.15}TiO_3$, but raises the level of permittivity below the Curie point. The donor additive raises the general level of permittivity for $(PbTiO_3)_{.57}(BaZrO_3)_{.43}$. These materials have washed out Curie peaks near room temperature.

B. Volume Resistivity-Temperature Curves

Figure 11 shows volume resistivity as function of reciprocal absolute temperature for $Ba_{.55}Sr_{.45}TiO_3$, $(Ba_{.55}Sr_{.45}TiO_3)_{0.99}(Ba_2Sc_2O_5)_{.01}$, and $(Ba_{.55}Sr_{.45}TiO_3)_{0.99}(BaNb_2O_6)_{.01}$. These data indicate that the base material, $Ba_{.55}Sr_{.45}TiO_3$, has n-type conductivity, with the acceptor additive (Sc^{3+}) acting to compensate and raise the level, the donor additive (Nb^{5+}) lowering the level.

It is not possible to predict the effects of donors and acceptors in the general case. They may have very little effect, at least within certain temperature limits, if mobilities are low or if the levels of acceptors and donors are deep (tightly bound). Usually, however, the levels of donors are quite shallow. Another factor which might limit the effects of acceptors is generation of compensating donors by the lattice; this often accompanies introduction of acceptors.

Figure 12 shows an example where neither the donor nor the acceptor appreciably affects the level of the volume resistivity. The curves of Fig. 12 are nearly coincident with the upper curve of Fig. 11.

Figure 13 shows volume resistivity as function of reciprocal absolute temperature for $Pb_{.15}Ba_{.7}Sr_{.15}TiO_3$ with and without the donor (Nb^{5+})

FIGURE 10.

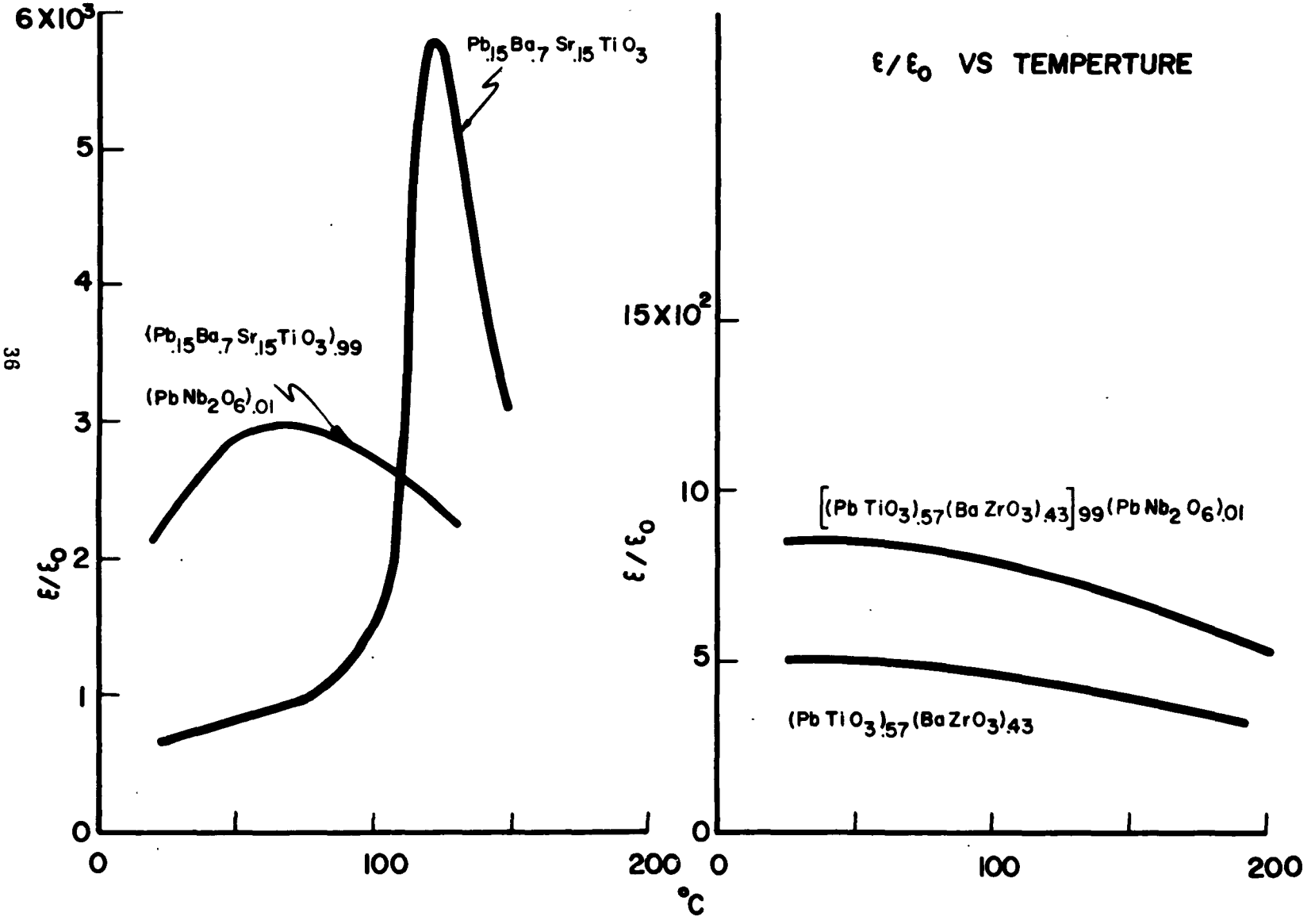
6X10³
5
4
3
2
1
0
ε/ε₀
0
100
200
°C
Pb.15 Ba.7 Sr.15 Ti O3
(Pb.15 Ba.7 Sr.15 Ti O3).99
(Pb Nb2 O6).01
ε/ε₀ VS TEMPERTURE
15X10²
10
5
0
ε/ε₀
[(Pb Ti O3).57 (Ba Zr O3).43].99 (Pb Nb2 O6).01
(Pb Ti O3).57 (Ba Zr O3).43
0
100
200

FIGURE 11.

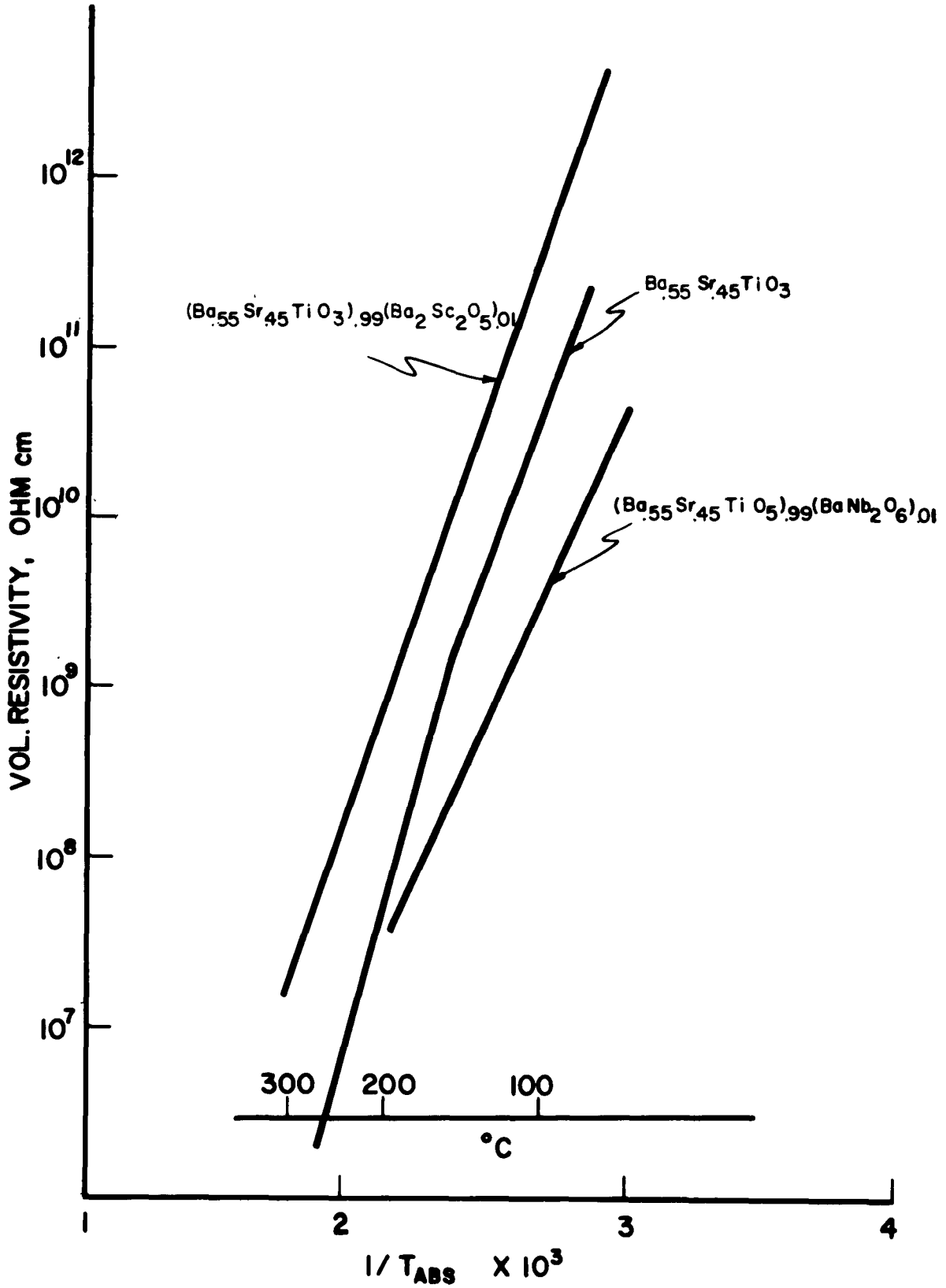

ERD 5704

FIGURE 12.

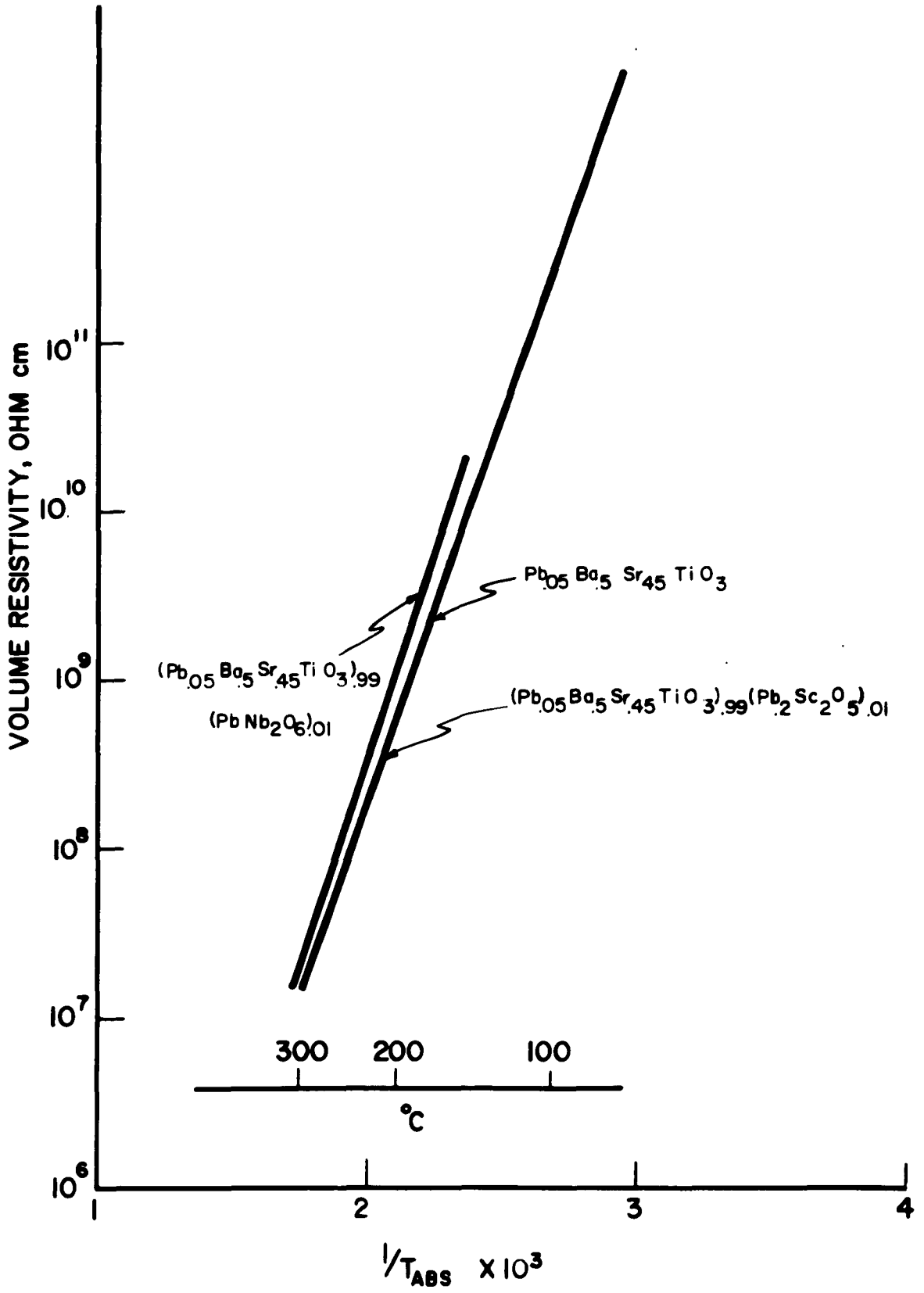

ERD 5705

FIGURE 13.

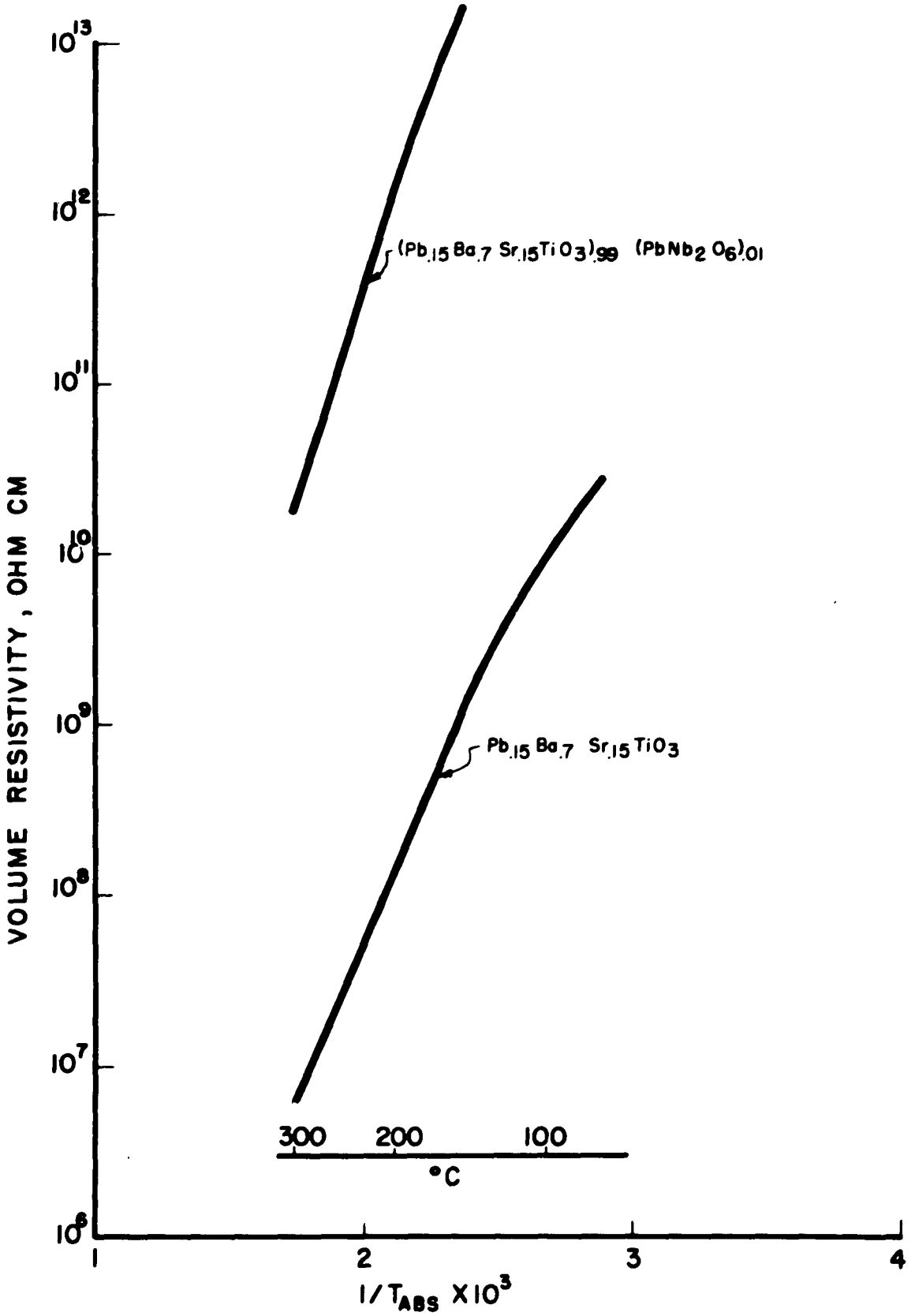

ERD 5706

additive. Here the donor had a profound effect on the volume resistivity, causing an increase of over three orders of magnitude. Due to experimental difficulties in measuring volume resistivities in excess of about 10^{13} ohm cm, no data are given for temperatures below which the volume resistivity rises to about this value. Comparison of Fig. 13 and 11 indicates that $Ba_{.55}Sr_{.45}TiO_3$ has n-type conductivity and $Pb_{.15}Ba_{.7}Sr_{.15}TiO_3$ has p-type conductivity. Neither the donor nor the acceptor additive has an appreciable effect on $Pb_{.05}Ba_{.5}Sr_{.45}TiO_3$, which is an intermediate composition (Fig. 12).

Figure 14 shows volume resistivity as function of reciprocal absolute temperature for $Ba_{.85}Sr_{.15}TiO_3$ with and without the donor (Nb^{5+}) additive. Here the donor brings about an increase in volume resistivity by about 2 orders of magnitude, indicating that the base material has p-type conductivity. It is interesting to note that the curve for $Ba_{.85}Sr_{.15}TiO_3$ with Nb^{5+} is nearly coincident with the curves of Fig. 12.

Figure 15 shows volume resistivity as function of reciprocal absolute temperature for various $(Pb,Sr)TiO_3$ compositions. The curves are nearly coincident for $Pb_{.3}Sr_{.7}TiO_3$ with donor (Nb^{5+}) and acceptor (Sc^{3+}) additives and with no addition, but the donor addition decreases the slope slightly. It is interesting to note that plain $Pb_{.5}Sr_{.5}TiO_3$ has markedly lower volume resistivity than plain $Pb_{.3}Sr_{.7}TiO_3$ and that with the former the donor additive causes a pronounced increase in volume resistivity ($\sim 10^3$).

Figure 16 shows volume resistivity as function of reciprocal absolute temperature for $Pb_{.05}Ba_{.8}Sr_{.15}TiO_3$ with and without donor addition. The effect of the donor is relatively slight.

FIGURE 14.

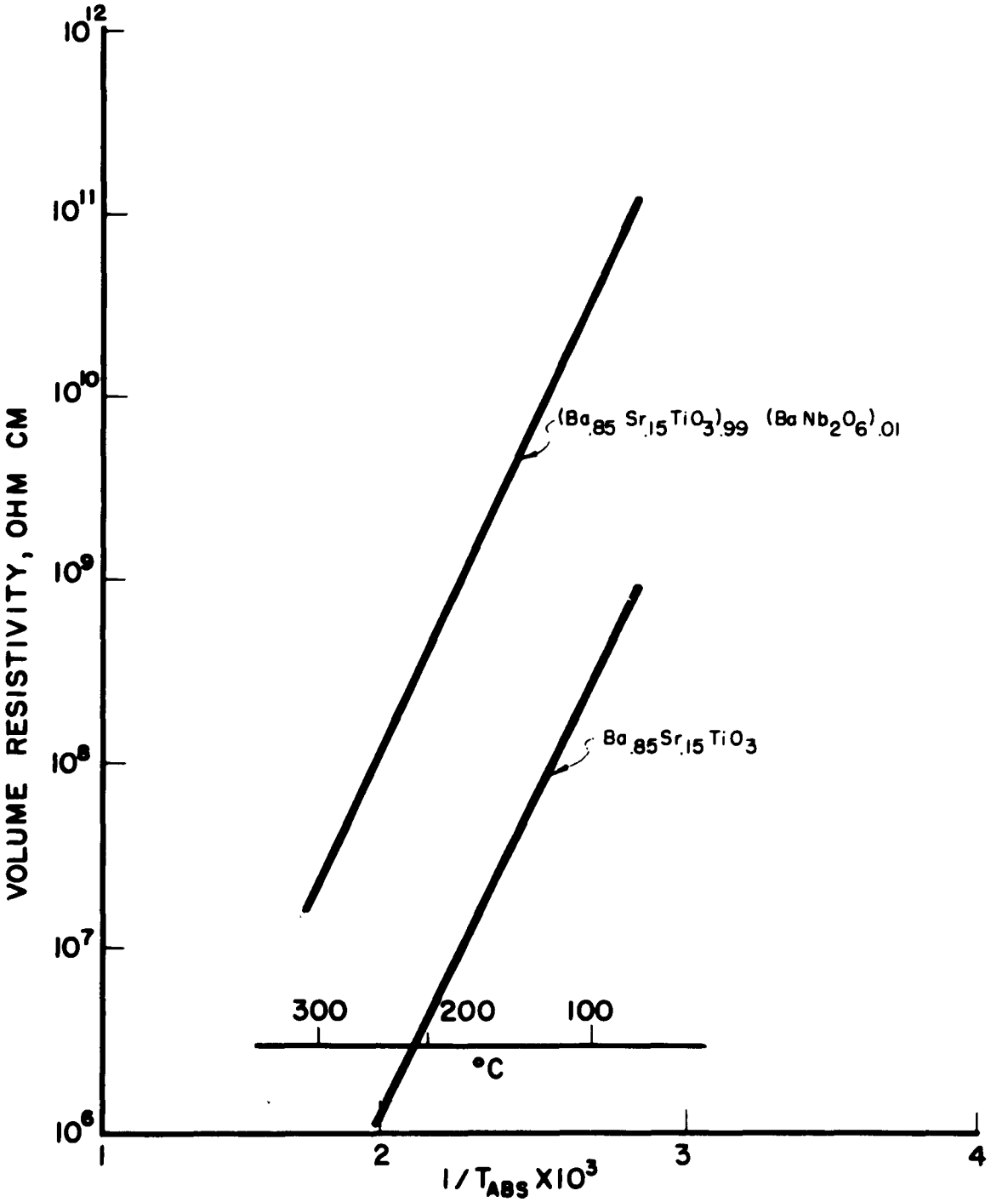

ERD 5707

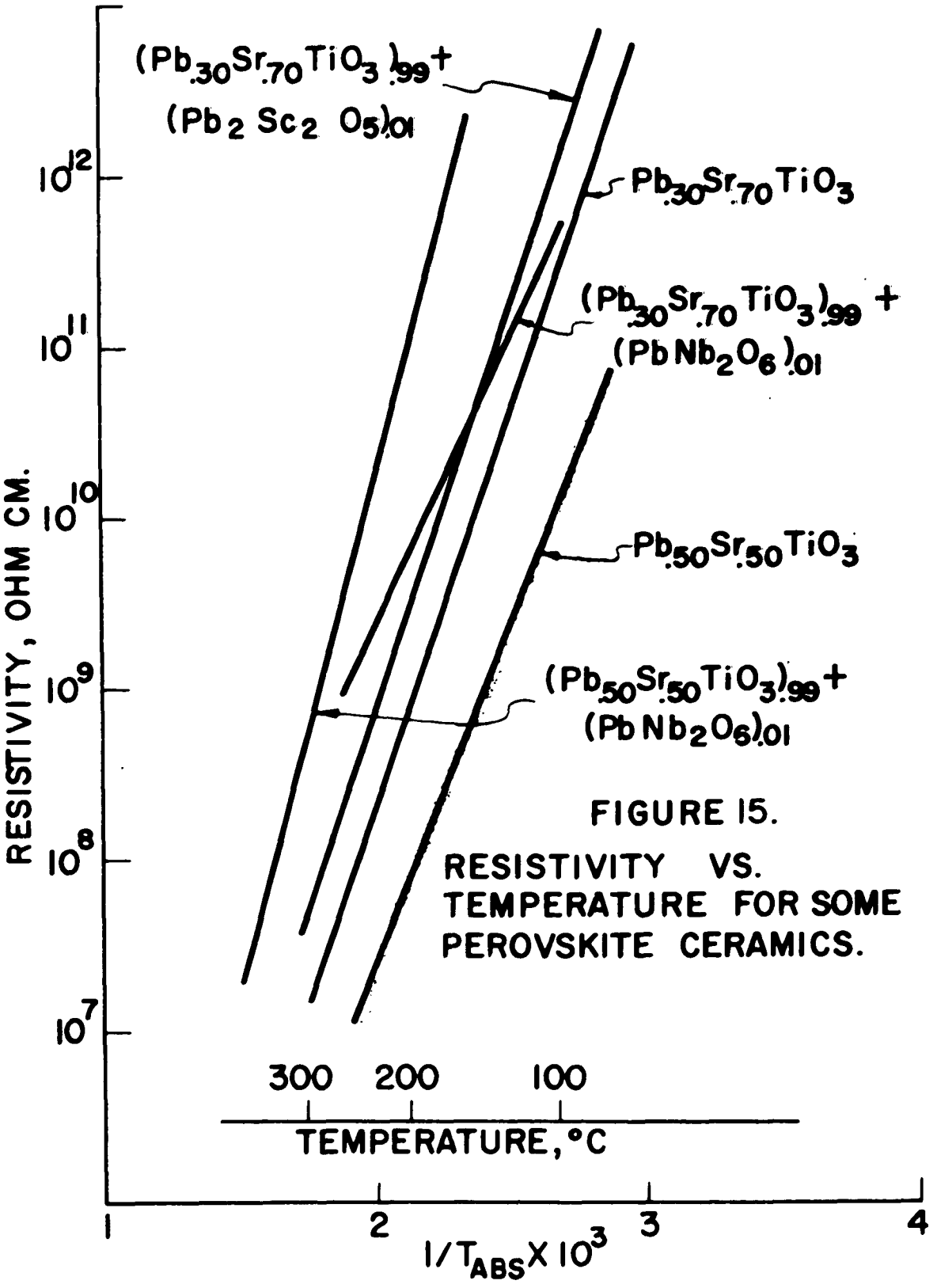

FIGURE 15.

RESISTIVITY VS. TEMPERATURE FOR SOME PEROVSKITE CERAMICS.

FIGURE 16.

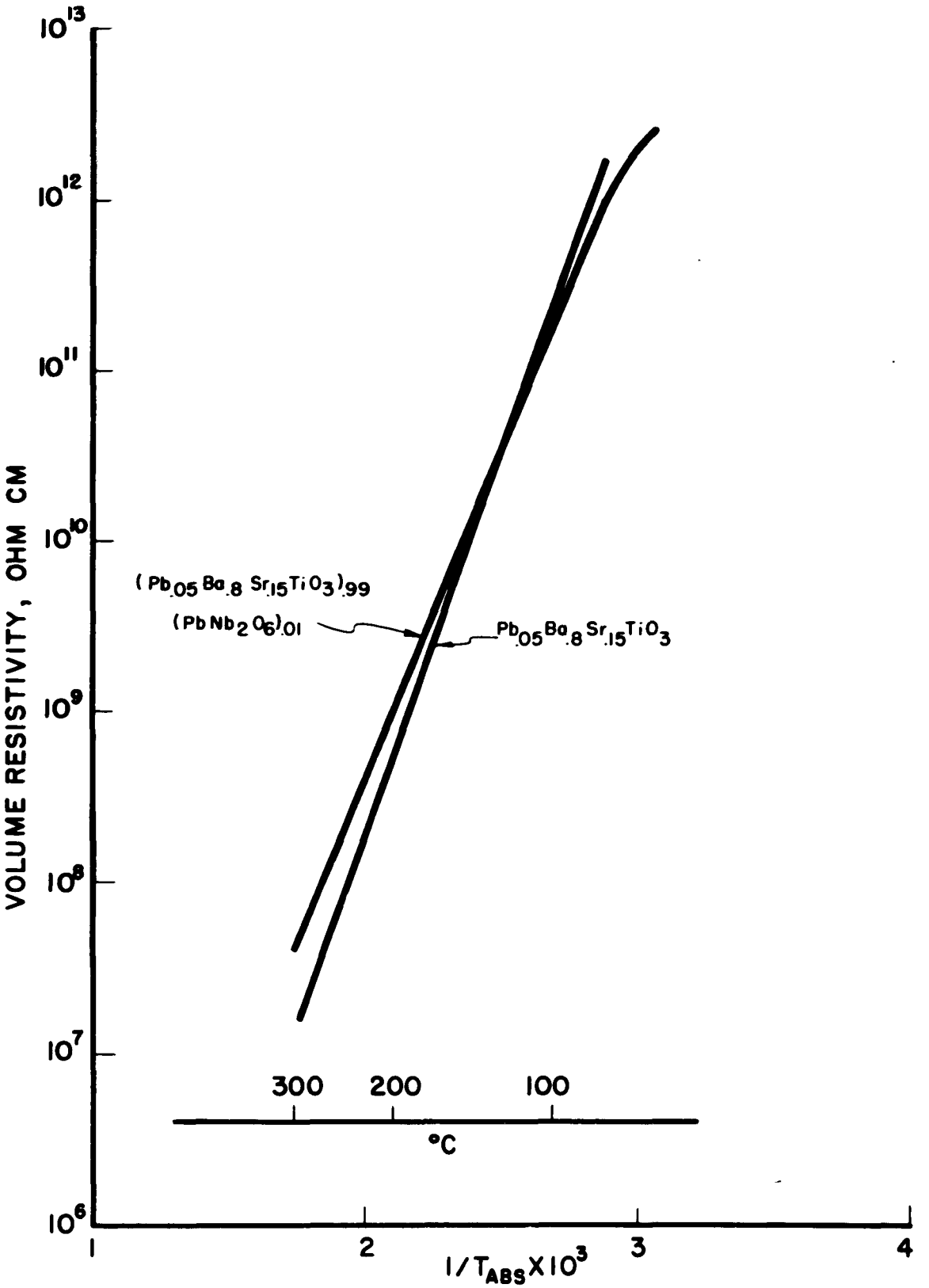

ERD 5708

All volume resistivity vs reciprocal absolute temperature curves shown previously are for titanates. Fig. 17 shows a plot for a mixed zirconate-titanate with and without donor additive. The donor in this case raises the volume resistivity by about two orders of magnitude.

Volume resistivity vs reciprocal absolute temperature curves in Figures 18 through 20 are for zirconates. Figure 18 shows the curves for $Pb_{.75}Ba_{.25}ZrO_3$ and $Pb_{.6}Ba_{.4}ZrO_3$; these are virtually coincident. The donor additive increases volume resistivity by about two orders of magnitude.

Figure 19 shows volume resistivity as function of reciprocal absolute temperature for plain $PbZrO_3$ and $PbZrO_3$ with donor and acceptor additives. Neither type of additive is particularly effective in altering the resistivity level, although the donor causes an increase of over one order of magnitude in the volume resistivity above about 250°C. The slopes with donor and acceptor are about equal and separated by about one order of magnitude. The slope is markedly higher for plain $PbZrO_3$.

Figure 20 shows volume resistivity as function of reciprocal absolute temperature for $Pb_{.5}Sr_{.5}ZrO_3$ with and without donor additive and for $Pb_{.75}Sr_{.25}ZrO_3$. The donor in this case raises the volume resistivity by about two orders of magnitude.

While all materials prepared in this work are insulators in ordinary temperature ranges, there may be as much as five orders of magnitude difference in conductivity between the most and least insulating materials at a given temperature. The slopes of all curves are <u>roughly</u> the same, implying similar activation energies and perhaps similar microscopic processes causing conduction in all compositions. There are changes in slope in some

FIGURE 17.

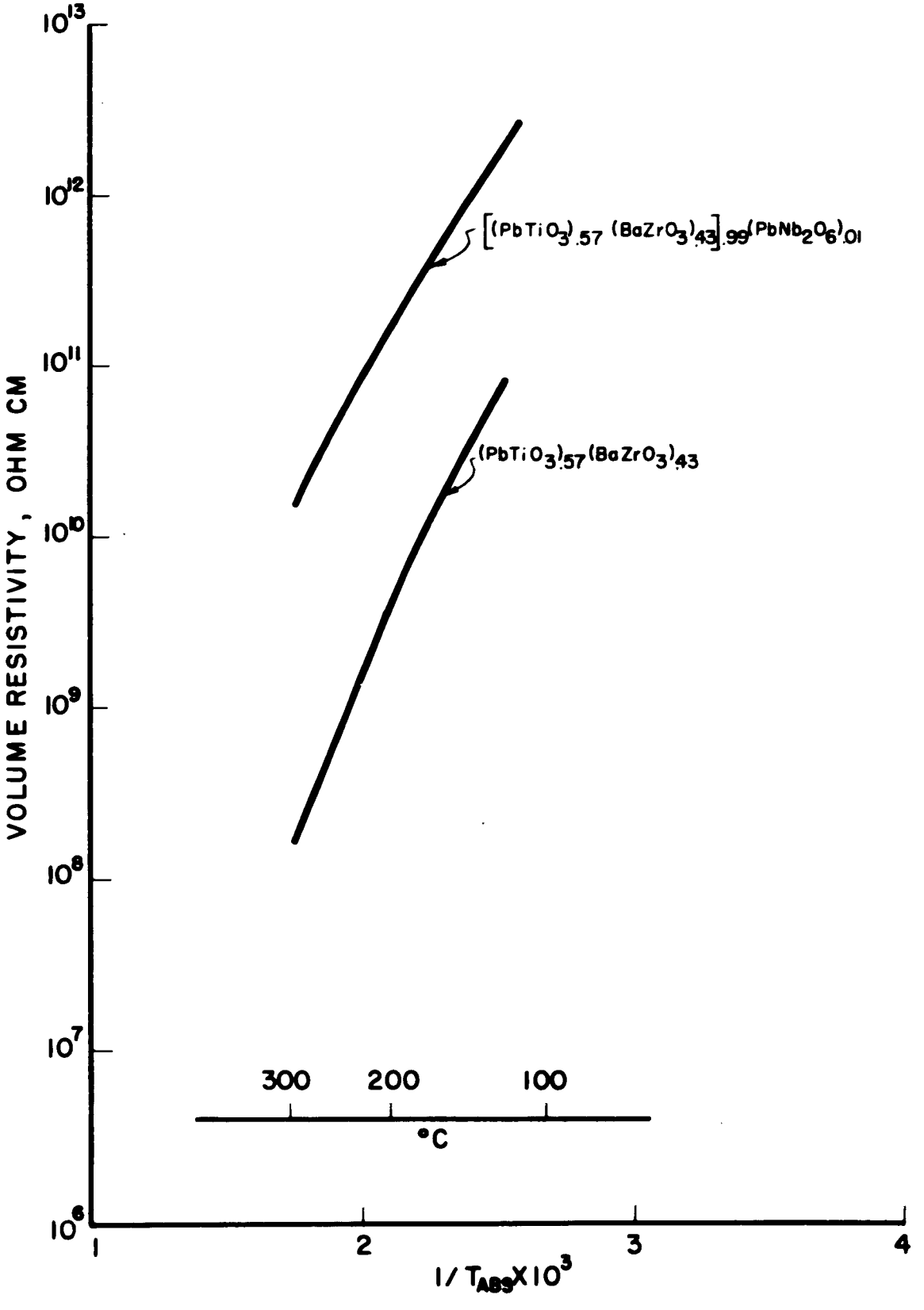

ERD 5709

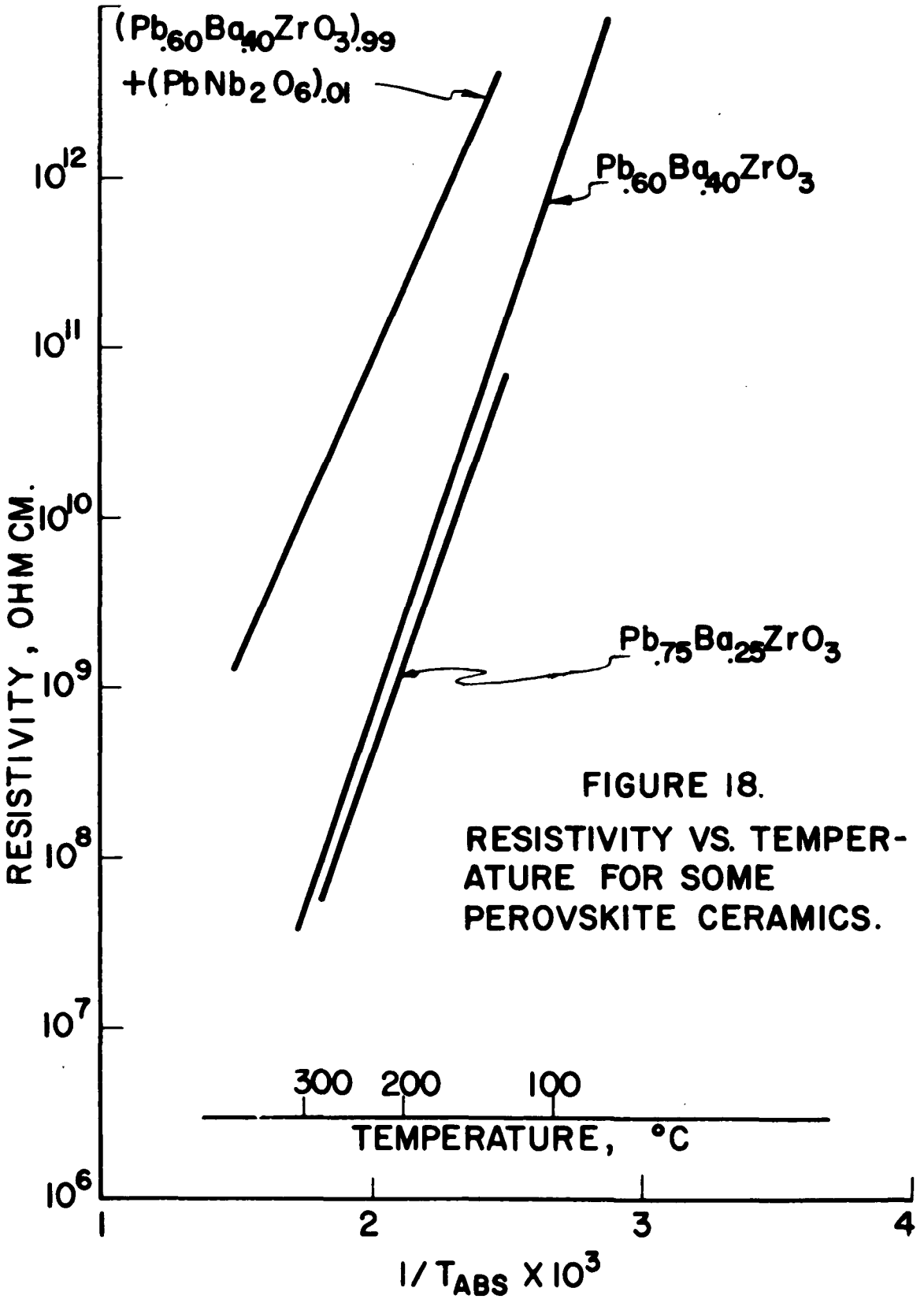

FIGURE 18.

RESISTIVITY VS. TEMPERATURE FOR SOME PEROVSKITE CERAMICS.

FIGURE 19.

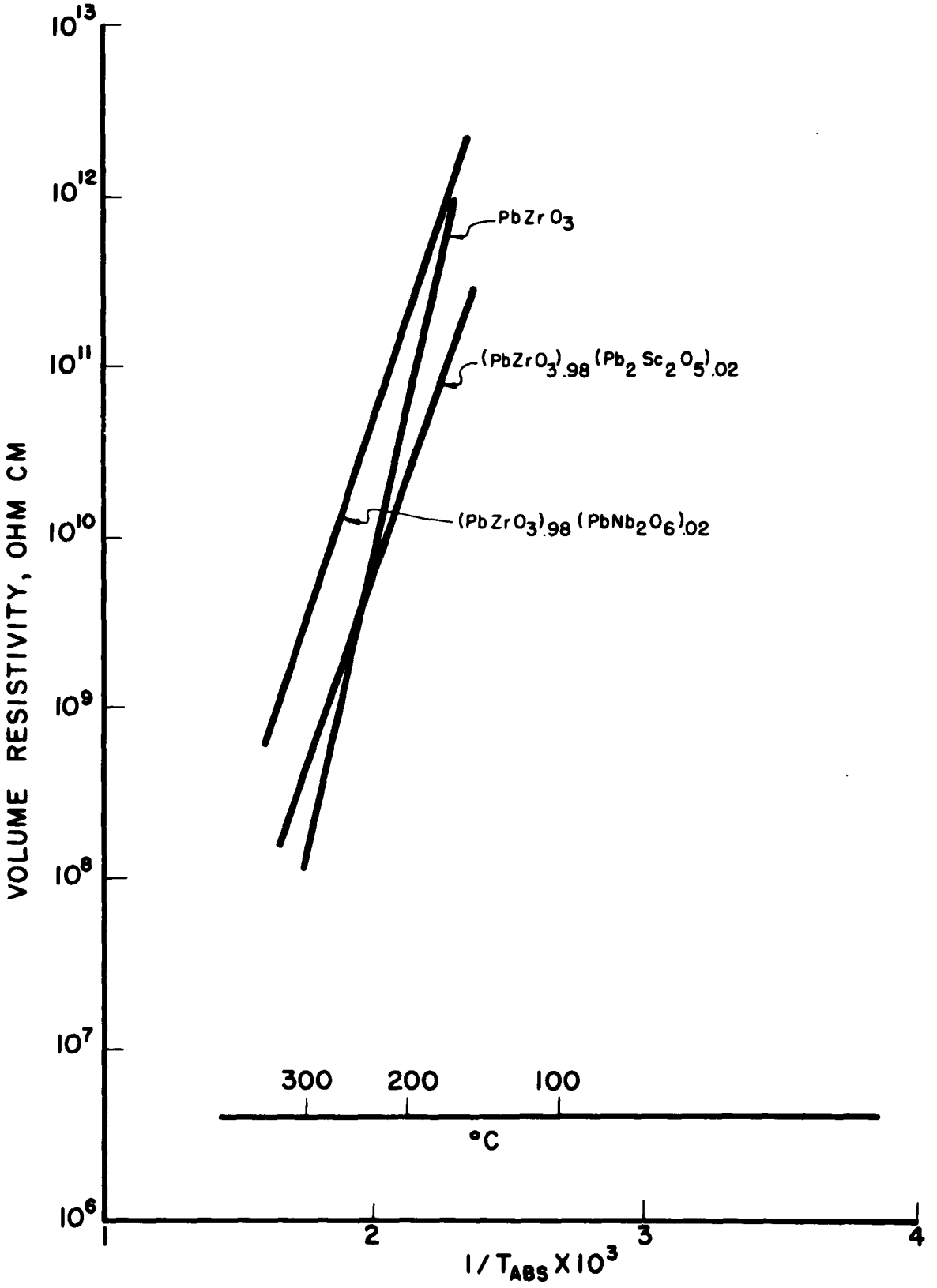

ERD 5710

FIGURE 20.

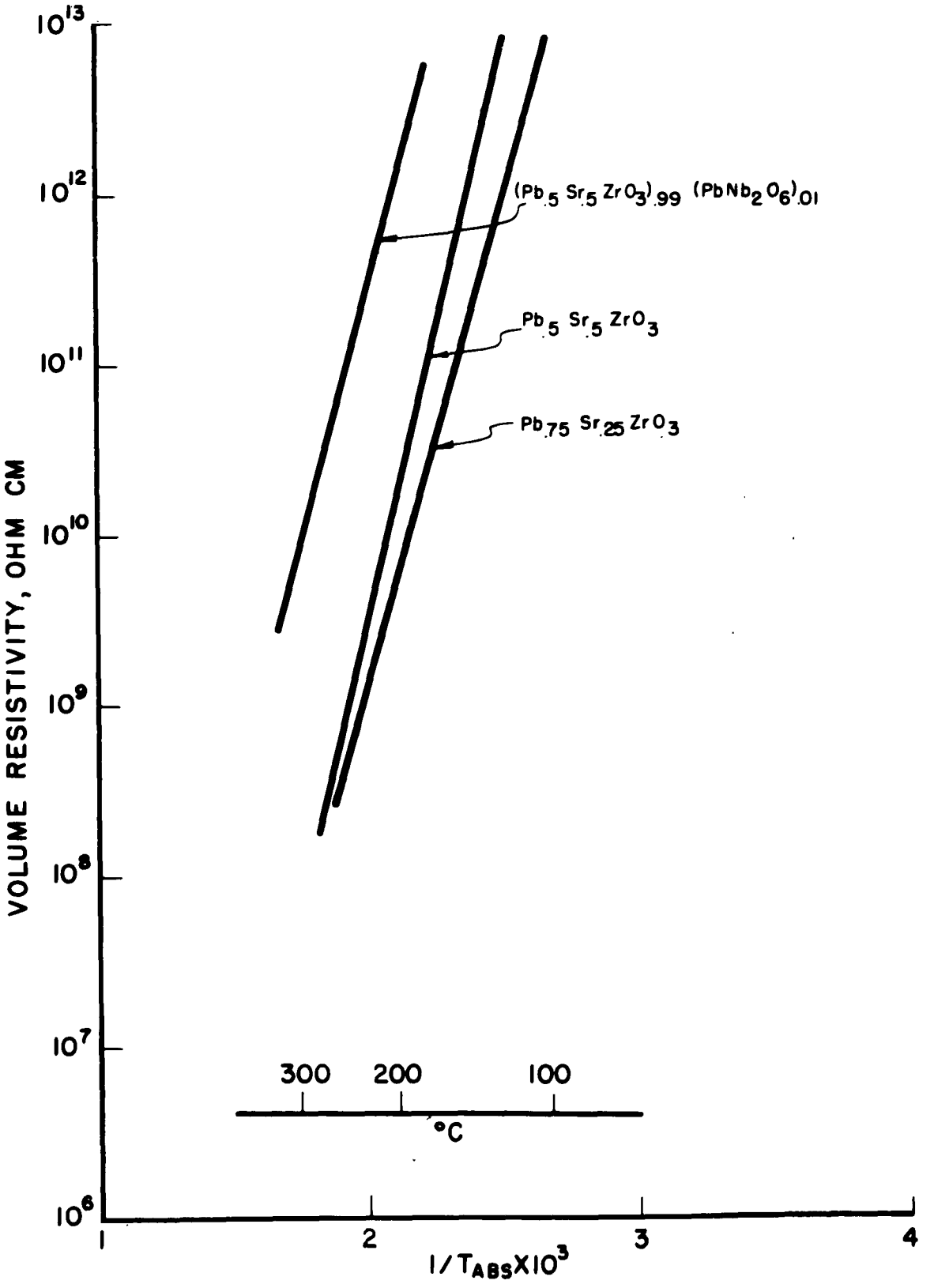

ERD 5711

instances, however, and these may be related to changes in the conduction process. Figure 21 summarizes some of the data of Figures 11 through 20. Here the various base materials studied are grouped in steps of one-half order of magnitude in their general level of volume resistivity. With the base materials alone there is a range of four orders of magnitude, with the zirconates in general grouped in the upper two orders of magnitude, the titanates in the lower two orders of magnitude.

The mechanisms of conduction in most oxides are electronic, with electrons and holes being generated by oxygen and metal vacancies, respectively, in the unmodified oxide. The data of Figs. 11 through 21 and Table II indicate that in nearly all cases the donor (Nb^{5+}) raises and the acceptor (Sc^{3+}) lowers the resistivity, indicating the normal conductivity is p-type. In only one case (Fig. 11) were clearly opposite effects noted and in this case the normal conductivity is n-type. It is important to note that the compositions of Figs. 11 and 14 were fired in a gas furnace, and all other compositions were fired in an electric furnace with an upper temperature limit near 1550°C. In a gas furnace the atmosphere is not air, but a combustible mixture which is not in chemical equilibrium. The atmosphere therefore tends to be reducing, in contrast to the usual oxidizing atmosphere of an electric furnace. This would tend to bring about n-type conductivity in the specimens prepared in a gas furnace. Furthermore, because of the greater susceptibility to reduction of Ti^{4+} in contrast to Zr^{4+}, one expects titanates to tend towards n-type conductivity in comparison to the zirconates.

The resistivity-temperature data presented and discussed in this section are representative of the bulk ceramic. There may be significant

FIGURE 21.

RELATIVE GENERAL LEVEL OF VOLUME RESISTIVITIES OF BASE MATERIALS

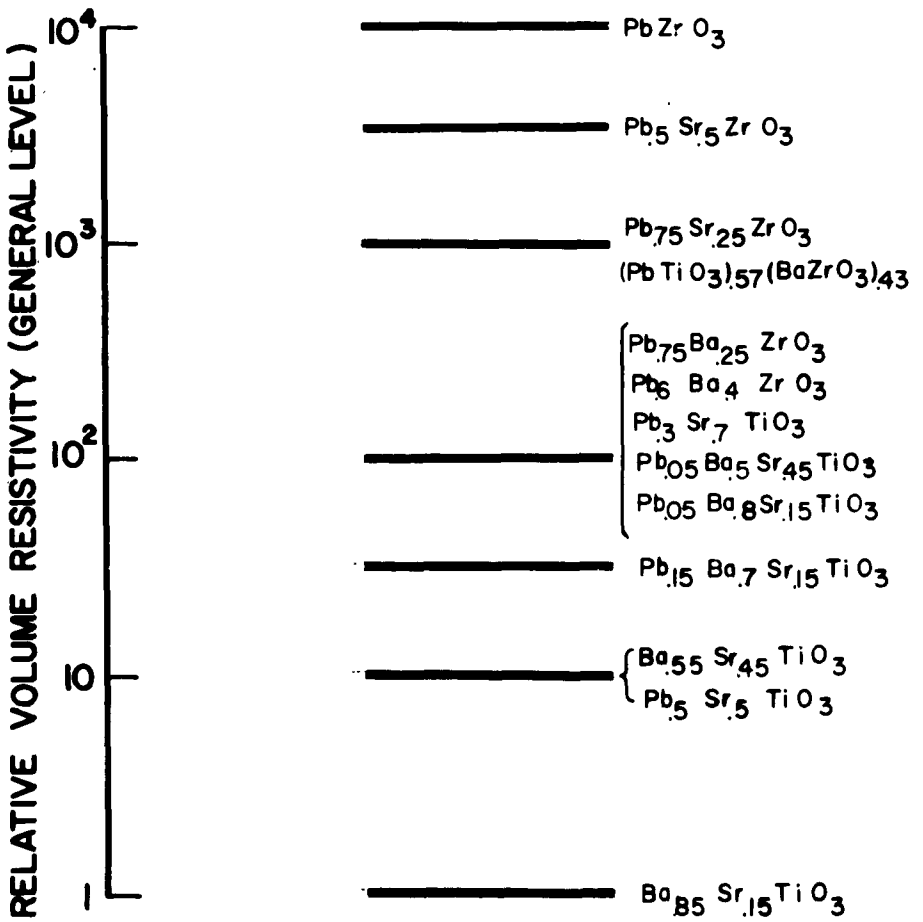

Table II. Effect of Donor (Nb^{5+}) and Acceptor (Sc^{3+})

Additives on General Level of Volume Restitivity

Base Material	Nb^{5+}	Sc^{3+}
$PbZrO_3$	up, especially at high temperature	down, especially at low temperature
$Pb_{.5}Sr_{.5}ZrO_3$	up ~ 10^2	----------
$Pb_{.75}Sr_{.25}ZrO_3$	----------	----------
$(PbTiO_3)_{.57}(BaZrO_3)_{.43}$	up ~ 10^2	----------
$Pb_{.6}Ba_{.4}ZrO_3$	up ~ 10^2	----------
$Pb_{.75}Ba_{.25}ZrO_3$	----------	----------
$Pb_{.3}Sr_{.7}TiO_3$	up at high temp.	up ~ 2
$Pb_{.05}Ba_{.5}Sr_{.45}TiO_3$	~ same	~ same
$Pb_{.05}Ba_{.8}Sr_{.15}TiO_3$	~ same	----------
$Pb_{.15}Ba_{.7}Sr_{.15}TiO_3$	up ~ 10^3	----------
$Ba_{.55}Sr_{.45}TiO_3$	down ~ 10	up ~ 10
$Pb_{.5}Sr_{.5}TiO_3$	up ~ 10^3	----------
$Ba_{.85}Sr_{.15}TiO_3$	up ~ 10^2	----------

variations at a microscopic level, such as conduction along grain boundaries, which have a great deal to do with dielectric degradation or breakdown. Variations of this type may be detected only indirectly, by, for instance, preparing a given composition with widely different grain size. If the material with smaller grain size then has significantly lower volume resistivity, one might conclude that the greater overall volume of material at the grain boundaries could account for this. Unfortunately, other factors must also be considered, such as the longer exposure to peak temperature necessary to encourage grain growth, the effect of atmosphere, etc. Studies of this type were not included in the scope of this project, but some attempts were made to determine whether there is a relation between grain size and dielectric degradation and dielectric strength (Sections IV and VIII).

IV. GRAIN STRUCTURE

The examination of the grain structure of ceramics requires a polishing and etching procedure which can reveal the details of grain boundaries and minimize scratching and grain tear-outs. The method developed in this work involves polishing carried out in six stages, four with silicon carbide polishing papers, two with rotating lapping wheels. The silicon carbide papers, in order of use, are of grit size 240, 320, 400, and 600. The test specimen is moved in a horizontal linear motion with no rotation. Running water is used as a lubricant, and moderate pressure is maintained on the test specimen. In instances in which the test specimen is initially flat (not warped), the first two or three grit sizes are omitted.

The first wheel lapping step is performed on a nylon-covered wheel with six-micron diamond paste. The second step is accomplished on a "Microcloth"* covered wheel with three-micron diamond paste. The rate of wheel rotation for both steps is 1150 rpm. The test specimen is rotated circumferentially about the wheel in a direction opposite to the rotation of the wheel with moderate vertical pressure maintained.

Etching is with a dilute solution of technical grade hydrofluosilicic acid (H_2SiF_6) at 25°C. In most cases significant etching begins during a five-second immersion in a 0.3% (by volume) water solution. After the five-second immersion the degree of etching is checked by a microscopic examination (about 1000 x). When insufficient etching has taken place, either the solution concentration or submersion time is increased by a factor of five to ten, and the process is repeated. The least severe etching process has been three seconds in a 0.3% solution, and the most severe was for twenty minutes in a 3% solution.

In some instances the grains of the ceramic dielectrics are so small (order of one to two microns) that detail cannot be brought out using normal optical magnification. In these cases electron micrographs were made. Extreme care is then required in the polishing procedure, and the procedure outlined above is further refined. There are three initial steps using respectively, 9-, 5-, and 3-micron Microgrit type WCA** abrasive in glycerine, mixed with one part abrasive to two parts glycerine (by volume). These slurries are used on a flat and scratch-free piece of plate glass. The test specimen is moved in

---

* A. B. Buelher, Ltd., Evanston, Illinois.

** Micro Abrasives Corp., Westfield, Mass.

a circular path and it is simultaneously slowly rotated. Each slurry is used for about two minutes.

The fourth step involves 3-micron abrasive in distilled water (one part abrasive to three parts water). The fifth and sixth steps involve Linde fine abrasive types C-5250 and A-5175* respectively, mixed as in step four. These slurries are used on a Pellon PAD** perforated polishing disc, with the disc backed by plate glass.

The polishing operation is monitored by intermittent examination of the test specimen under a microscope at about 1000 x. The test specimen must be carefully washed between steps in order to prevent contamination of a given slurry with the preceding larger grit. Etching is accomplished as described before. The electron micrographs were actually made on replicas.

Microphotographs of most of the ceramics are shown in Figures 22 through 33 and electron micrographs of some ceramics with smaller grains are shown in Figures 34 through 36. It is at once clear that there are pronounced differences in grain size and in distribution of grain sizes. These results are discussed in connection with results of degradation and dielectric strength tests in Section VIII.

V. DIELECTRIC BREAKDOWN STUDIES

Dielectric breakdown in insulators was the subject of considerable theoretical and experimental study before World War II, especially by von

---

* Linde Air Products Co., New York 17, N. Y.

** Geoscience Instruments Corp., New York 38, N. Y.

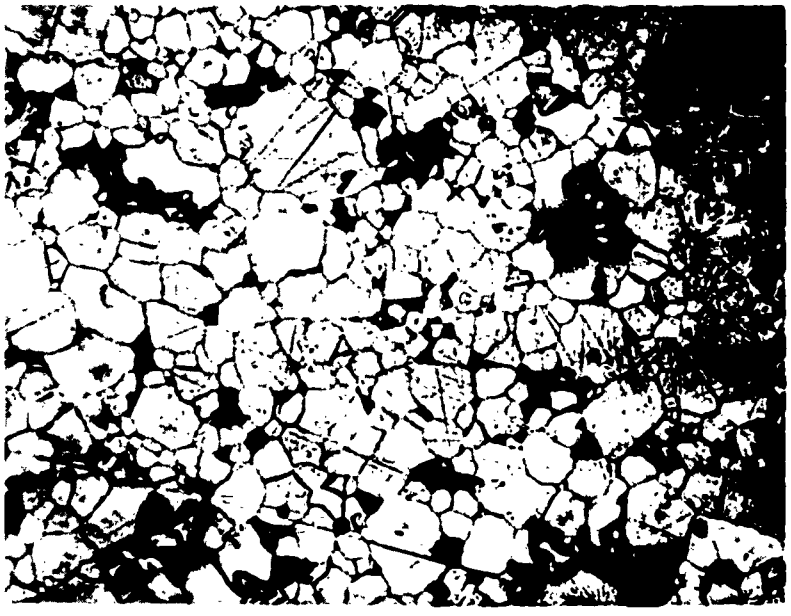

$Pb_{0.05}Ba_{0.80}Sr_{0.15}TiO_3$
DENSITY: 97% THEORETICAL
ETCH: H_2SiF_6 SOLN. 1000X

Figure 22

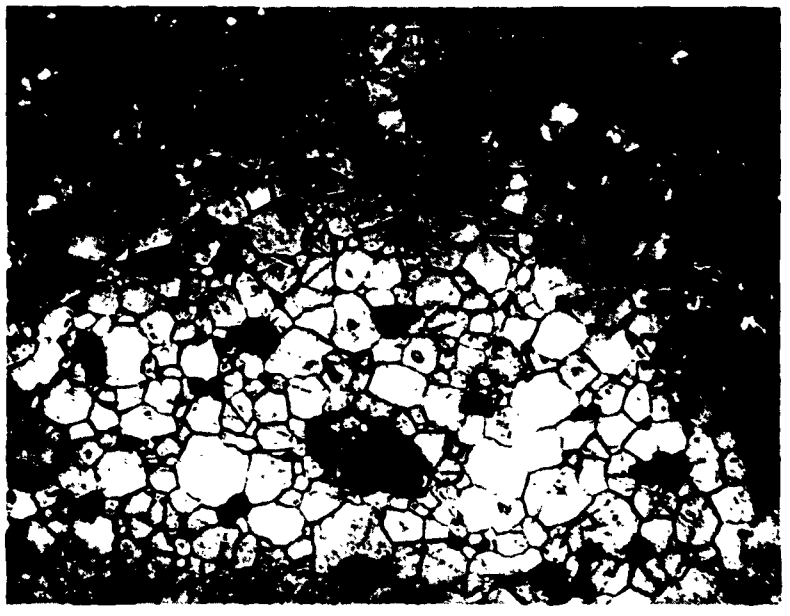

$Pb_{0.05}Ba_{0.50}Sr_{0.45}TiO_3$
DENSITY: 98% THEORETICAL
ETCH: HF, HNO_3 SOLN. 1000X

Figure 23

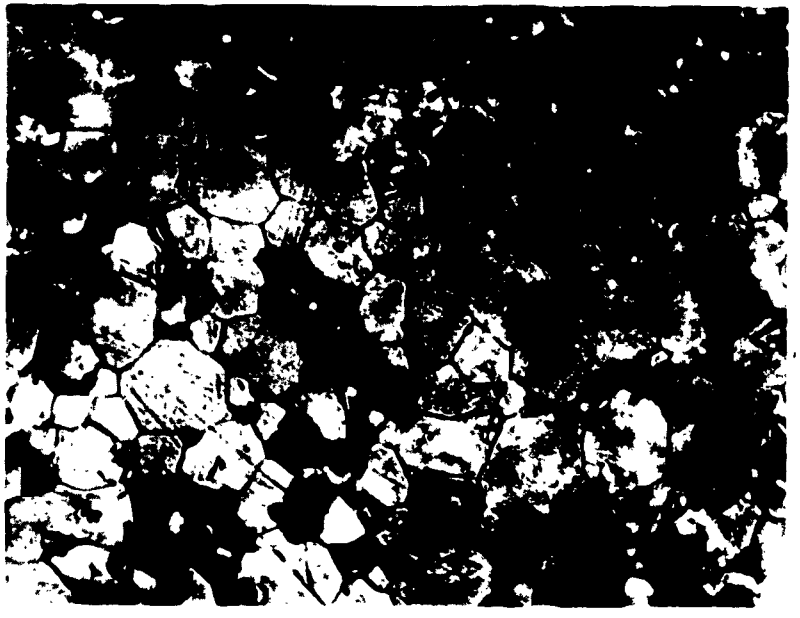

$Pb_{0.30}Sr_{0.70}TiO_3$
DENSITY: 96% THEORETICAL
ETCH: H_2SiF_6 SOLN. 1000X

Figure 24

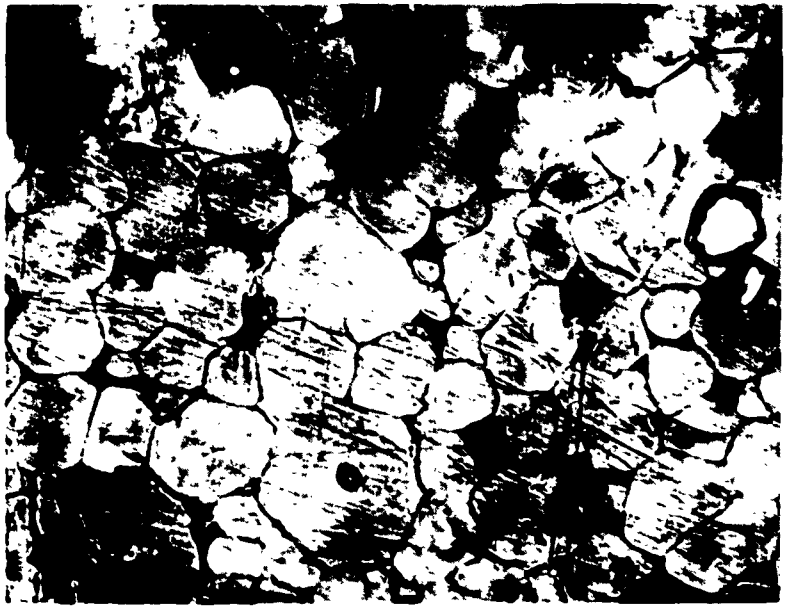

$Pb_{0.50}Sr_{0.50}TiO_3$
DENSITY: 96% THEORETICAL
ETCH: H_2SiF_6 SOLN. 1000X

Figure 25

$(Pb_{0.30}Sr_{0.70}TiO_3)_{0.99} + (Pb_2Sc_2O_5)_{0.01}$
DENSITY: 97% THEORETICAL
ETCH: H_2SiF_6 SOLN. 1000X

Figure 26

$(Pb_{0.50}Sr_{0.50}TiO_3)_{0.99} + (PbNb_2O_6)_{0.01}$
DENSITY: 98% THEORETICAL
ETCH: H_2SiF_6 SOLN. 1000X

Figure 27

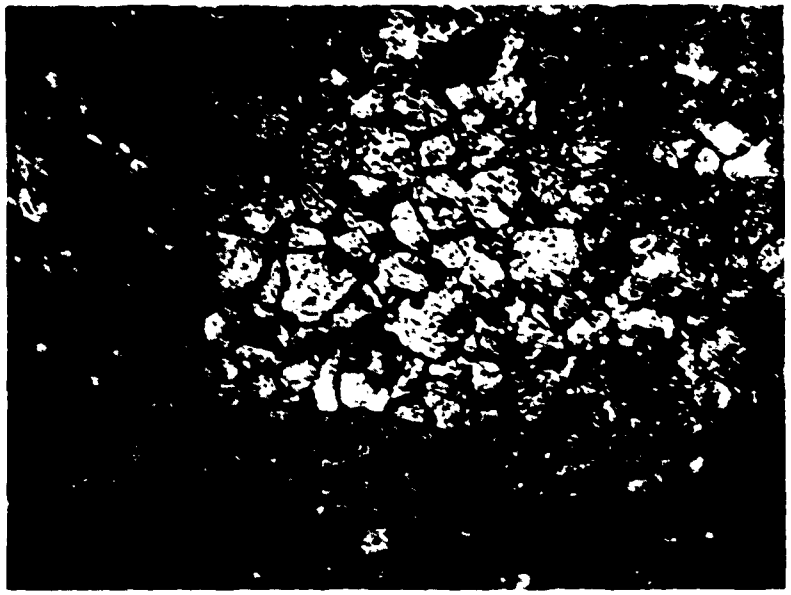

$Pb_{0.50}Sr_{0.50}ZrO_3$
DENSITY: 99% THEORETICAL
ETCH: H_2SiF_6 SOLN. 1000X

Figure 28

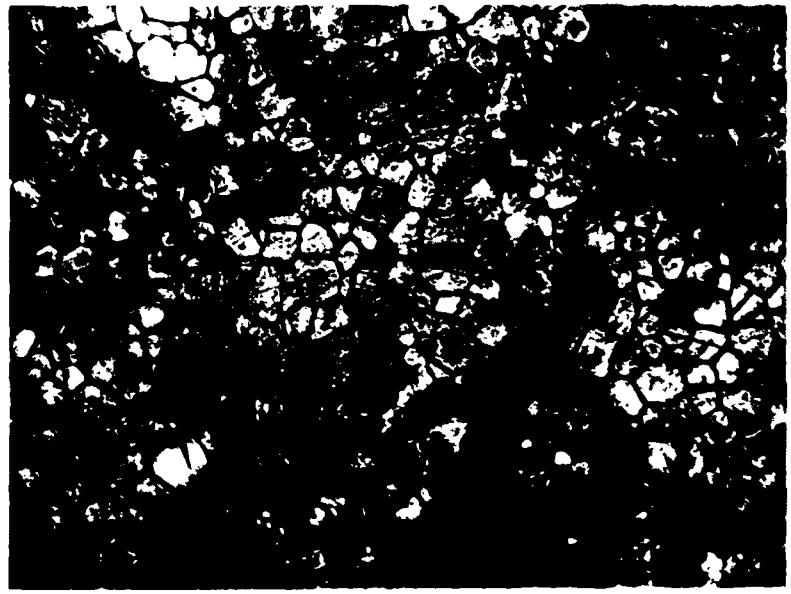

$Pb_{0.75}Sr_{0.25}ZrO_3$
DENSITY: 98% THEORETICAL
ETCH: H_2SiF_6 SOLN. 1000X

Figure 29

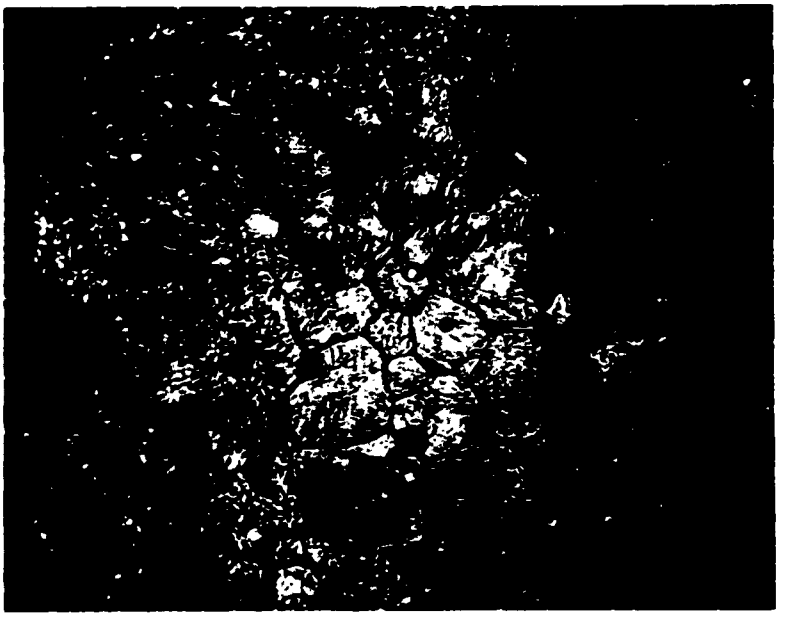

$(Pb_{0.50}Sr_{0.50}ZrO_3)_{0.99} + (PbNb_2O_6)_{0.01}$
DENSITY: 99% THEORETICAL
ETCH: H_2SiF_6 SOLN. 1000X

Figure 30

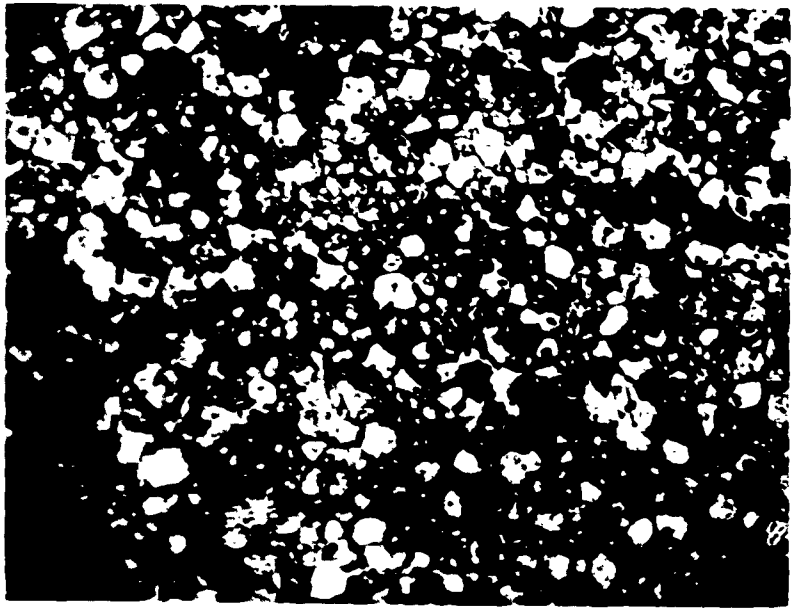

$Pb_{0.60}Ba_{0.40}ZrO_3$
DENSITY: 96% THEORETICAL
ETCH: H_2SiF_6 SOLN. 1000X

Figure 31

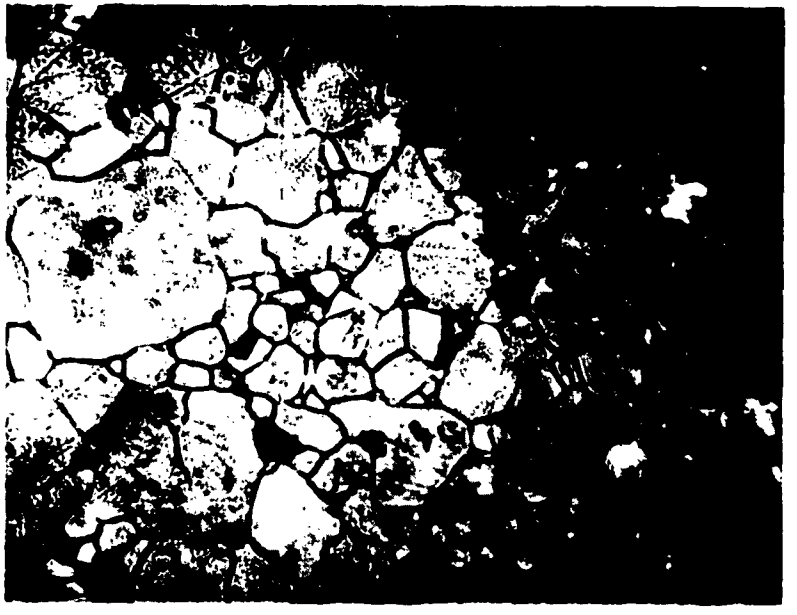

$(Pb_{0.60}Ba_{0.40}ZrO_3)_{0.99} + (PbNb_2O_6)_{0.01}$
DENSITY: 99% THEORETICAL
ETCH: H_2SiF_6 SOLN. 1000X

Figure 32

$PbZrO_3$
DENSITY: 99% THEORETICAL
ETCH: H_2SiF_6 SOLN. 15000X

Figure 33

$(PbZrO_3)_{0.98} + (PbNb_2O_6)_{0.02}$
DENSITY: 99% THEORETICAL
ETCH: H_2SiF_5 SOLN. 15000X

Figure 34

$(Pb_{0.30}Sr_{0.70}TiO_3)_{0.99} + (PbNb_2O_6)_{0.01}$
DENSITY: 99% THEORETICAL
ETCH: HF, HNO_3 SOLN. 14000X

Figure 35

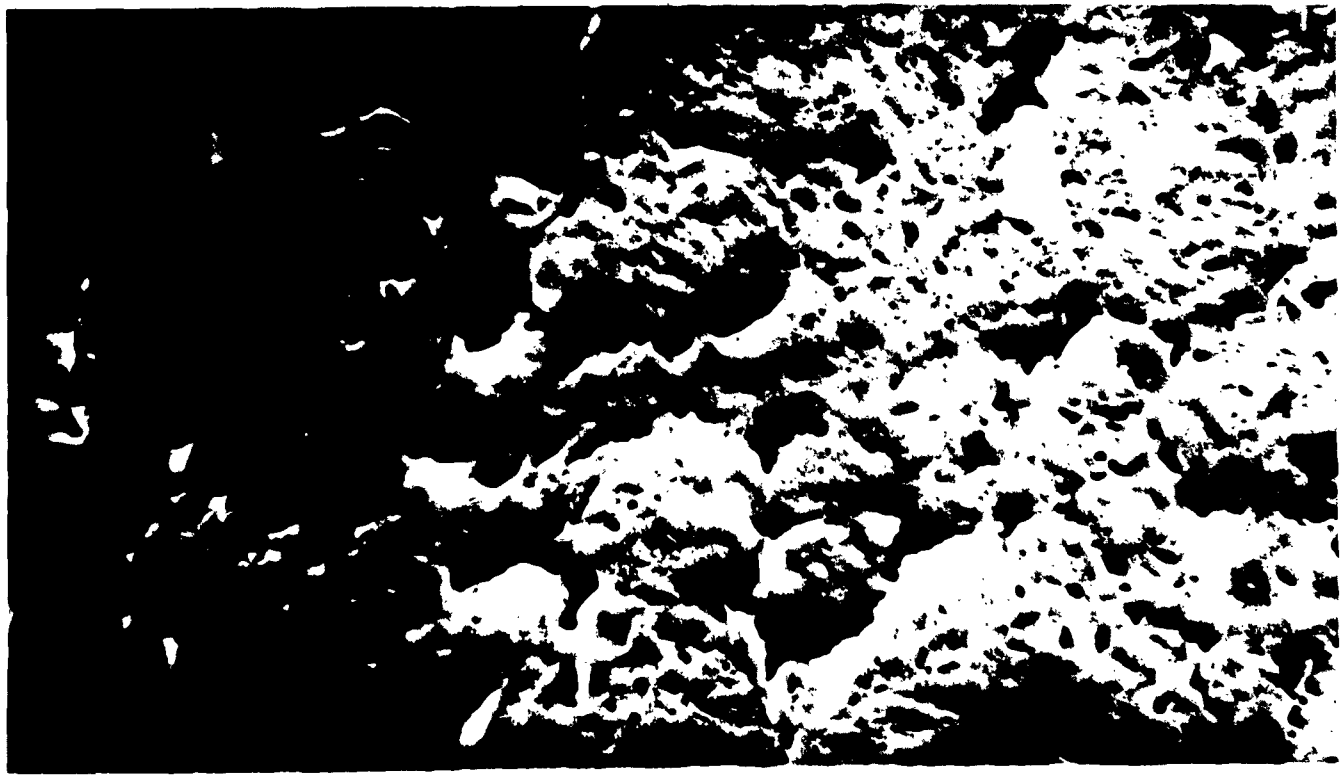

$Pb_{0.75}Ba_{0.25}ZrO_3$
DENSITY: 97% THEORETICAL
ETCH: H_2SiF_6 SOLN. 16000X

Figure 36

Hippel and Fröhlich. The theory of von Hippel[3] may be very briefly outlined as follows. Conducting electrons are provided from outside the insulator or by ionizing radiation. At voltages below the breakdown voltage acceleration of electrons sufficient to cause impact ionization and avalanche formation is prevented by excitation of vibrations or oscillations of the structure. When the voltage is sufficient to permit the electrons to traverse the vibration barrier (or in other words when the electrons gain more energy from the electric field than they lose in stimulating vibrations), the electrons are accelerated to cause impact ionization and avalanche formation, and dielectric breakdown occurs. Fröhlich's theory[4] differs from von Hippel's in that he does not consider that the electrons are always accelerated or that they always move in the direction of the electric field. He allows for scattering and assumes that breakdown occurs when some of the electrons have a net gain of energy, and there are sufficient electrons with a gain in energy to maintain breakdown.

The largely qualitative theories of dielectric breakdown discussed briefly above are difficult to formulate quantitatively, and there has not been the concentration of effort since World War II that there was in preceding years. Von Hippel states that "the disquieting outcome of all this effort is that every theoretical approach has claimed good agreement with the experimental facts, while the experimentalist knows that the theoretical models used are inadequate and that the experimental data do not yet represent the inherent strength of materials."[5]

---

[3] A. von Hippel, Z. Physik 75, 145 (1932); Z. Elecktrochem. 7b, 506 (1933).

[4] H. Fröhlich, Phys. Soc. Reports on Progress in Physics 6, 411 (1939).

[5] A. von Hippel, Tech. Rep. 136, Laboratory for Insulation Research, Massachusetts Institute of Technology (1959).

With ceramic materials the intrinsic dielectric strength of the material is never realized due to voids or inclusions and the additional complication of grain boundaries. Even with perfect single crystals one may not realize the intrinsic dielectric strength due to prebreakdown or ionization of the surrounding medium or on the surface of the test specimen. Furthermore with crystals or ceramics high field ionic conductivity may cause thermal breakdown, again limiting the actual dielectric strength to a value considerably lower than intrinsic. With piezoelectric (including ferroelectric) materials there is an additional complication of interrelated mechanical and electrical effects. These coupling effects are intrinsic for all piezoelectric materials, but it is clear that mechanical stress and strain related to an applied electric field can degrade dielectric strength. In such case the dielectric strength is not independent of the configuration of the test specimen, since relief of internal stress may play an important role. As mentioned previously, a transition from antiferroelectric or paraelectric to ferroelectric in perovskite materials involves a large lattice strain (volume increase by as much as 0.9%). Furthermore, strains associated with domain wall movement in ferroelectrics subjected to an electric field may cause linear strains as high as 0.5%.

It is furthermore important to note that insulators tend to have lower dielectric strength with increasing thickness. Von Hippel attributes this to predischarges and edge breakdown favored by higher total voltage.[5] He states that elimination of these causes with ionic crystals and plastics leads to independence of dielectric strength and thickness down to about 0.01 mm. It is nevertheless true that for practical purposes dielectric strength is not

independent of thickness, and this may be inherent in ceramic specimens, which lack the perfection of mylar or alkali halide crystals.

Relatively little effort has been directed to study of the extent to which imperfections in ceramic specimens influence dielectric strength. Gerson and Marshall,[6] however, used a statistical approach to determine the effects of porosity on dielectric strength. Their theory showed that the actual measured dielectric strength in porous materials is a function of porosity, void size, and specimen dimensions. Agreement between theory and experiment was good, but voids were artificially introduced and they were of uniform size and shape. It is clear that the problem is much more difficult with typical ceramics having widely varying void sizes and shapes.

Most materials prepared in this work were tested for dielectric strength. It is clear that these tests do not determine the inherent dielectric strength, but it is likely that the results provide an adequate basis for comparison. In these tests three to six discs of each composition were subjected to an electric field increasing from zero to the breakdown field in about ten to twenty seconds. The discs were 6 mm in diameter and about 0.28 mm thick. They were coated with air-drying silver paint allowing a margin of one mm at the edge. Unless breakdown occurred at the electrode edge, which is the region of highest electric stress, data were not considered valid. In all but one or two instances failure occurred at the electrode edge. Results are summarized in Table III. The breakdown experiments were made in silicone oil maintained at 110°C to eliminate moisture. The table also shows % theoretical density of the specimens used for dielectric strength measurements, the relative dielectric

[6] R. Gerson and T. C. Marshall, J. Appl. Phys. 30, 1650 (1959).

TABLE III. ELECTRICAL BREAKDOWN STR

Material	% Crystal Density of Specimens Tested	Average Breakdown Field at 110° C	Temperature of Peak Permittivity °C		$\varepsilon/\varepsilon_o$ at 110° C	Volun Resisti at 100 ohm c
$(Pb_{.05}Ba_{.80}Sr_{.15}TiO_3)$	97%	163 KV/cm		88	4,600	3×10^{1}
$Pb_{.05}Ba_{.50}Sr_{.45}TiO_3$	98	196	Below	20	850	3×10^{1}
$(Pb_{.05}Ba_{.80}Sr_{.15}TiO_3).99(PbNb_2O_6).01$	84	—		35	800	10^{11}
$(Pb_{.05}Ba_{.50}Sr_{.45}TiO_3).99(PbNb_2O_6).01$	89	—	Below	25	500	3×10^{1}
$(Pb_{.05}Ba_{.50}Sr_{.45}TiO_3).99(Pb_2Sc_2O_5).01$	91	—		-50	500	3×10^{1}
$(Pb_{.30}Sr_{.70}TiO_3)$	97	130		0	750	3×10^{1}
$(Pb_{.50}Sr_{.50}TiO_3)$	96	—		145	1,300	10^{10}
$(Pb_{.30}Sr_{.70}TiO_3).99(PbNb_2O_6).01$	99	—		-5	2,350	7×10^{1}
$(Pb_{.50}Sr_{.50}TiO_3).99(PbNb_2O_6).01$	98	113		120	4,500	2×10^{1}
$(Pb_{.30}Sr_{.70}TiO_3).99(Pb_2Sc_2O_5).01$	97	206		45	1,000	2×10^{1}
$(PbZrO_3).98(PbNb_2O_6).02$	97	121		200	950	10^{13} e
$(PbZrO_3)$	97	107		230	200	10^{13} e
$(PbZrO_3).98(Pb_2Sc_2O_5).02$	84	—		230	480	3×10^{1}
$(Pb_{.75}Sr_{.25}ZrO_3)$	99	162		200	250	10^{13} e
$(Pb_{.50}Sr_{.50}ZrO_3)$	98	126	Below	-200	145	2×10^{1}
$(Pb_{.50}Sr_{.50}ZrO_3).99(PbNb_2O_6).01$	97	242	Below	-200	137	10^{14} e
$(Pb_{.75}Ba_{.25}ZrO_3)$	97	86		110	13,000	10^{12}
$(Pb_{.60}Ba_{.40}ZrO_3)$	96	96		25	3,000	2×10^{1}
$(Pb_{.60}Ba_{.40}ZrO_3).99(PbNb_2O_6).01$	97	131		-25	2,300	2×10^{1}
$Ba_{.85}Sr_{.15}TiO_3$	90	—		25	1,100	3×10^{8}
$(Ba_{.85}Sr_{.15}TiO_3).99(BaNb_2O_6).01$	95	—	Below	25	400	3×10^{1}
$(Ba_{.55}Sr_{.45}TiO_3)$	96	34.5		-37	600	4×10^{1}
$(Ba_{.55}Sr_{.45}TiO_3).99(BaNb_2O_6).01$	98	26		-55	600	3×10^{8}
$(Ba_{.55}Sr_{.45}TiO_3).99(Ba_2Sc_2O_5).01$	92	—		-50	600	3×10^{1}
$Pb_{.15}Ba_{.70}Sr_{.15}TiO_3$	93	—		120	3,000	10^{10}
$(Pb_{.15}Ba_{.70}Sr_{.15}TiO_3).99(PbNb_2O_6).01$	98	—		65	2,600	3×10^{1}
$(PbTiO_3).57(BaZrO_3).43$	89	—	Below	25	450	2×10^{1}
$\left[(PbTiO_3).57(BaZrO_3).43\right] 0.99(PbNb_2O_6).01$	89	—	Below	25	750	3×10^{1}

AL BREAKDOWN STRENGTH OF SOME PEROVSKITE CERAMICS

e /	$\varepsilon/\varepsilon_o$ at 110° C	Volume Resistivity at 100° C ohm cm	Time Const. ($\rho\epsilon$) seconds at 100°C	Structures Detected by x-ray Diffraction	Perovskite Unit Cell $\sqrt[3]{\text{Vol.}}$, Å	c/a	State at 25° C
8	4,600	3×10^{11}	125	Tetr.	3.98_6	1.006_3	Ferroelectric
0	850	3×10^{11}	23	Cubic	3.95_5		Paraelectric
5	800	10^{11}	7	Pseudocubic?	3.99_4		Very weak ferroelectric probably
5	500	3×10^{11}	21	Cubic?	3.95_7		Paraelectric
0	500	3×10^{11}	13	Cubic	3.96_1		Paraelectric
0	750	3×10^{11}	19	Cubic	3.92_2		Paraelectric
5	1,300	10^{10}	1.2	Tetr.	3.92_9	1.008_9	Ferroelectric
5	2,350	7×10^{11}	150	Cubic	3.92_2		Paraelectric
0	4,500	2×10^{13} est.	8000	Tetr.		1.008_6	Ferroelectric
5	1,000	2×10^{12}	180	2 Perov. Phases	3.96 and 3.93		Very weak ferroelectric probably
0	950	10^{13} est.	900	RH + Minor O.	RH = 4.14_9		Antiferroelectric, with mostly ferroelectric mixed
0	200	10^{13} est.	180	Ortho.	4.14_1	.9888	Antiferroelectric
0	480	3×10^{12} est.	130				Probably antiferroelectric
0	250	10^{13} est.	230	Tetr. (+Ortho?)	4.12_9	.9923	Antiferroelectric
0	145	2×10^{13} est.	260	Cubic	-----		Paraelectric
0	137	10^{14} est.	1200	Cubic	-----		Paraelectric
0	13,000	10^{12}	1200	Rhomb.	4.16_9	Rhomb. angle	Ferroelectric
5	3,000	2×10^{12}	540	Cubic	-----	89° 52'	Paraelectric
5	2,300	2×10^{13} est.	4200	Cubic	-----		Paraelectric
5	1,100	3×10^{8}	0.03	Reacted	-----		Paraelectric
5	400	3×10^{10}	1	2 Similar Perov. Phases. one weak	-----		Paraelectric
7	600	4×10^{10}	2	Reacted powder	-----		Paraelectric
5	600	3×10^{9}	0.16	2 Simil. Perov. Phases, Disim.	-----		Paraelectric
0	600	3×10^{11}	16	Latt. Con. Multiple Perovs.	-----		Paraelectric
0	3,000	10^{10}	3	Phases. +1 wk line -------	-----		Ferroelectric
5	2,600	3×10^{13} est.	7000	-------	-----		Ferroelectric
5	450	2×10^{11}	8	Cubic Perov.			Paraelectric
5	750	3×10^{12}	200	Cubic + wk pyro Perovskite			Paraelectric

2

constant (110°C), and the volume resistivity (low field) at 100°C. The Curie points are also listed, and the states (ferroelectric, paraelectric, or antiferroelectric) at 110°C and with no applied electric field are also noted. The c/a ratios of tetragonal materials and rhombohedral angles of rhombohedral materials are also listed in the table. Where determined, the cube root of the unit cell volume is given. The crystal densities of materials for which the unit cell volume was not measured were determined by interpolation (for instance between those for $BaTiO_3$ and $SrTiO_3$).

VI. DEPENDENCE OF VOLUME RESISTIVITY ON ELECTRIC FIELD STRENGTH

Volume resistivity for a given material is dependent not only on temperature, but also upon the electric field strength and the period of exposure to electric field. Work described in this section is concerned with dependence of volume resistivity on electric field strength, where the total exposure period is relatively short.

Figure 37 shows volume resistivity as function of electric field for $(Pb_{.6}Ba_{.4}ZrO_3)_{.99}(PbNb_2O_5)_{.01}$ at 300°C. Each point on the curve represents the average of two virgin specimens (never before subjected to an electric field). The total fluctuation in volume resistivity was by a factor of only about two, and the volume resistivity, about $10^{10.5}$ at 10 kv/cm, 300°C is remarkably high.

Figure 38 shows volume resistivity as function of electric field at 230°C for $Pb_{.6}Ba_{.4}ZrO_3$. Here also the total variation in resistivity was less than a factor of two in the range to 10 kv/cm. It is interesting to note that with Nb^{5+} addition (Fig. 37) the volume resistivity at 10 kv/cm is two orders of magnitude higher at 300°C than that for plain $Pb_{.6}Ba_{.4}ZrO_3$ at 230°C.

FIGURE 37.

VOLUME RESISTIVITY VS. FIELD

$(Pb_{.6}\ Ba_{.4}\ Zr\ O_3)_{0.99}\ (PbNb_2\ O_6)_{0.01}$

VIRGIN SPECIMENS (AVG. OF TWO)
300 °C

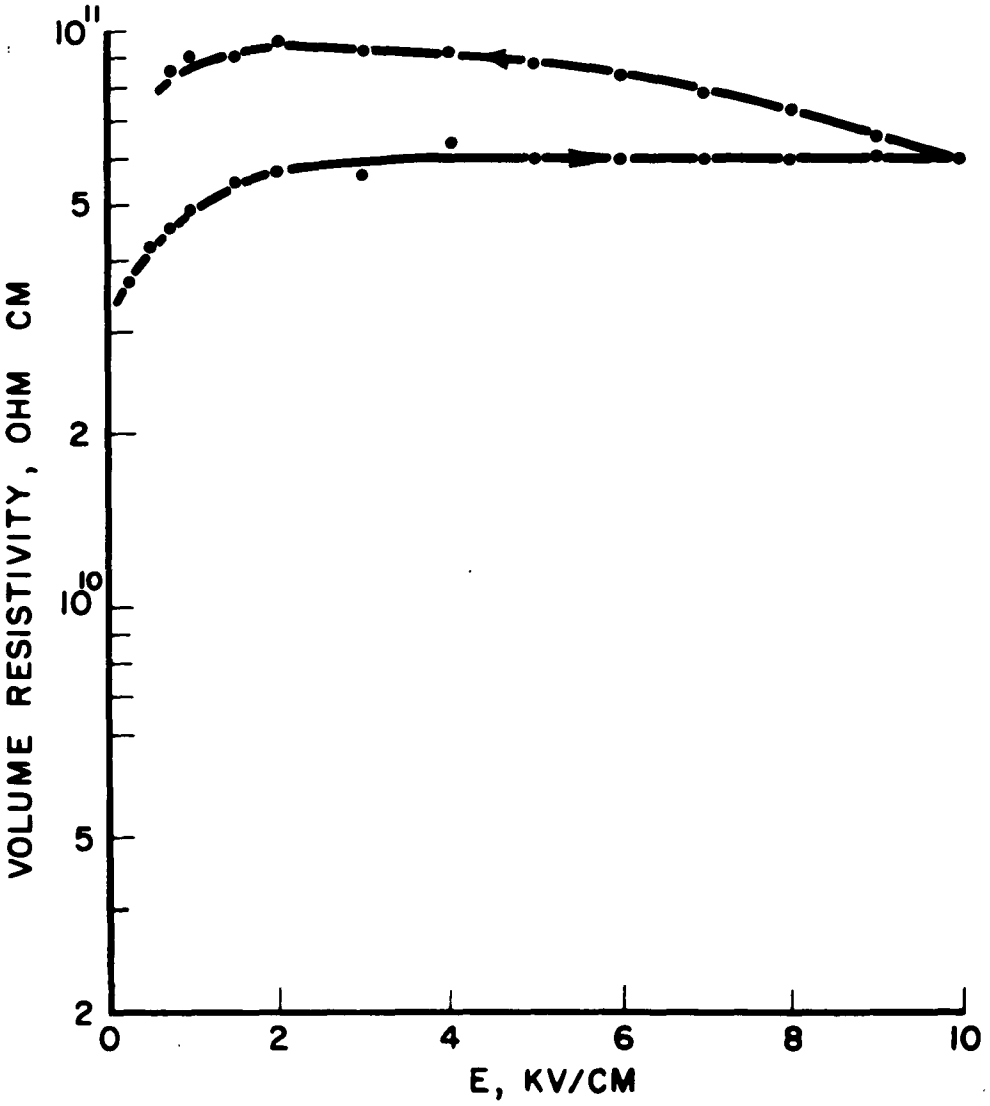

ERD 5713

FIGURE 38.

VOLUME RESISTIVITY VS FIELD

$Pb_{.6}\ Ba_{.4}\ ZrO_3$

VIRGIN SPECIMENS (AVE. OF TWO)

230°C

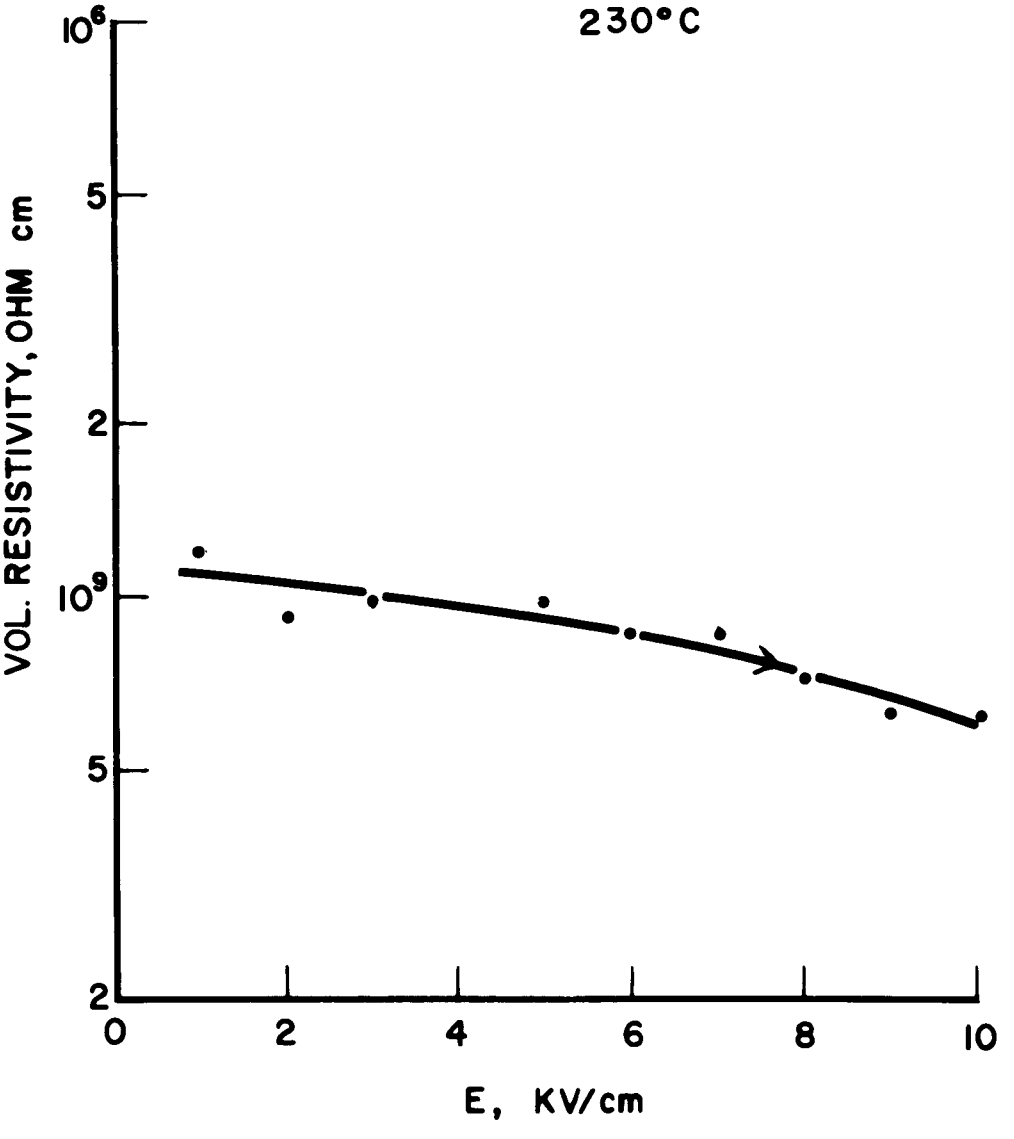

ERD 5714

Figure 39 shows volume resistivity as function of electric field at 230°C for $(Pb_{.5}Sr_{.5}TiO_3)_{.99}(PbNb_2O_6)_{.01}$. The upper curve is for virgin material, the lower for the same material after a 265-hour life test at 230°C with a maintained electric field of 10 kv/cm. The results of the dielectric degradation study for this material are summarized in Figure 48. The life test caused a decrease of one order of magnitude in the 10 kv/cm volume resistivity at 230°C (shown in Figs. 39 and 48), but the decrease in low signal resistivity was nearly two orders of magnitude. It is interesting to note that the volume resistivity is about three times higher at 10 kv/cm than at 2 kv/cm after the life test (polarity of applied voltage never changed).

Figure 40 shows volume resistivity at 230°C as function of electric field for $PbZrO_3$ for a virgin specimen and for another specimen previously subjected to an electric field of 10 kv/cm for 190 hours at 230°C. For both curves the resistivity was determined just three minutes after each change of electric field (noted by the points) in order that conditions be as nearly alike as possible. The chief difference between the two curves is the more pronounced hysteresis of the virgin specimen.

VII. RESULTS OF DIELECTRIC DEGRADATION TESTS

Dielectric degradation, the gradual decrease in volume resistivity during long exposure to dc fields substantially below the dielectric strength, was studied at 230 and 300°C. For reasons discussed in the introduction, the tests were made under conditions which were expected to bring about failure in a reasonable period of time. The failure expected under these conditions is a very large decrease in volume resistivity throughout the volume of the material.

FIGURE 39.

VOLUME RESISTIVITY VS. ELECTRIC FIELD

$(Pb_{.5}\ Sr_{.5}\ TiO_3)_{.99}\ (Pb\ Nb_2\ O_6)_{.01}$

230 °C

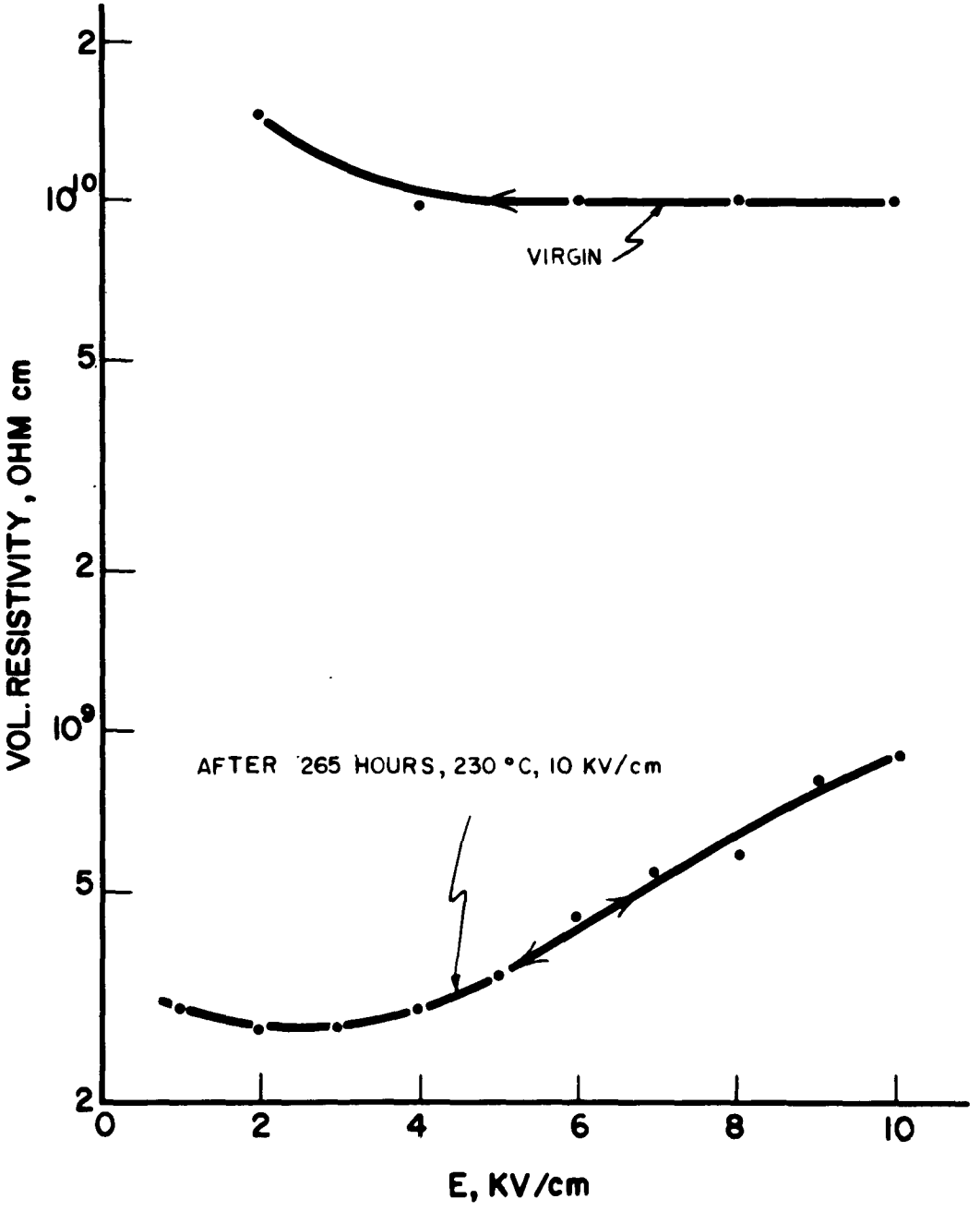

ERD 5715

FIGURE 40.

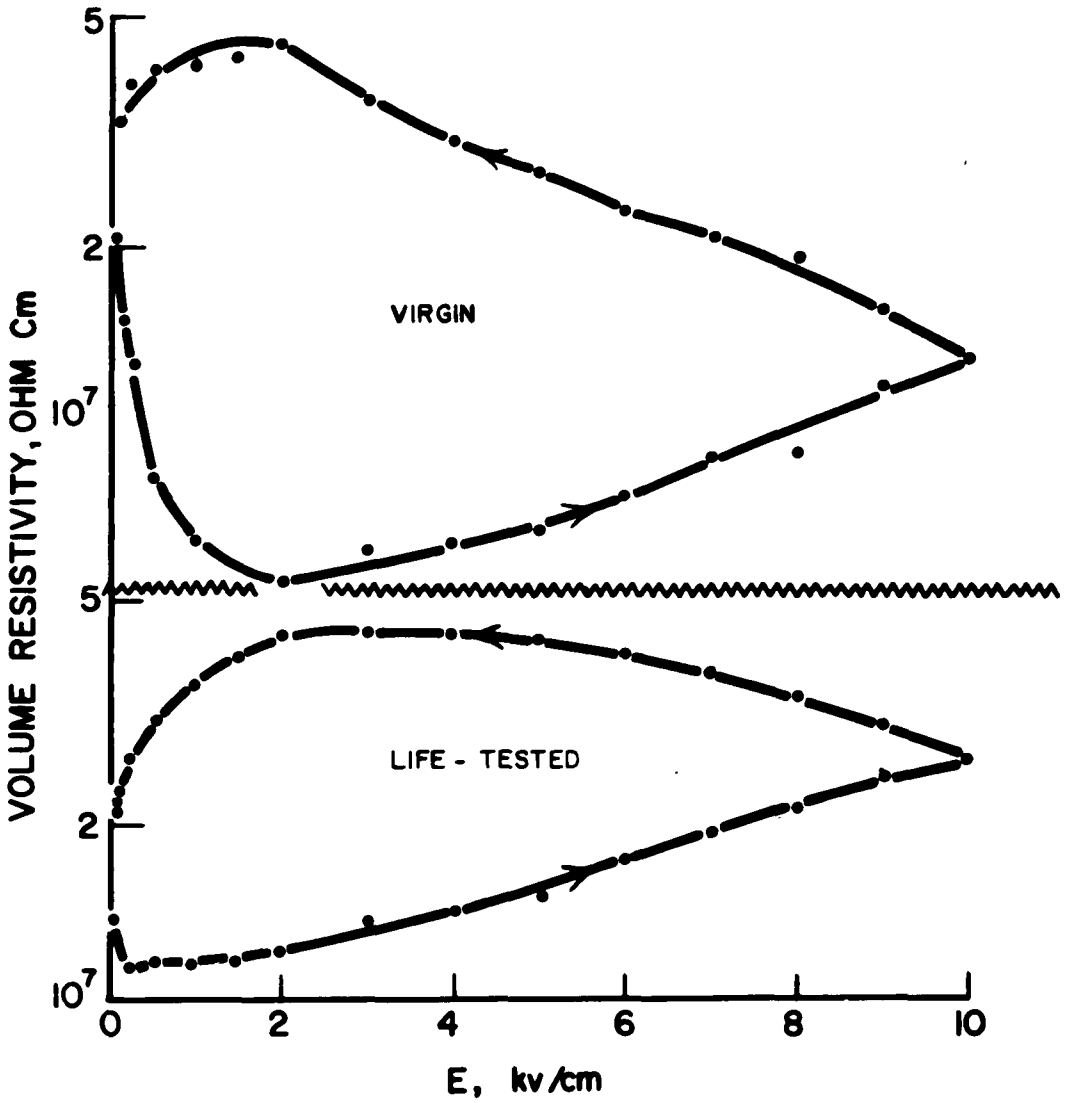

VOLUME RESISTIVITY VS ELECTRIC FEILD

$PbZrO_3$, 300 °C

UPPER CURVE - VIRGIN SPECIMEN

LOWER CURVE - AFTER EXPOSURE TO 10KV/cm AT 230 °C FOR 190 HOURS

As will be shown in section, most materials did not fail in this manner, but rather appeared to suffer dielectric breakdown in specific paths, usually at the electrode edge where the electric stress is maximum. The tests here desribed were made at 230 or 300°C with an electric field (dc) of 10 kv/cm.

Test specimens as fired are 3/4" in diameter by 0.040 to 0.060 inches thick. For the degradation tests the specimens were lapped to 0.010" thickness in two stages of lapping with silicon carbide grit. Then discs of 6 mm diameter were cut from the larger discs with an ultrasonic impact grinder. Gold electrodes about 4 mm in diameter were then applied using DuPont 3N Gold paste;* the electrodes were baked on at 600°C for one hour. Gold is thought to be superior in comparison, for instance, with silver, since electrochemical effects involving the electrode may be an important factor in these tests.

The circuit used in the degradation studies is shown in Figure 41. The power supply is a Lambda Model 71 regulated power supply. R_2 is a two-watt potentiometer whose resistance is about 0.5 megohm. The power dissipated in R_2 is therefore less than 0.5 watts with 500 volts input. R_2 was set so that the tapped output was 250 volts, thus providing an electric field of 10 kv/cm across the test specimens. R_1 is a current-metering resistance for determination of the current through the test specimen. Its value was chosen such that the voltage drop across it was less than 2.5 volts. With this arrangement the power supply could not be overloaded in case the test specimen should suffer dielectric failure, and in such case the power dissipation in the upper half of R_2 would reach only one watt. The voltages V_1 and V_2 are measured

* E. I. DuPont de Nemours Co., Wilmington 98, Delaware

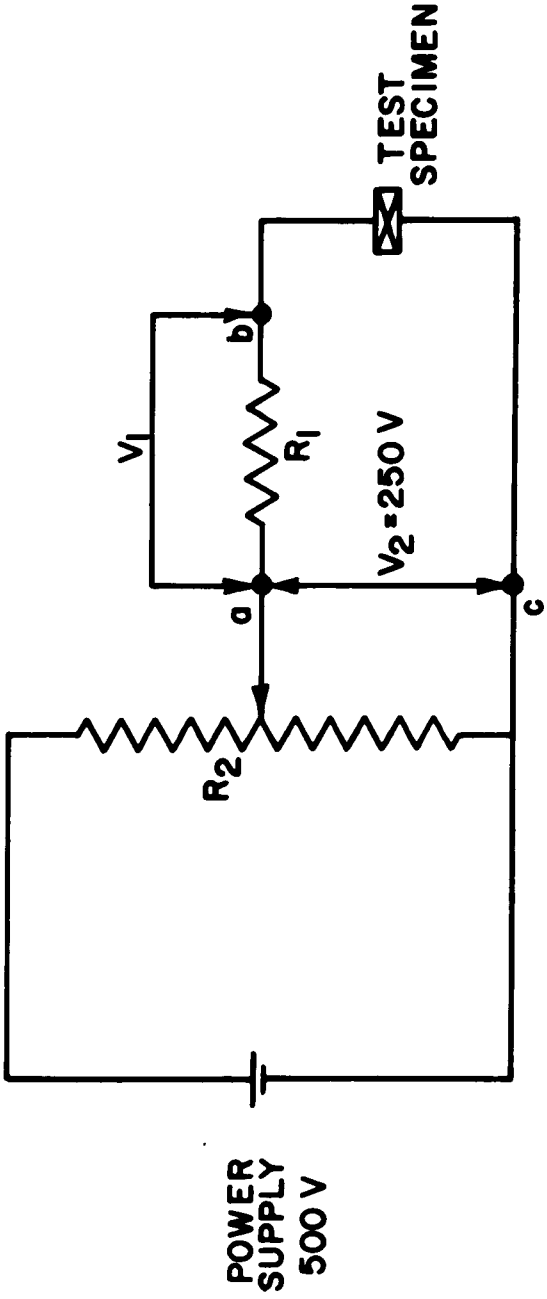

FIGURE 41.
LIFE TEST CIRCUIT

with electronic electrometers (Keithley Models 610 and 210 respectively) with point a grounded. This circuit is not satisfactory for measurements of volume resistivity greater than about 10^{12} ohm cm, since the electrometer and power supply cannot both be grounded. In such case R_2 is eliminated. This offers less protection to the power supply, but eliminates the difficulty in measurements of volume resistivity to about 10^{13} ohm cm.

For the circuit of Fig. 41 the resistance of the test specimen R_{TS} is given by:

$$R_{TS} = R_1 \frac{V_2 - V_1}{V_1} \sim R_1 \frac{V_2}{V_1} .$$

Potentiometer R_2 (when used) and metering resistance R_1 are mounted on an insulated panel (lucite). The test specimen is placed in a furnace, Hevi-Duty type 051. Points a and b are accessible on the lucite panel.

A diagram of the experimental arrangement for holding the test specimens in the furnace is shown in Fig. 42. Electrical connection to the test specimens is made via the silver rods A. The lower ends of these rods are coated with DuPont 3N gold paste to prevent formation of oxide layers. This is probably not necessary, since silver oxide is a relatively good conductor, but it was felt that this might help prevent electrochemical effects not directly the fault of the test specimen. The upper ends of the rods A are connected to the respective resistances R_1 by alligator clipped fine wire (phonograph pickup arm cable). The plates B_1 and B_2 were fabricated from boron nitride in order to prevent leakage currents between the silver rods A. The thermal insulation inside the furnace door was removed around the alumina tubes F, also to

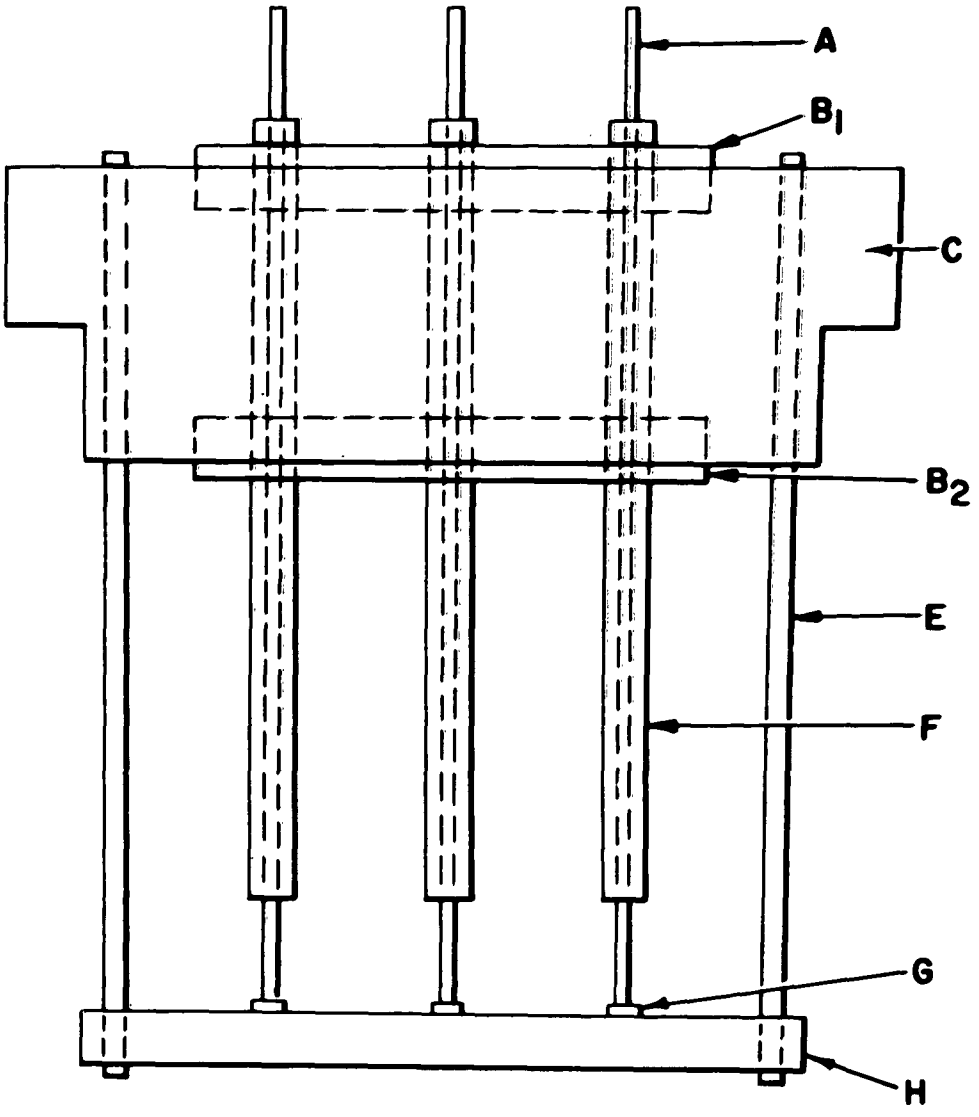

FIGURE 42.
LIFE TEST JIG

prevent leakage currents. The sole function of the alumina connecting rods E is to support plate H, which holds the test specimens. In one experimental set-up plate H is silver coated with DuPont 3N gold paste. In the other plate H is gold with a stainless steel plate underneath for support.

The results of the first degradation tests at 230°C are summarized in Figs. 43 through 49. Volume resistivity increased with time (up to 200 hours) for some compositions, specifically the zirconates, and decreased for others, the titanates. It is especially interesting to note the differences in the results obtained with the titanates and zirconates. There were no cases of dielectric breakdown in these tests of 100 to 200 hours duration. A word should perhaps be written about the manner in which these curves are plotted. Volume resistivity is plotted on a logarithmic scale in order to show properly the total range, about two orders of magnitude in Figs. 43 to 49. A logarithmic scale was also used for time in view of the relatively linear (log resistivity vs log time) plots resulting. This tends to put undue emphasis on the early periods of exposure. Results of longer tests are plotted to linear as well as logarithmic time scales (Fig. 53).

Dielectric degradation actually involves more than simply a decrease in volume resistivity. The dielectric properties are also altered by a period of exposure to a relatively high dc electric field. This is shown in Table IV, where the results of the degradation studies of Figs. 43 through 49 are summarized. The first column of this table shows the ratio of volume resistivity at the beginning to that at the end of the degradation tests. Here the behavior of zirconates as a class is quite different from that of the titanates, as mentioned previously in connection with Figs. 43 through 49. The next two columns

FIGURE 43.

RESISTIVITY VS. ELAPSED TIME

10 KV/CM 230°C

$(Pb_{0.50}Sr_{0.50}ZrO_3)_{0.99} + (PbNb_2O_6)_{0.01}$

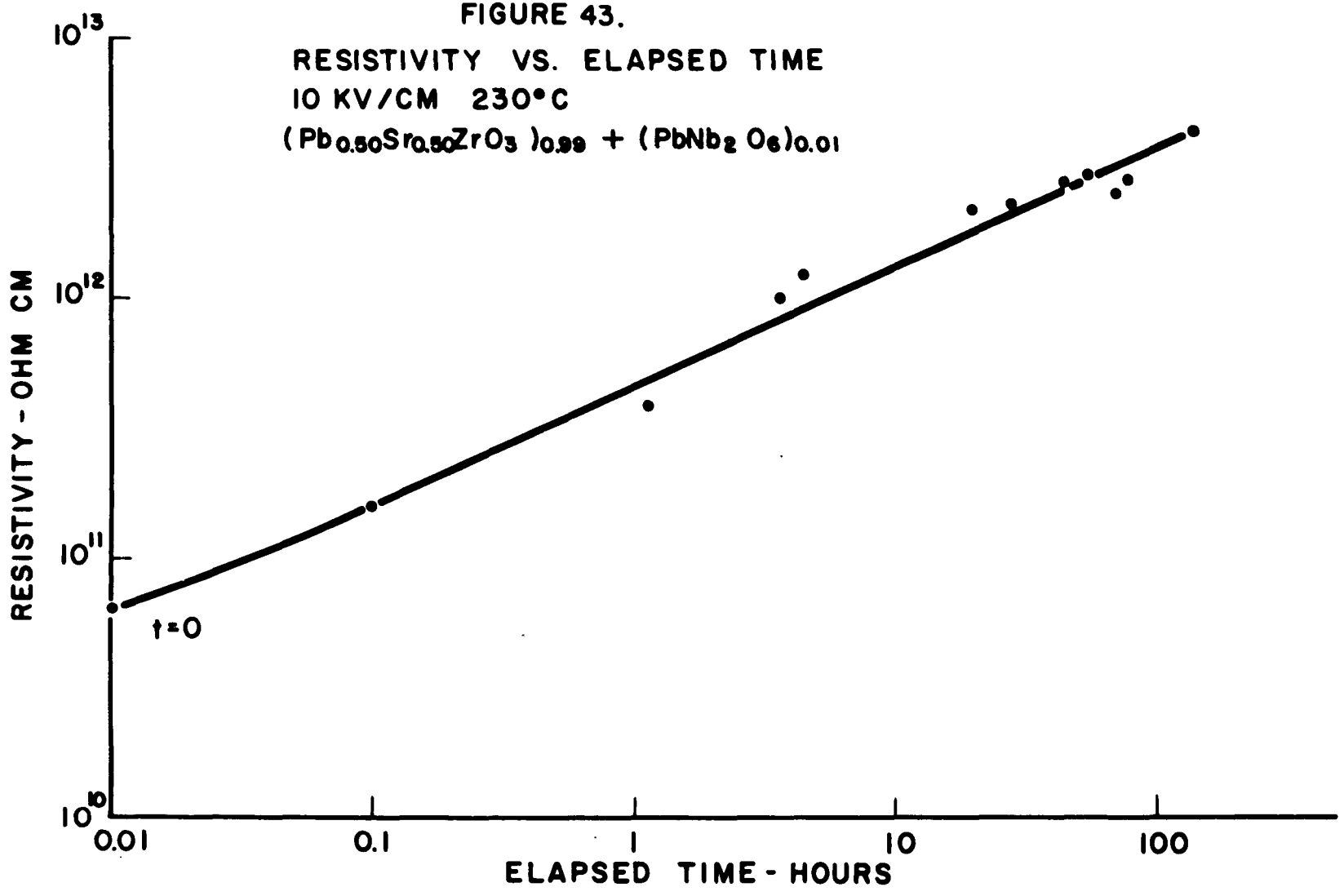

FIGURE 44.
RESISTIVITY VS. ELAPSED TIME

AVERAGE CURVE FOR 2 SAMPLES
10 KV/CM 230°C
$(PbZrO_3)_{0.98} + (PbNb_2O_6)_{0.02}$

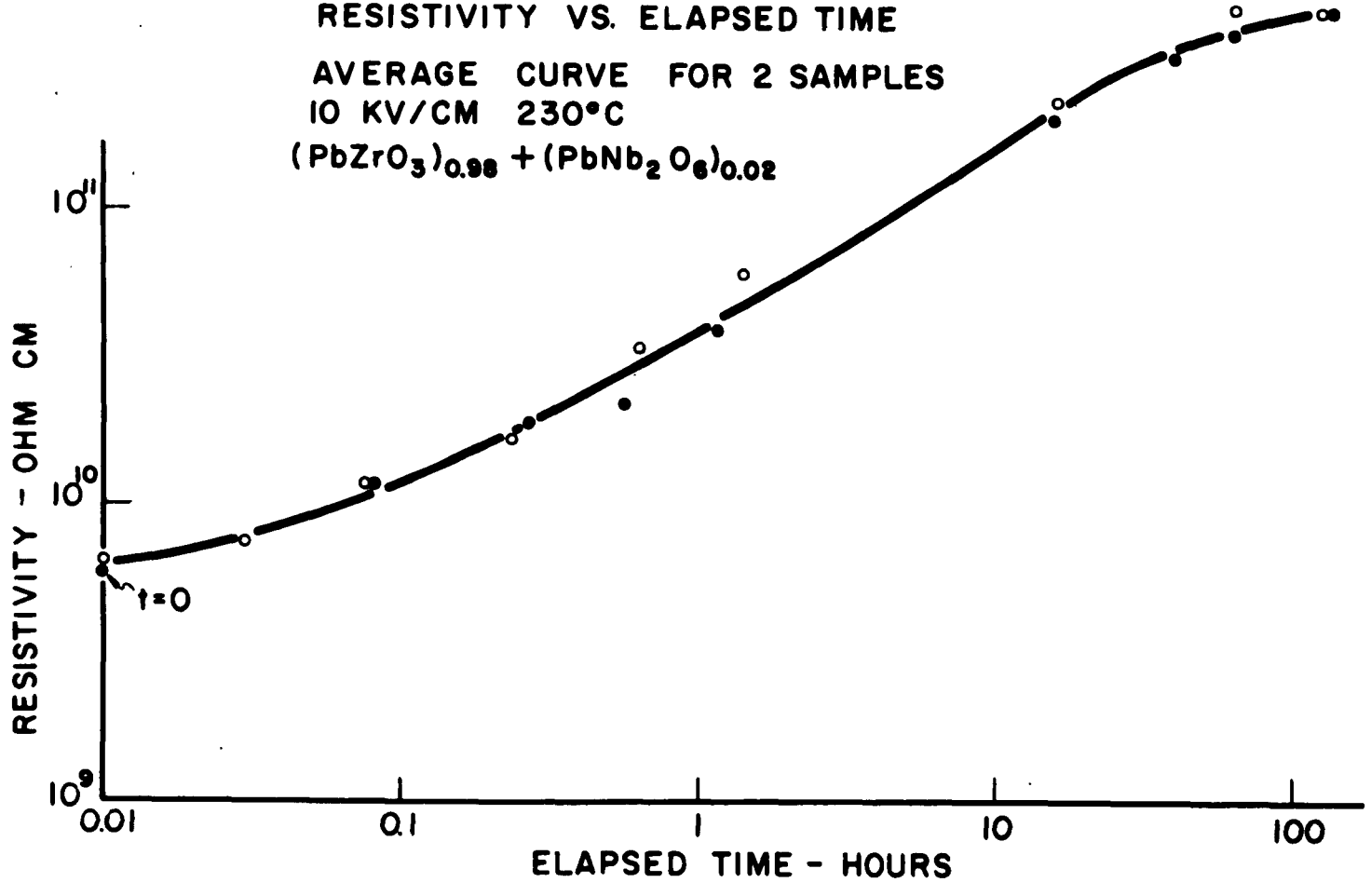

FIGURE 45.
RESISTIVITY VS. ELAPSED TIME
AVERAGE CURVE FOR 3 SAMPLES
10 KV/CM 230°C
$PbZrO_3$

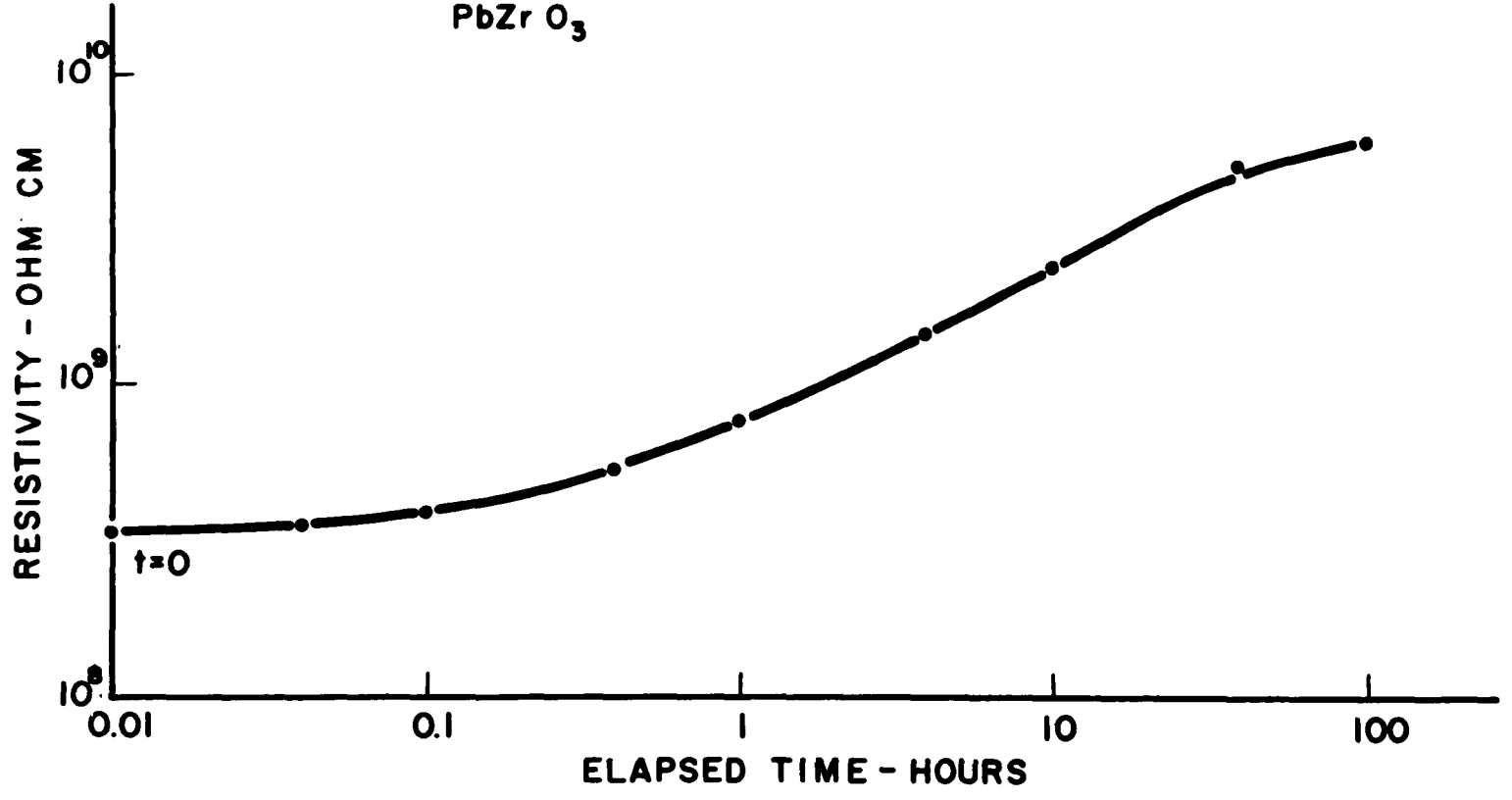

FIGURE 46.

RESISTIVITY VS. ELAPSED TIME

10 KV/CM 230°C

$(Pb_{0.60}Ba_{0.40}ZrO_3)_{0.99} + (PbNb_2O_6)_{0.01}$

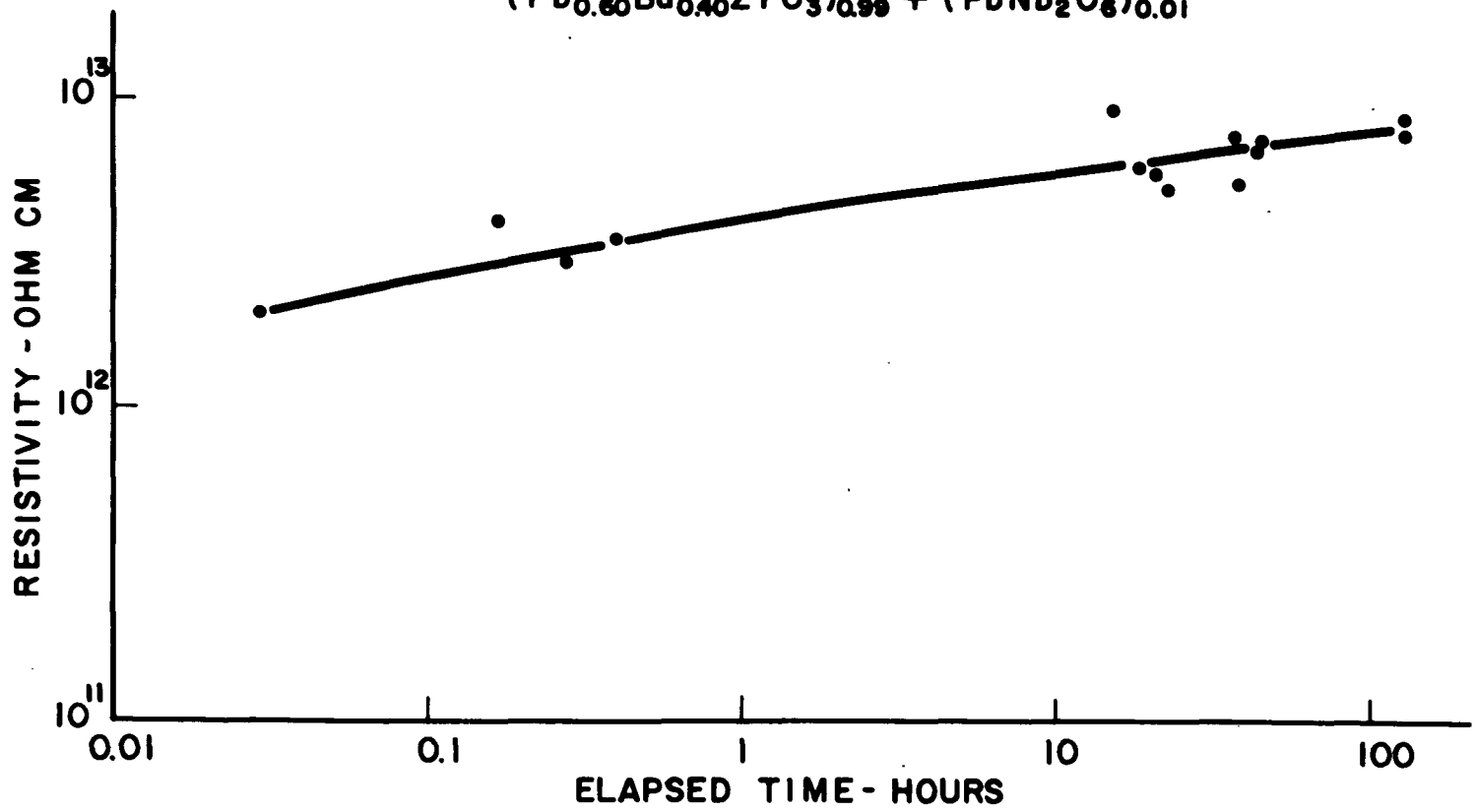

FIGURE 47.

RESISTIVITY VS. ELAPSED TIME
AVERAGE CURVE FOR 3 SAMPLES
10 KV/CM 230°C
$Pb_{0.30}\ Sr_{0.70}\ TiO_3$

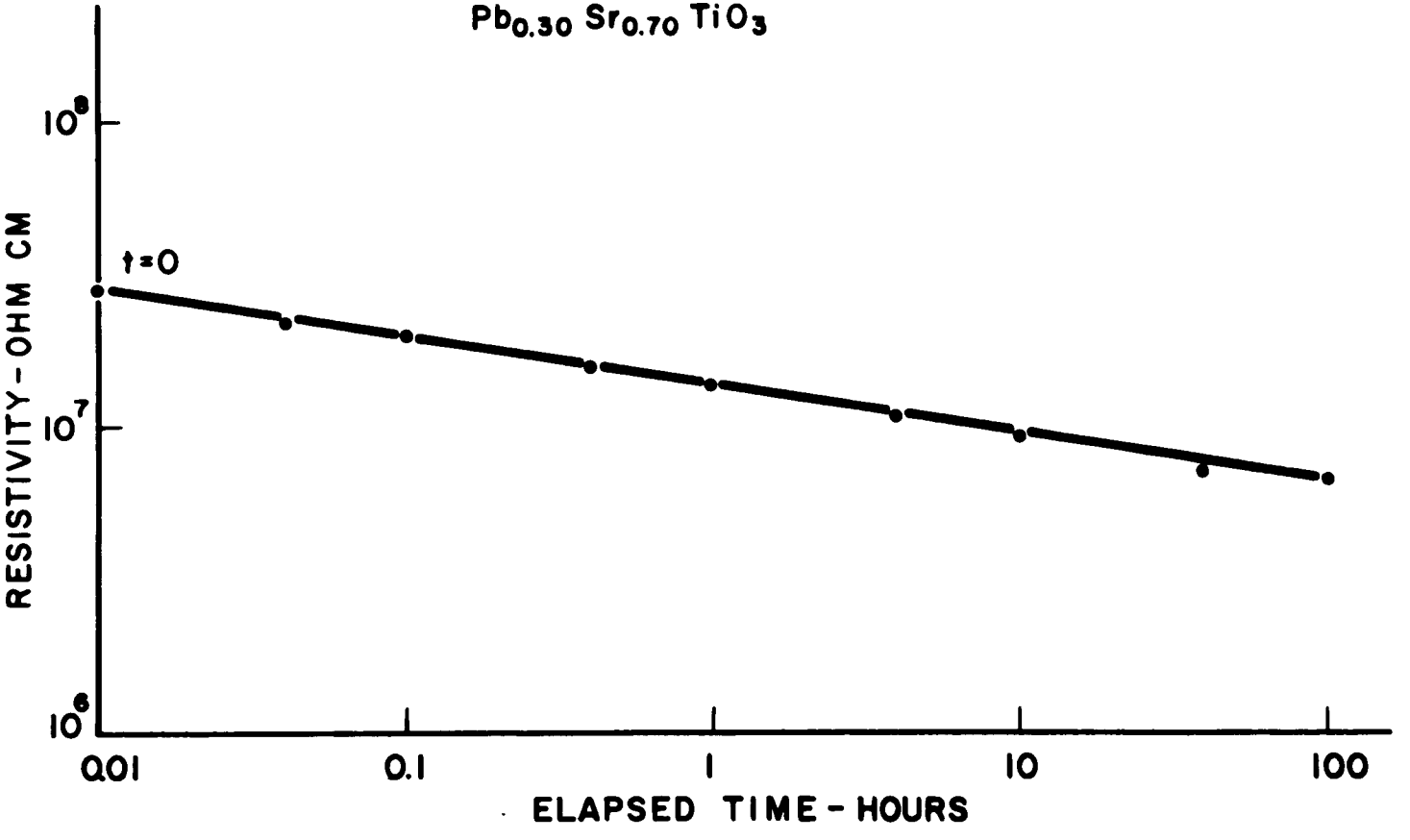

FIGURE 48.
RESISTIVITY VS. ELAPSED TIME.
AVERAGE CURVE FOR 3 SAMPLES
10 KV/CM 230°C
$(Pb_{0.50}Sr_{0.50}TiO_3)_{0.99} + (PbNb_2O_6)_{0.01}$

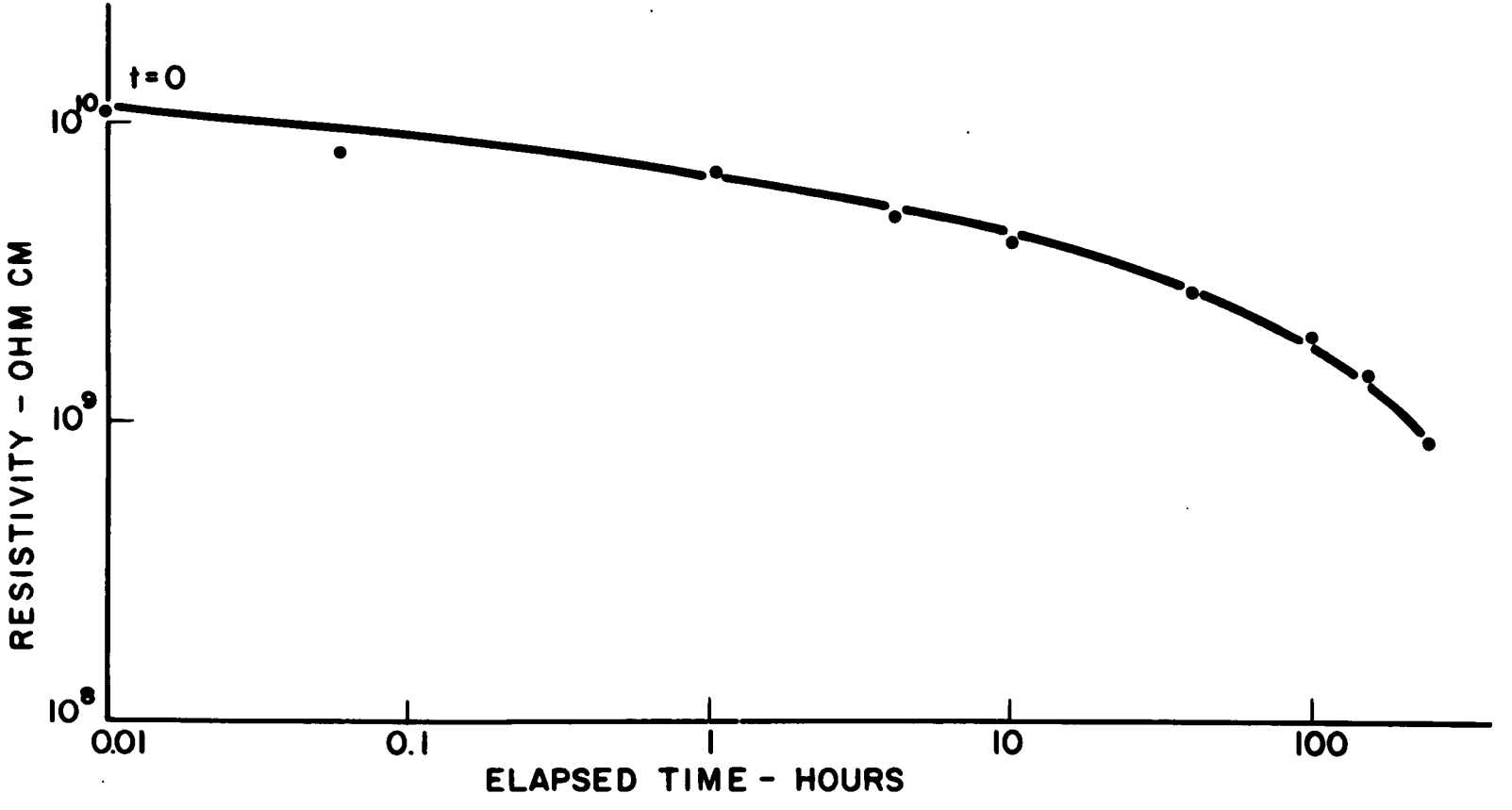

FIGURE 49.
RESISTIVITY VS. ELAPSED TIME
10 KV/CM 230°C
$(Pb_{0.30}Sr_{0.70}TiO_3)_{0.99} + (Pb_2Sc_2O_5)_{0.01}$

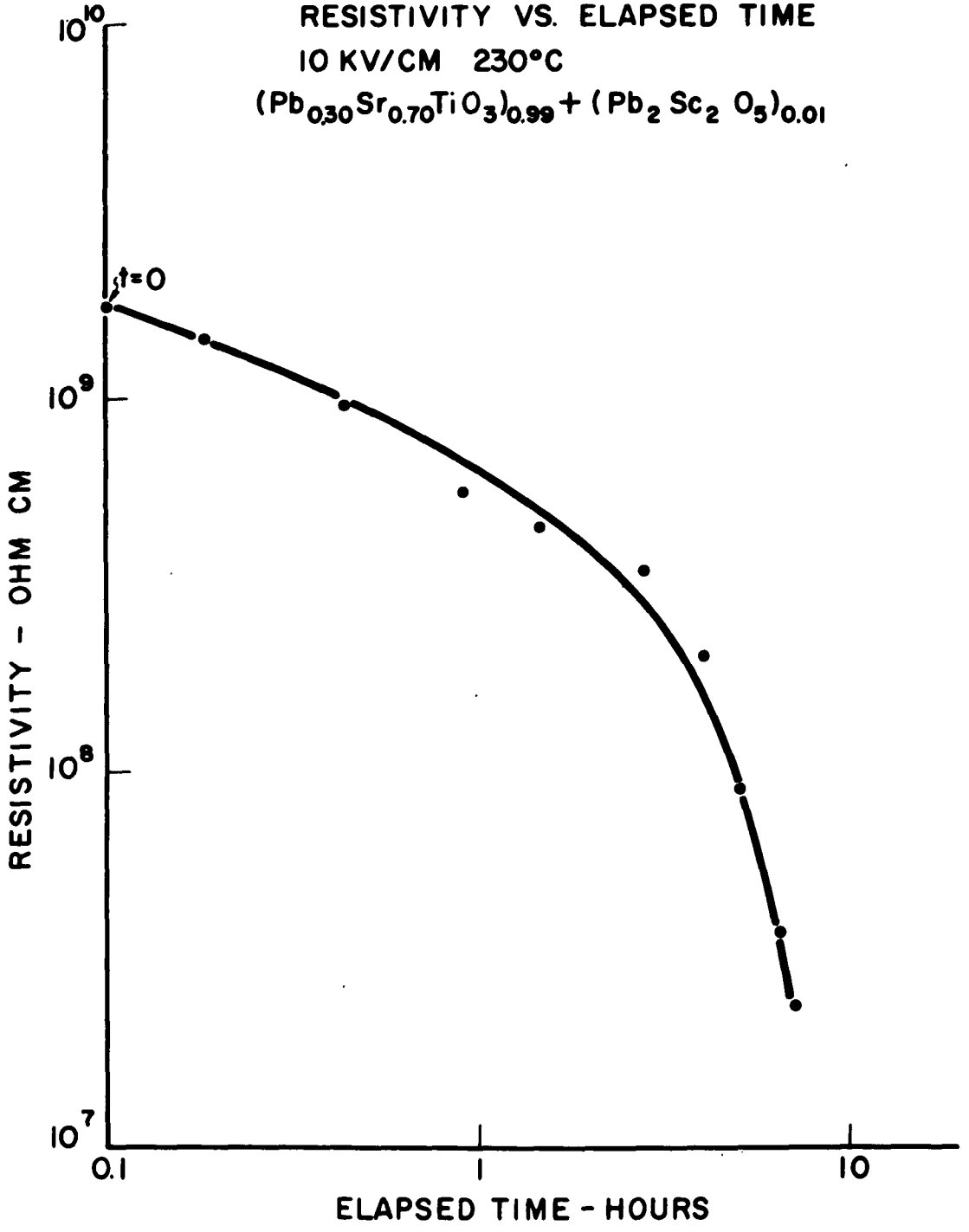

Table IV. Classification of Compositions with Respect to Their Behavior During Degradation Tests for 100 to 200 hours at 230°C with an Electric Field of 10 kv/cm

Composition	ρ after /ρ before 10 kV/cm, 230°C	ϵ/ϵ_o at 1 mc, 25°C Before	ϵ/ϵ_o at 1 mc, 25°C After	tan δ at 1 mc, 25°C Before	tan δ at 1 mc, 25°C After	ϵ/ϵ_o at 230°C 1 mc Before	ρ (230°C, 10Kv/cm) Before life test
$(PbZrO_3)_{0.98}$ + $(PbNb_2O_6)_{0.02}$	78	590 (1kc)	510	0.032 (1kc)	0.030	3375 (1kc)	6×10^9
$(Pb_{0.50}Sr_{0.50}ZrO_3)_{0.99}$ + $(PbNb_2O_6)_{0.01}$	69	166 (1kc)	166	---	---	121	6.2×10^{10}
$PbZrO_3$	18	169 (1kc)	134	0.0031 (1kc)	0.0056	4800 (1kc)	3.4×10^8
$(Pb_{0.60}Ba_{0.40}ZrO_3)_{0.99}$ + $(PbNb_2O_6)_{0.01}$	3.8	3712	3425	0.02	0.0038	700	2.0×10^{12}
$(Pb_{0.30}Sr_{0.70}TiO_3)_{0.99}$ + $(PbNb_2O_6)_{0.01}$	1.2	4950	5840	0.062	0.017	1500	9.8×10^6
$Pb_{0.30}Sr_{0.70}TiO_3$	0.23	2880 (1kc)	2650	0.012 (1kc)	0.024	400	2.9×10^7
$(Pb_{0.30}Sr_{0.70}TiO_3)_{0.99}$ + $(Pb_2Sc_2O_5)_{0.01}$	0.016	1100	---	0.014	---	500	1.7×10^9

of Table IV list the permittivities at 25°C before and after the degradation test. With one exception, which may be anomalous, the permittivities were less after the degradation test. The fourth and fifth columns list values of tan δ at 25°C before and after the degradation test. In most instances values of tan δ were higher after the degradation tests. With the titanates values of tan δ at frequencies below about 100 cps are substantially increased by the degradation of resistivity. Direct effects of decreased volume resistivity are not detected in values of tan δ measured at 1 mcps.

Since the volume resistivities of all zirconates increased throughout the period of the degradation studies of Figs. 43 through 46, further degradation studies under the same conditions were extended to 1000 hours on $PbZrO_3$, $(PbZrO_3)_{.98}(PbNb_2O_6)_{.02}$, and $Pb_{.6}Ba_{.4}ZrO_3$. Results of these tests are summarized in Figs. 50 through 52. In these tests there was unfortunately considerable scatter during the period 100 to 1,000 hours, and anomalous points were eliminated from the plots. Anomalous points were identified as points where there were wide differences in volume resistivities of specimens of the same composition. The reason for these anomalous points is formation of distinct breakdown paths, which were often healed by the simple process of destruction of the electrode in close proximity to the breakdown path by excessive current flow. Comparison of Figs. 52 and 45 and Figs. 53 and 46 indicates that behavior during the first 100 hours of the 1000-hour tests was somewhat different than that during the 100-hour tests. The reason for this is not known, but the general features of the tests are the same.

Figure 53 shows the curves of Figs. 50 through 52 replotted with a linear time scale. Here the relatively rapid increase in volume resistivity

FIGURE 50.
VOLUME RESISTIVITY VS ELAPSED TIME AVERAGE CURVE FOR TWO SPECIMENS
$Pb_{.6}\ Ba_{.4}\ Zr\ O_3$
10KV/cm, 230°C

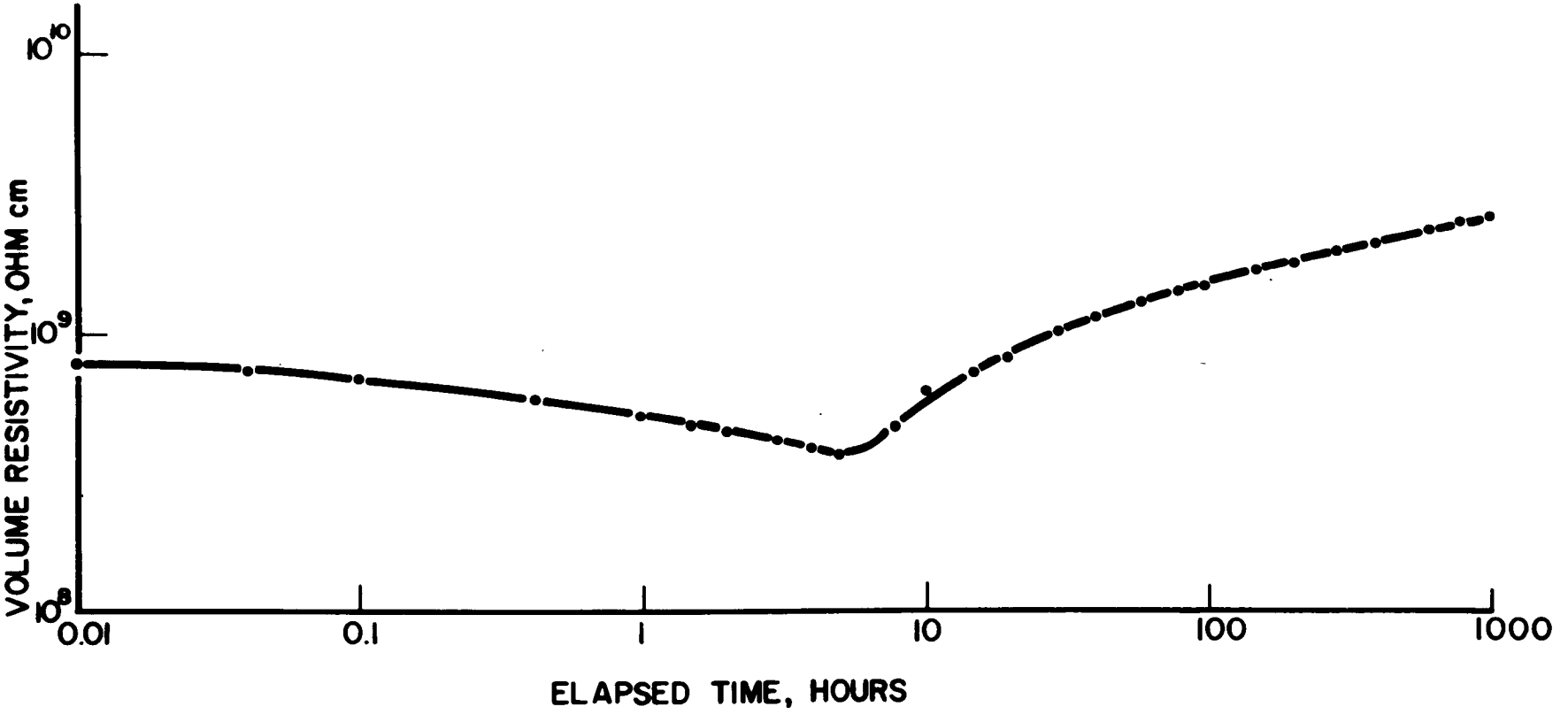

ERD 5717

FIGURE 51.

VOLUME RESISTIVITY VS ELAPSED TIME AVERAGE CURVE FOR THREE SPECIMENS.

$(Pb\ Zr\ O_3)_{.98}(PbNb_2O_6)_{.02}$

10KV/cm, 230 °C

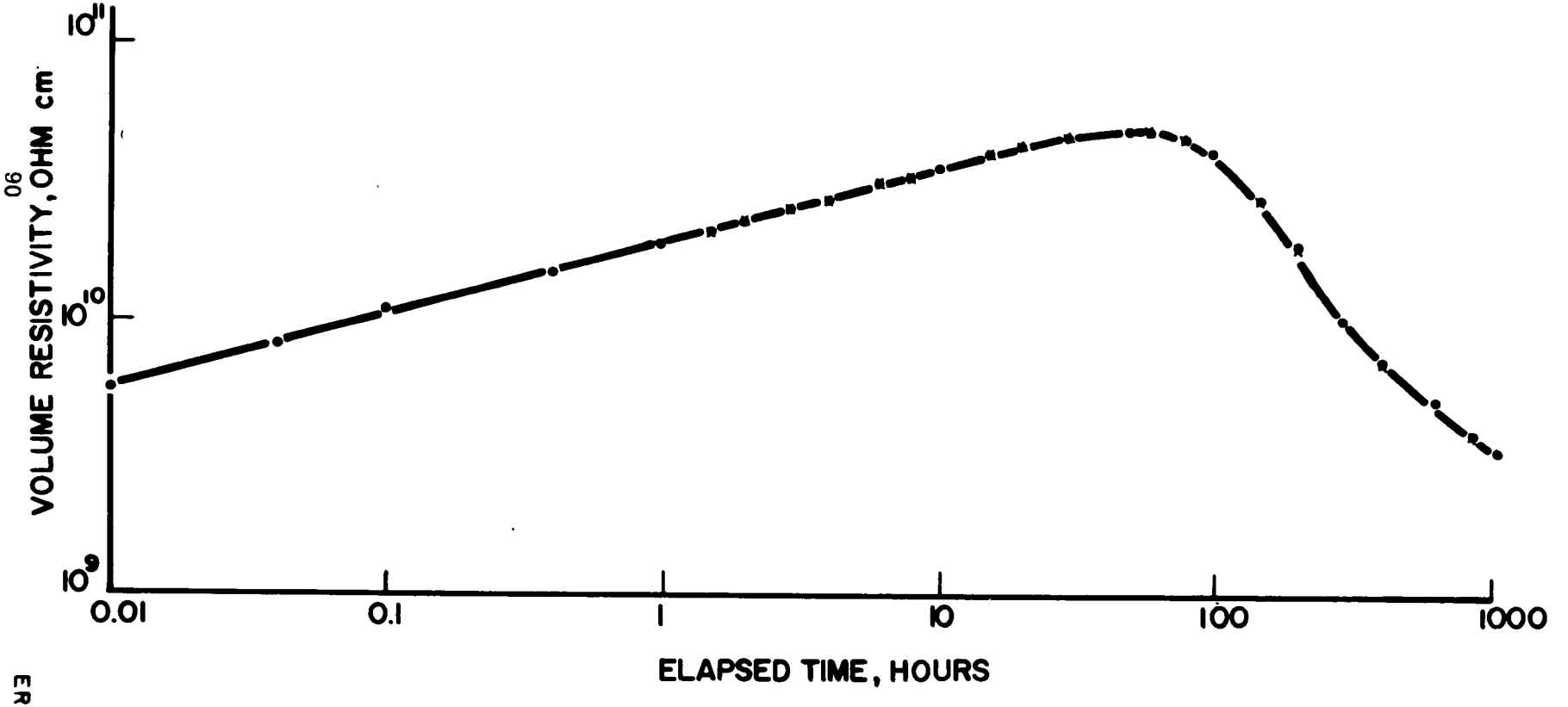

ERD 5718

FIGURE 52.

VOLUME RESISTIVITY VS ELAPSED TIME AVERAGE CURVE FOR THREE SPECIMENS.

$PbZrO_3$

10 KV/cm, 230 °C

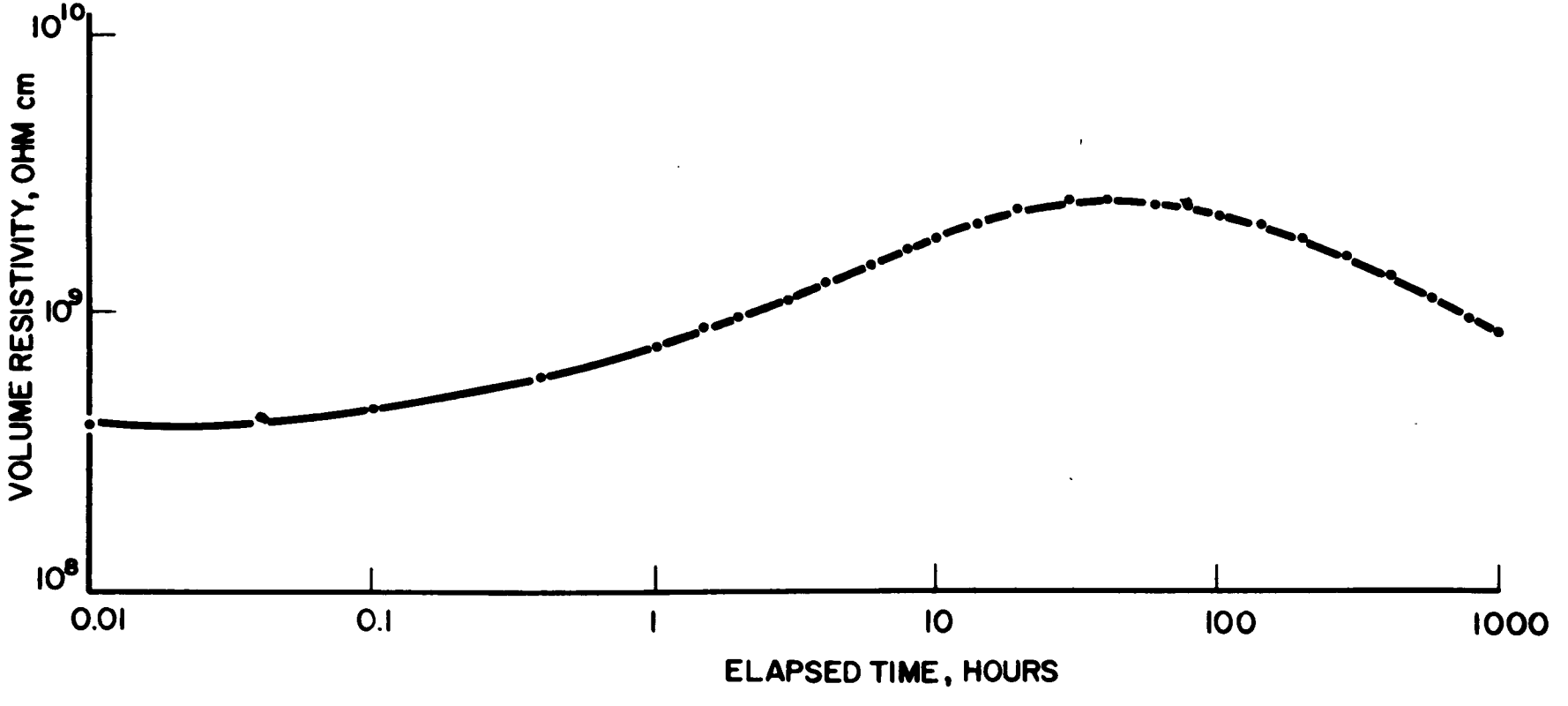

FIGURE 53.

VOLUME RESISTIVITY VS. ELAPSED TIME.

230 °C, 10 KV/CM

EACH CURVE AVG. OF TWO OR THREE SPECIMENS.

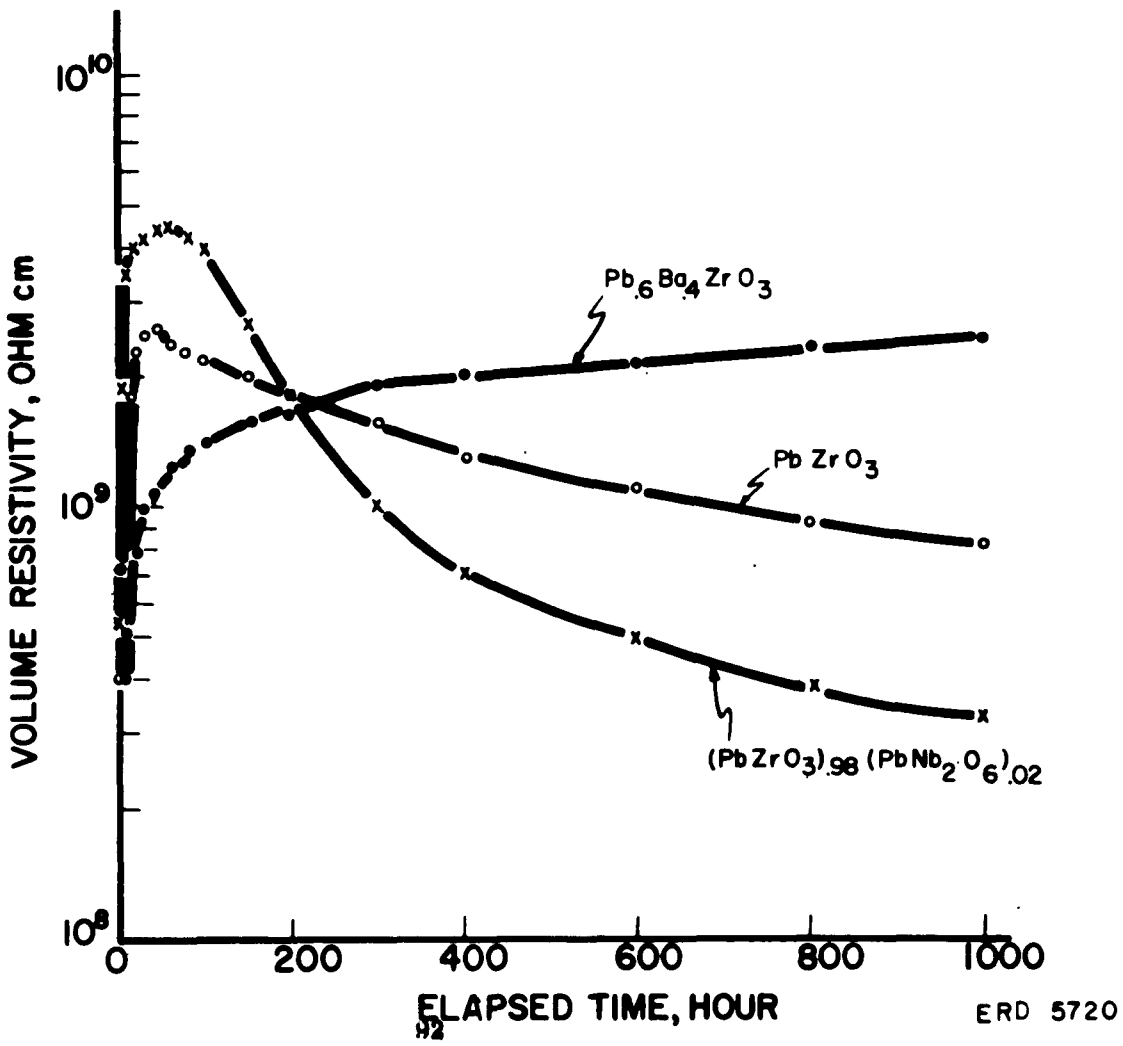

during the first 20 or 30 hours becomes a less significant feature of the plot. This is probably a more meaningful presentation of the degradation data than the logarithmic time scale plots. It is interesting to note that the $Pb_{.6}Ba_{.4}ZrO_3$ showed increasing volume resistivity to 1000 hours. The complicated behavior of this composition through the first six or seven hours (Fig. 50) does not show up on the linear plot (Fig. 53).

Photographs of the test specimens subjected to the 1000-hour tests are shown in Figures 54 (positive side) and 55 (negative side). Only two discs escaped mechanical failure and only one disc escaped dielectric breakdown. These failures account for the anomalous volume resistivity data obtained during the 1000-hour tests. Most dielectric breakdowns were "self-healed," i.e., high current quickly burned away the electrode surrounding the breakdown paths. Most of the dielectric breakdown paths formed around the periphery of the electrode where electric stress is highest, but there were exceptions which must indicate points of weakness in the ceramic. Even so, the test specimens had 97% of crystal density. In most cases mechanical failure did not remove a significant portion of the test specimen from the circuit due to the nature of the connection, so values of volume resistivity calculated using the initial specimen dimensions are not significantly altered.

Only one disc was available after the 1000 hour tests for dielectric measurements, and this disc ($Pb_{.6}Ba_{.4}ZrO_3$) did not change significantly in either permittivity or tan δ.

It was further noted that the rods making electrical connection to the test specimens became coated with a light yellowish substance during the tests. Some deposits are also evident on the peripheries of the electrodes on the

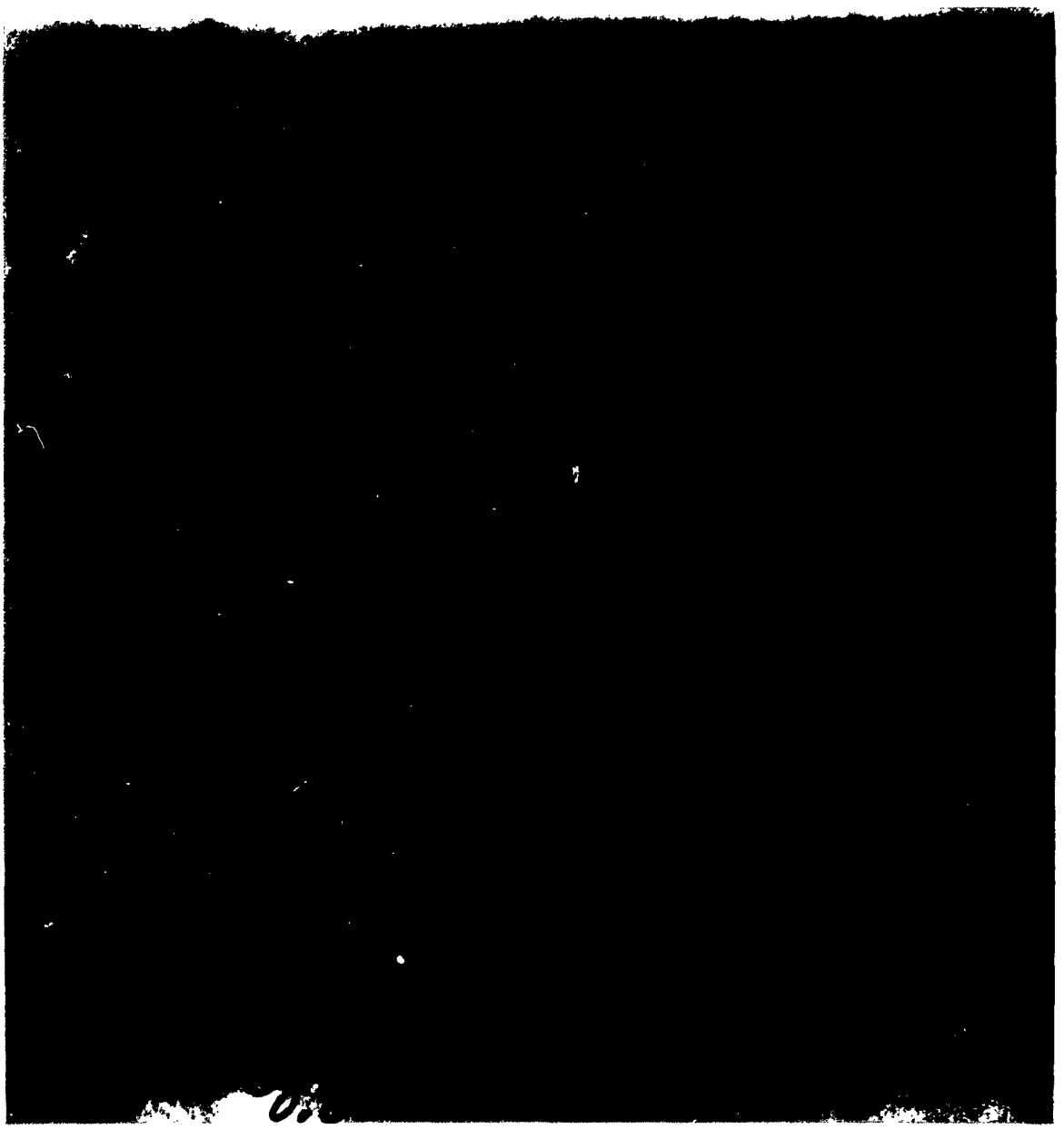

Figure 54. Appearance of Discs After 1000 Hour Degradation Studies, 230°C, 10 kv/cm, (+) Side.

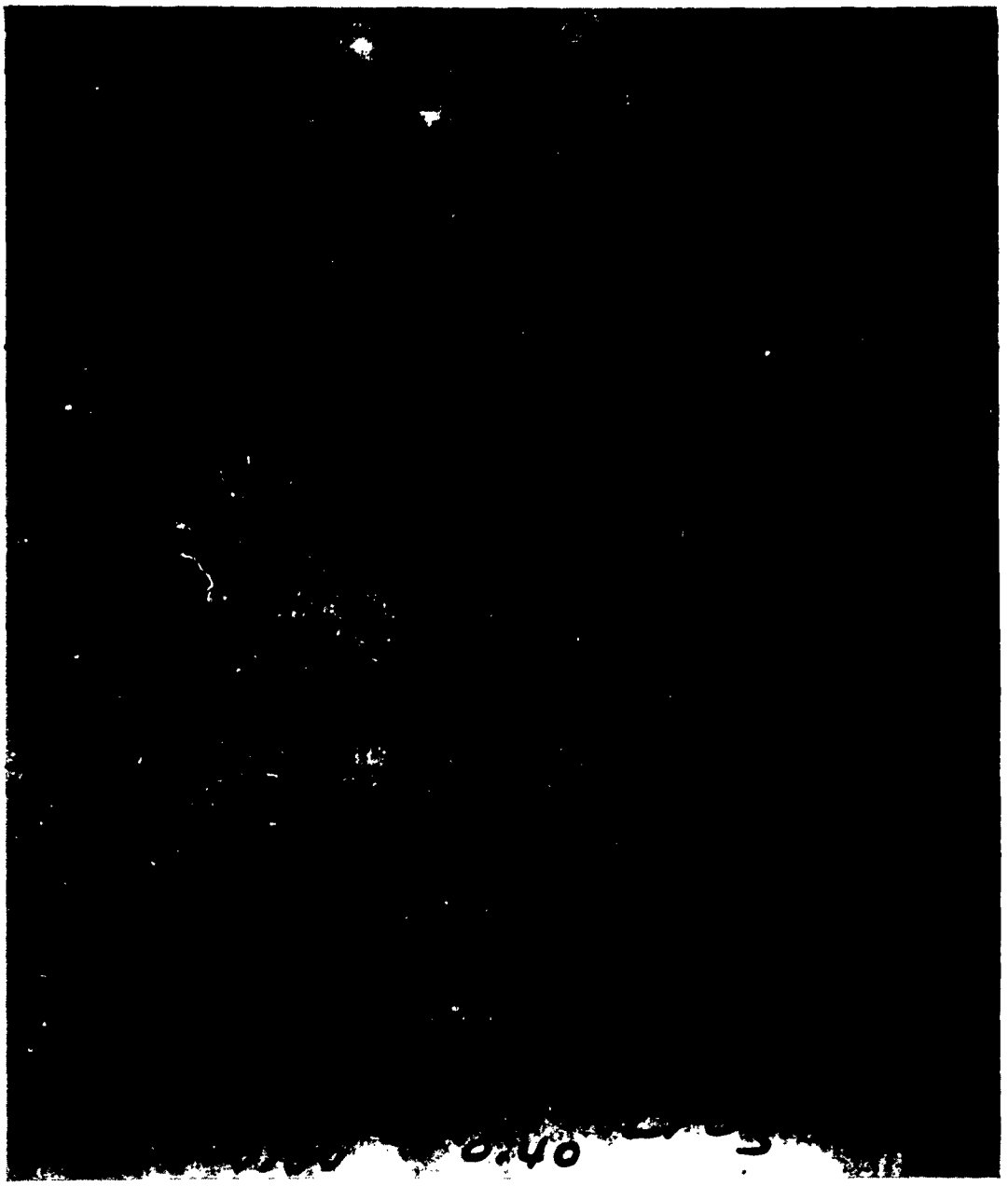

Figure 55. Appearance of Discs After 1000 Hour Degradation Studies, 230°C, 10 kv/cm, (-) Side.

positive sides of the test specimens (Fig. 54). Only lead was identified in substantial quantity by spectrographic analysis of this substance. It is unlikely that substantial quantities of PbO were driven off at 230°C, but it is likely that heavy current flow through localized breakdown paths may have generated sufficient heat in small volumes of the test material to cause some decomposition.

The rather severe degradation studies described here thus include two features which should be absent in the use of ordinary capacitors. These are loss of PbO and dielectric breakdown.

In an attempt to speed the degradation process further without substantially increasing the likelihood of dielectric breakdown, a degradation study at 300°C was undertaken. Results are summarized in Figs. 56 and 57 with time on a logarithmic scale and Fig. 58 with time on a linear scale. In this case there was somewhat less tendency for anomalous data in the range over 100 hours. Figure 59 shows the four $(Pb_{.6}Ba_{.4}ZrO_3)_{.99}(PbNb_2O_6)_{.01}$ discs after 900 hours at 10 kv/cm, 300°C. Only one disc escaped mechanical and dielectric breakdown. The tests on $(Ba_{.15}Pb_{.7}Sr_{.15}TiO_3)_{.99}(PbNb_2O_6)_{.01}$ were terminated after 600 hours due to catastrophic failure of all four discs. Chalky deposits indicative of PbO loss were again evident after these tests.

Figure 58 illustrates the general nature of behavior under severe temperature-field exposure for the zirconates and titanates. With the zirconates there is a rapid increase in volume resistivity following application of the electric field, often by about one order of magnitude. There is then a gradual decrease of volume resistivity with further exposure. With the titanates the volume resistivity decreases very sharply at first, often by nearly two orders of magnitude, and then this decrease slows. The difficulties of separating

FIGURE 56

VOLUME RESISTIVITY VS. ELAPSED TIME

$(Pb_{.6}\ Ba_{.4}\ ZrO_3)_{.99}\ (PbNb_2O_6)_{.01}$

300°C, 1.0 KV/CM. AVG. OF FOUR SPECIMENS

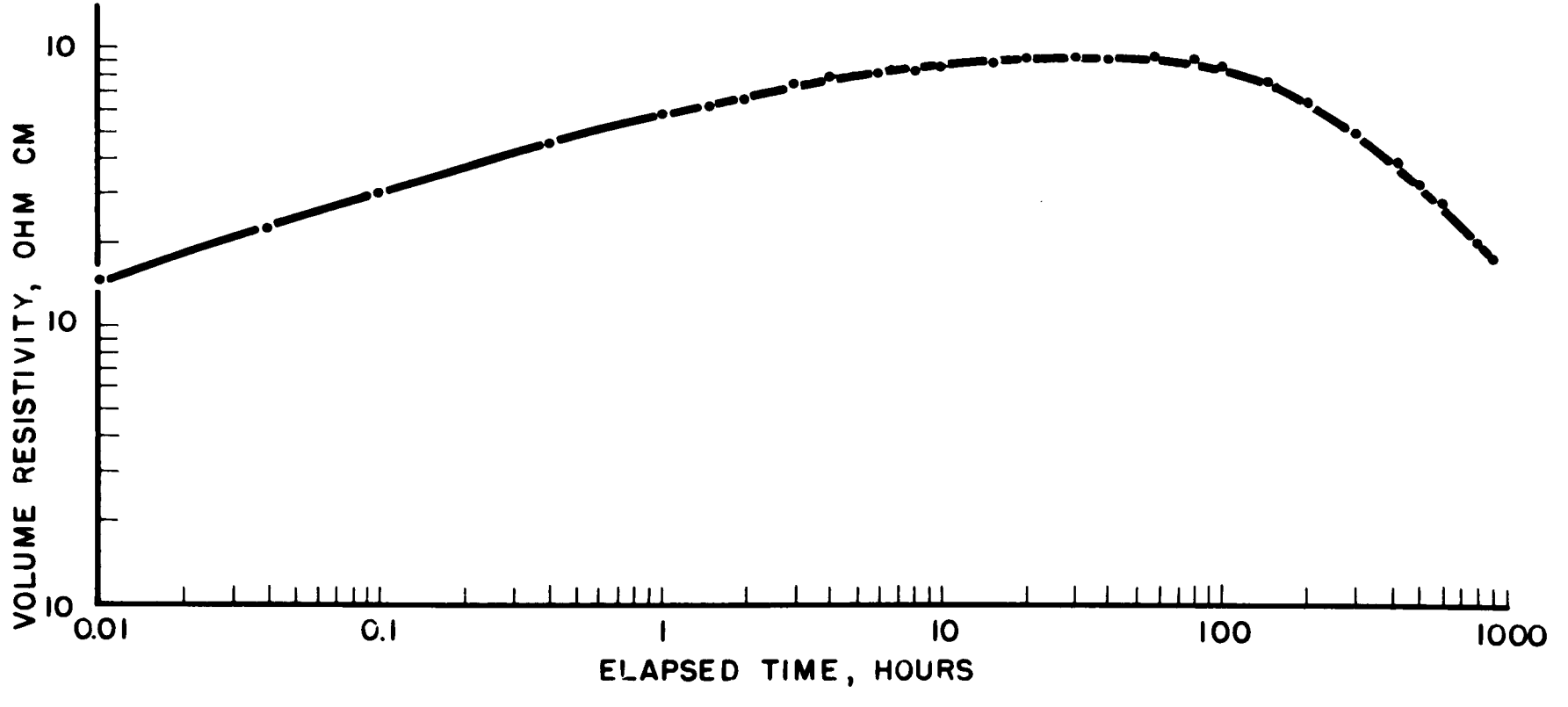

FIGURE 57.
VOLUME RESISTIVITY VS ELAPSED TIME

$(Pb_{.15}\ Ba_{.7}\ Sr_{.15}\ TiO_3)_{.99}\ (PbNb_2O_6)_{.01}$

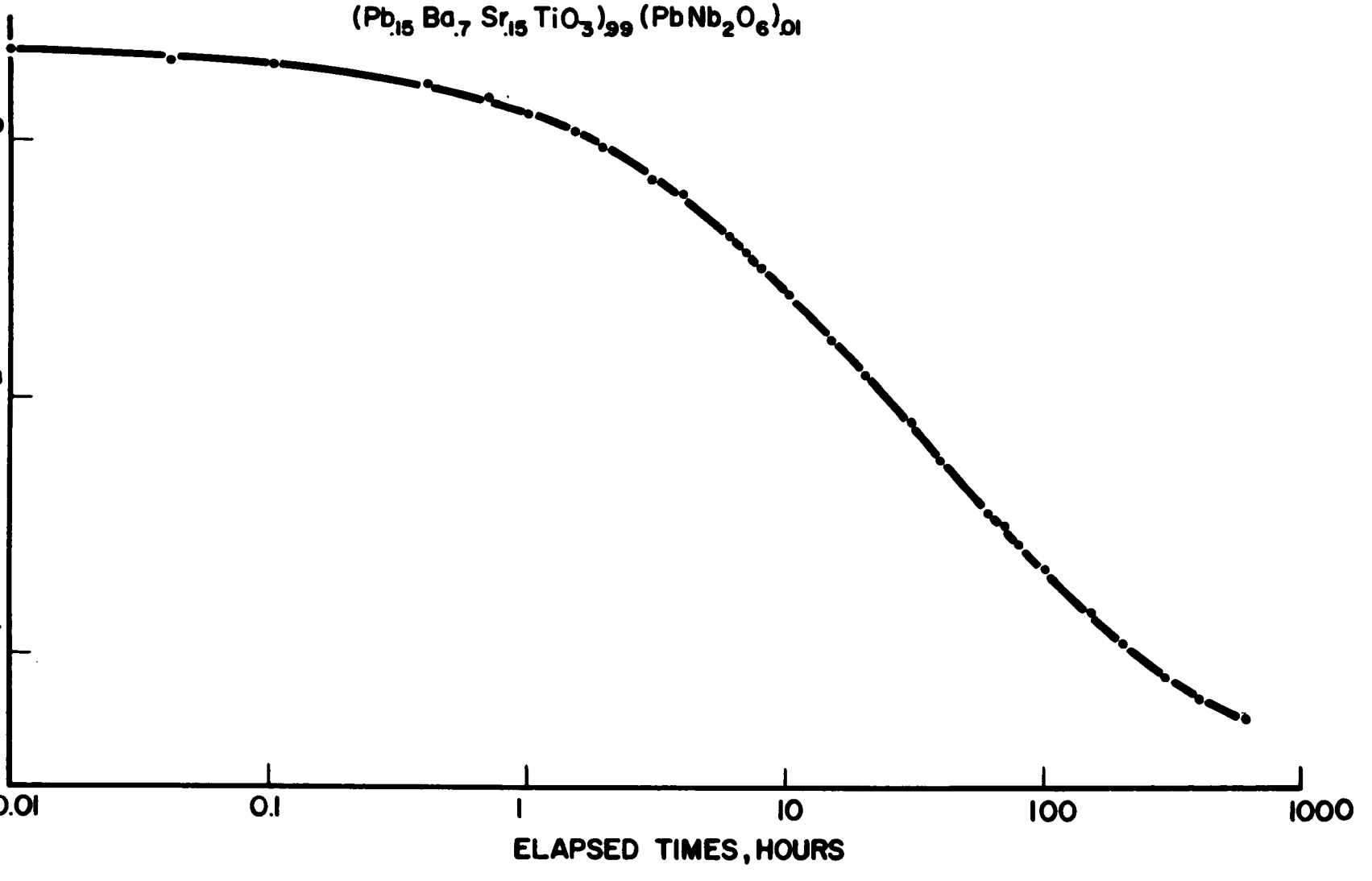

ERD 5722

FIGURE 58.
VOLUME RESISTIVITY VS ELAPSED TIME
10 KV/cm, 300 °C

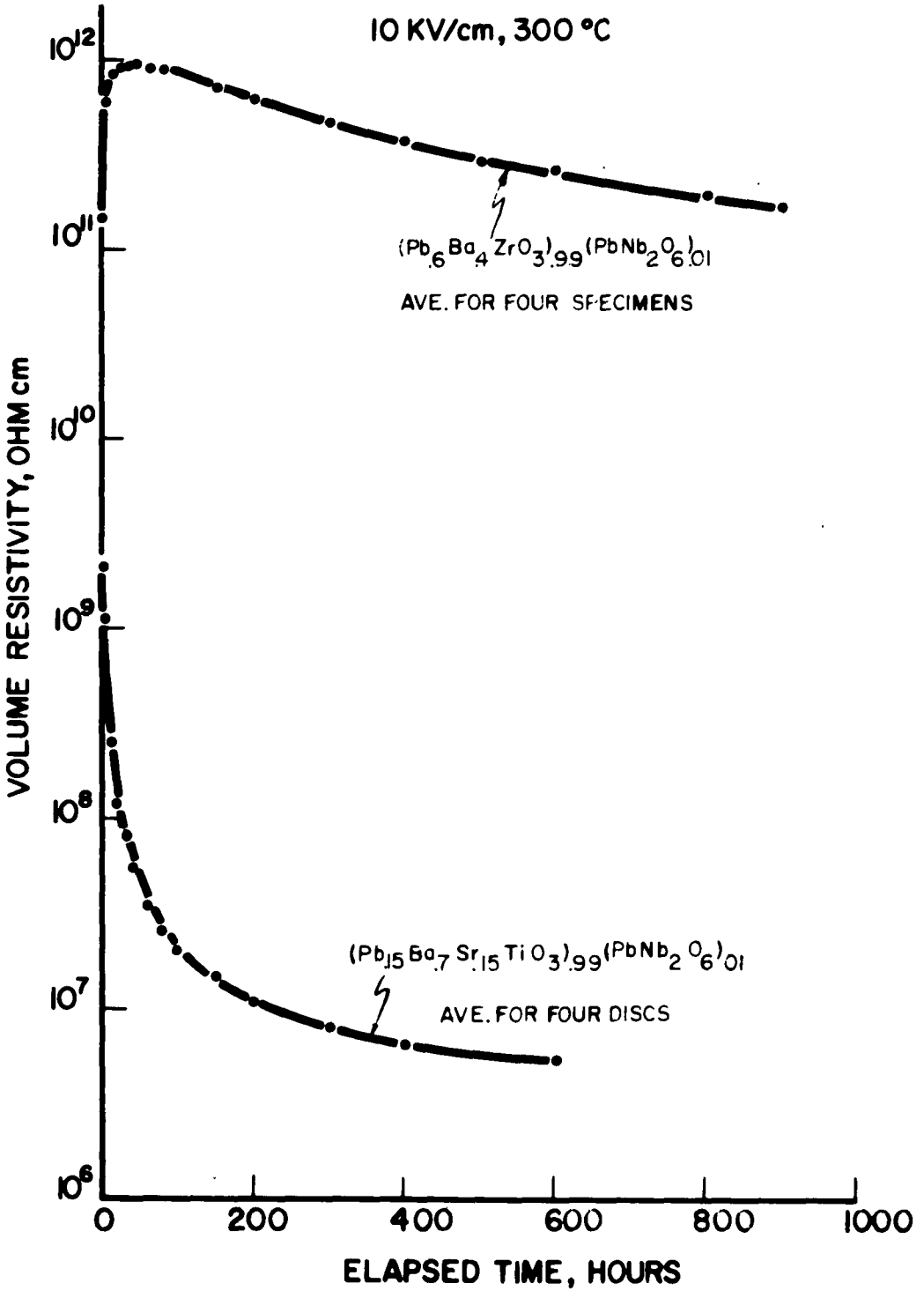

ERD 5723

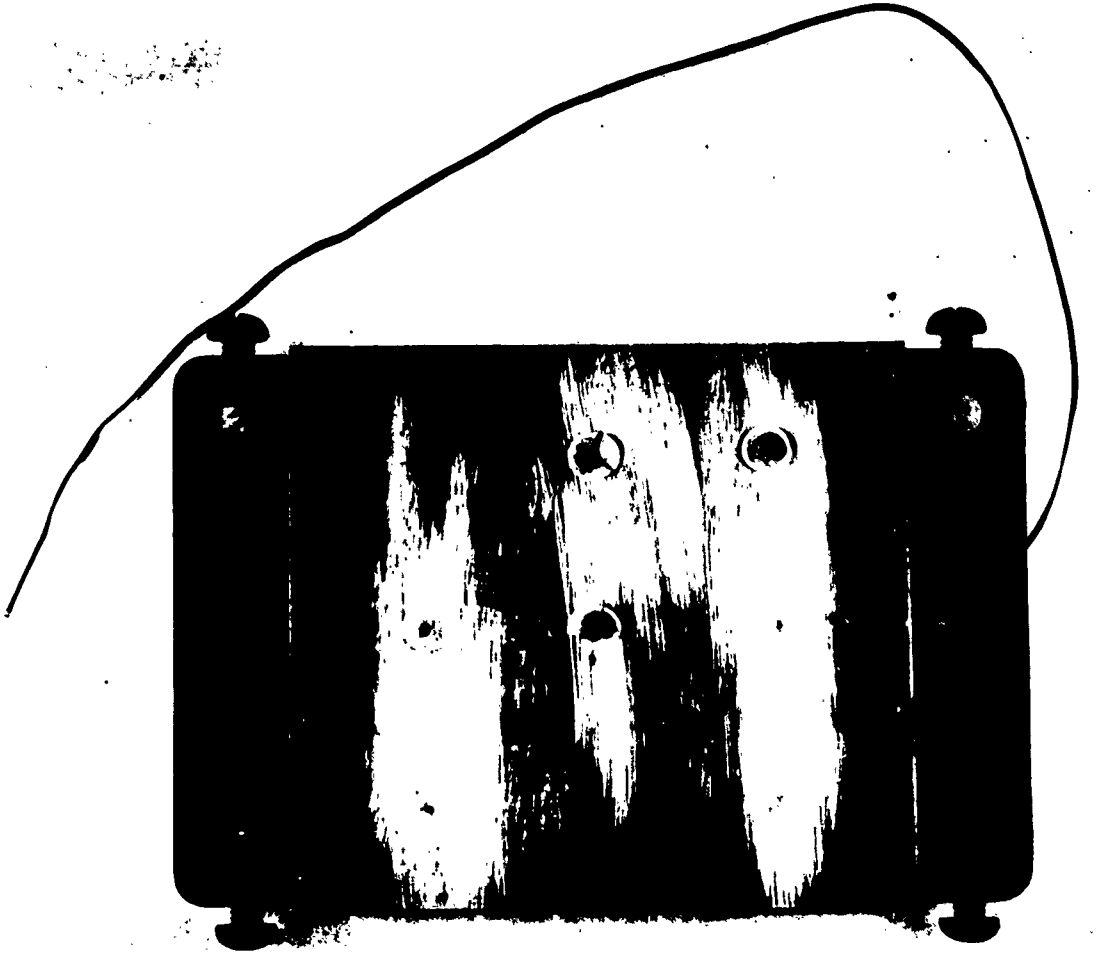

Figure 59. $(Pb_{0.60}Ba_{0.40}ZrO_3)_{0.99} + (PbNb_2O_6)_{0.01}$
Life Tested, 900 Hours, 300°C, 10 kv/cm.

volume degradation from formation of distinct breakdown paths prevent further clarification of this behavior. In the sense, however, that degradation contributes to formation of breakdown paths, however, it is not correct to say that the degradation process slows.

VIII. CORRELATION OF DEGRADATION AND DIELECTRIC BREAKDOWN WITH LOW SIGNAL PROPERTIES, GRAIN SIZE, AND CHEMICAL COMPOSITION

The objectives of this work, summarized in Section I, were to correlate various properties of the perovskite materials prepared with their dielectric breakdown strength and resistance to dielectric degradation. Insofar as possible the measurements presented in the preceding sections of this report are used as a basis for this correlation in this section.

Figure 60 shows the dielectric strength measured at 110°C for most of the compositions prepared as function of their permittivity at 110°C. There is a rough correlation only, with dielectric strength tending to decrease with increasing permittivity. This is the expected behavior. The energy storage of a linear capacitor per unit volume is $1/2\ \epsilon E^2$, where E is the limiting electric field. The limiting field must be well below the dielectric strength for any practical application, but if one assumes most ceramic dielectrics are approximately alike with respect to energy storage at breakdown, one must expect the square of the dielectric strength to be inversely proportional to the square root of the permittivity. Assuming E = 200 kv/cm at $\epsilon/\epsilon_o = 100$, the stored energy is 0.18 joules/cm^3, and the expected dependence of dielectric strength on permittivity is shown as a dashed line in Fig. 60. In mks units (E in volts/meter, ϵ in farads/meter) this curve is given by $E = 600/\sqrt{\epsilon}$, and at <u>every</u> point on this

FIGURE 60.
DIELECTRIC BREAKDOWN STRENGTH VS. DIELECTRIC CONSTANT FOR PEROVSKITE CERAMICS.

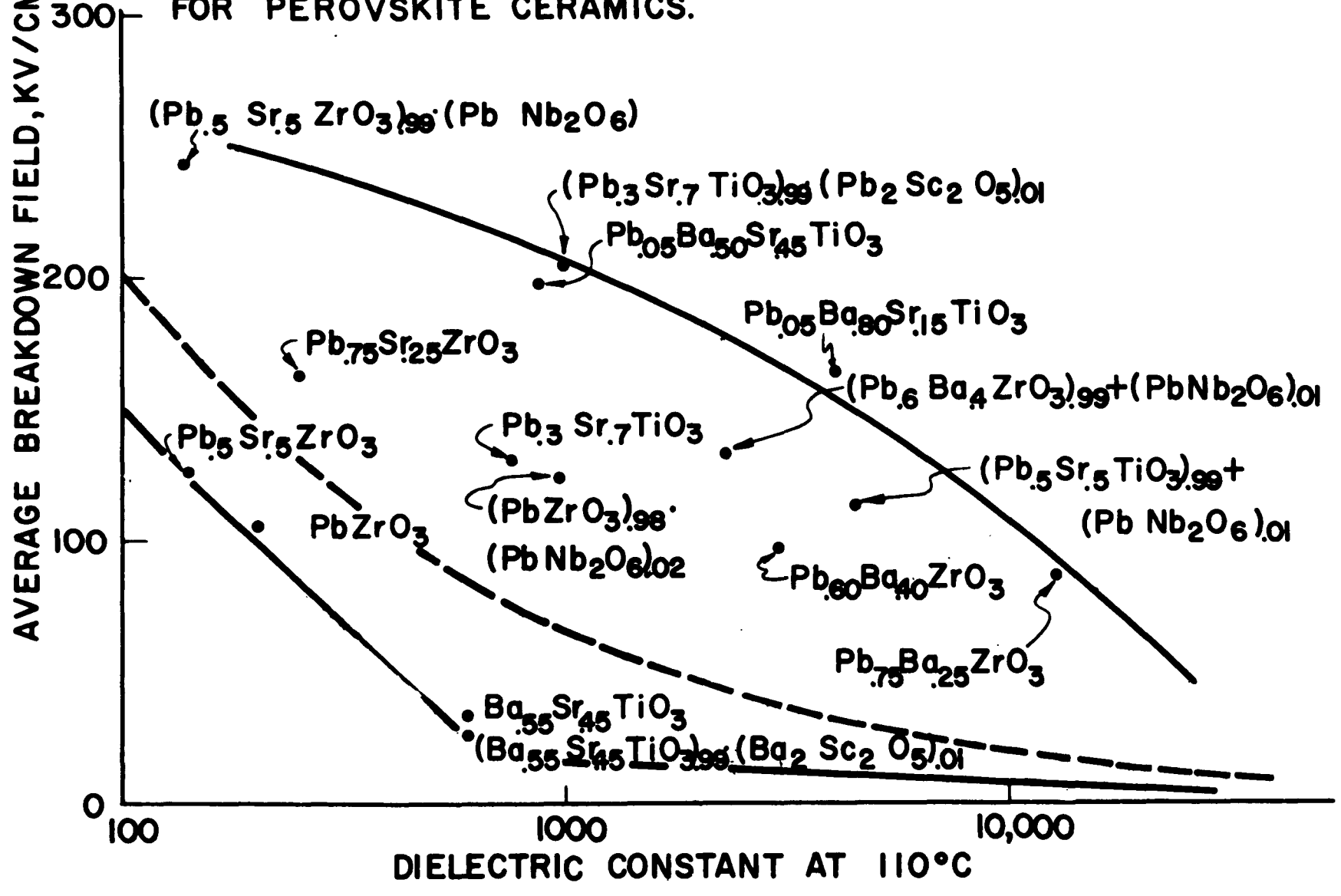

FIGURE 60.
DIELECTRIC BREAKDOWN STRENGTH VS. DIELECTRIC CONSTANT FOR PEROVSKITE CERAMICS.

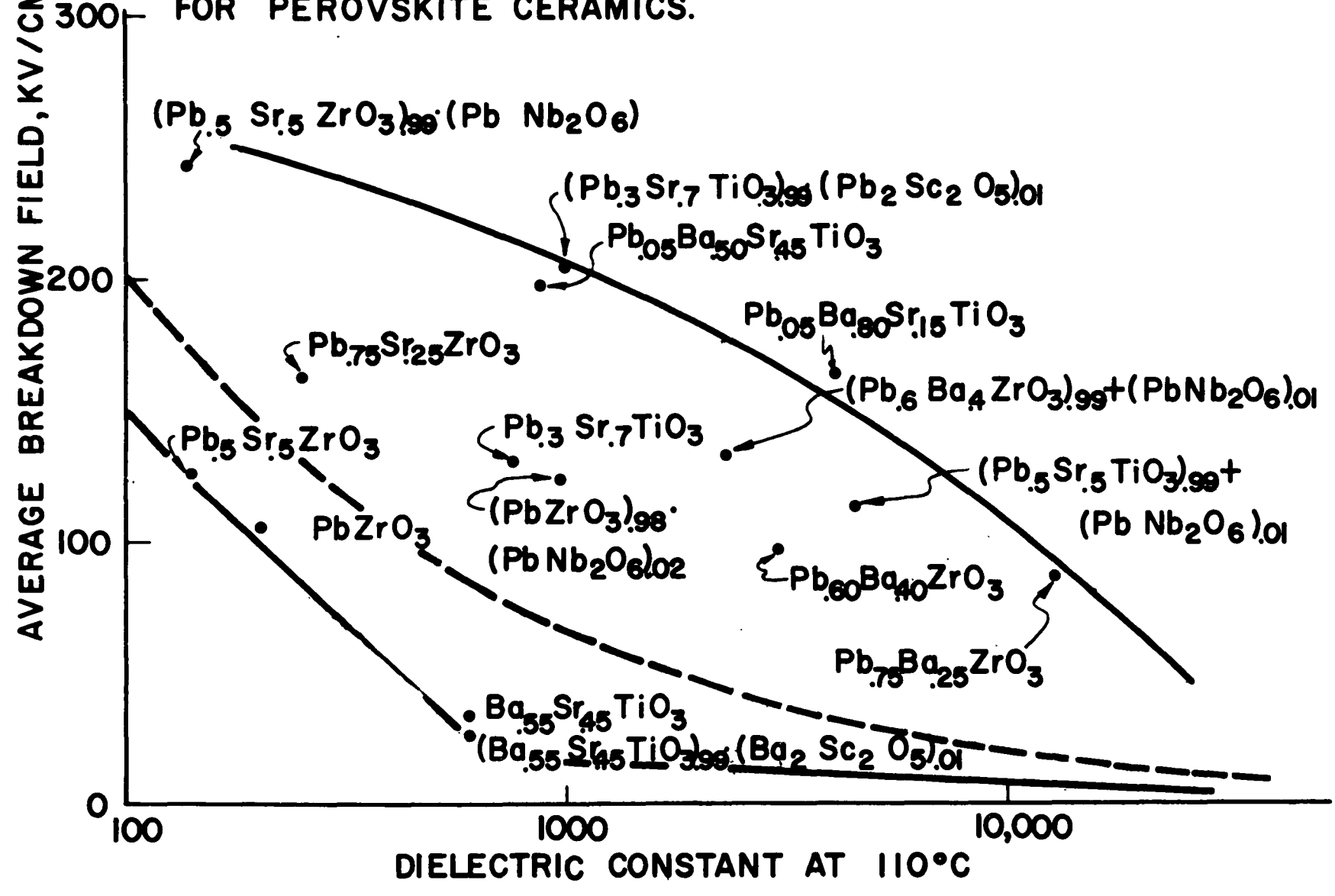

FIGURE 60.
DIELECTRIC BREAKDOWN STRENGTH VS. DIELECTRIC CONSTANT FOR PEROVSKITE CERAMICS.

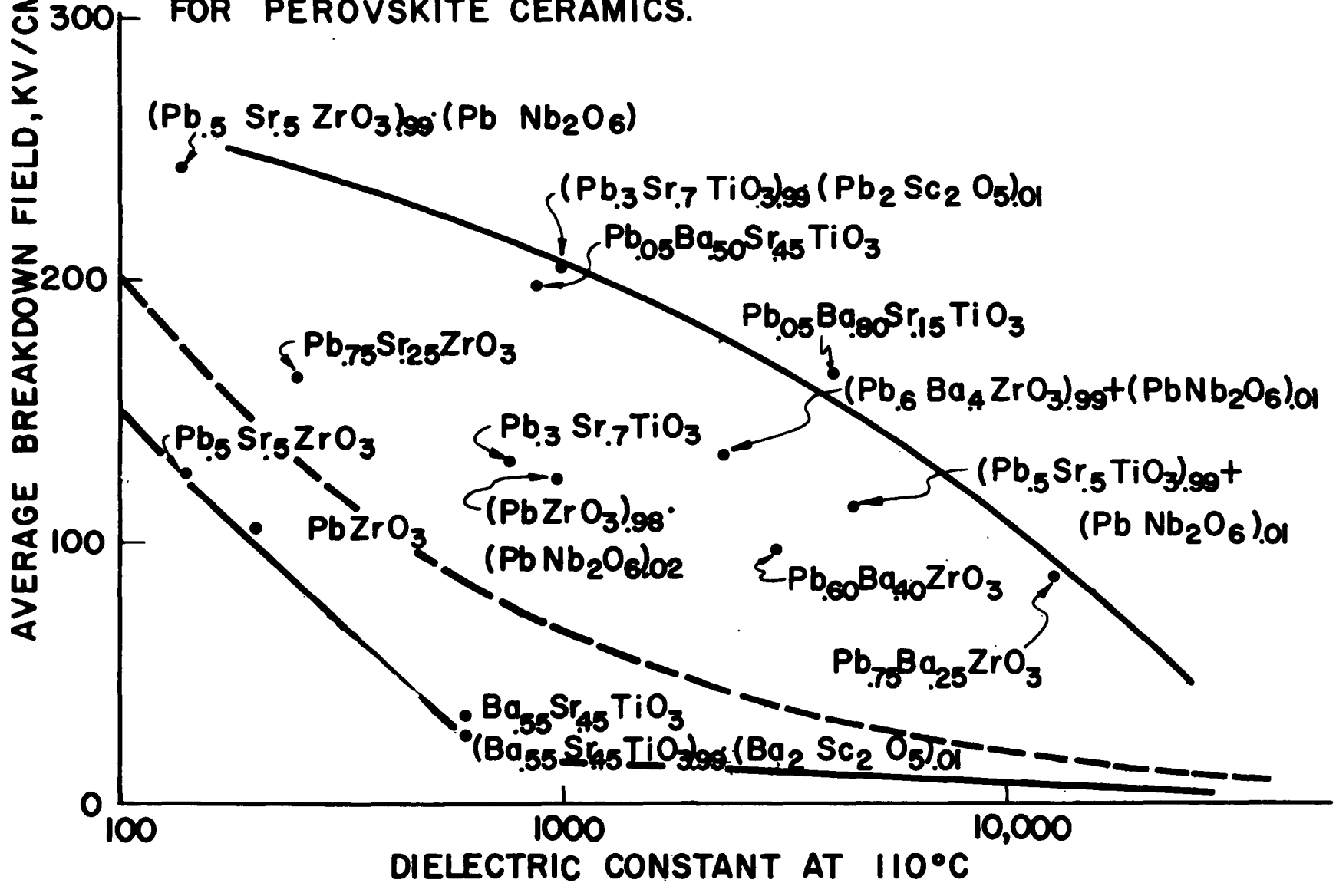

curve, the energy storage is the same, 0.18 joules/cm^3. This, of course, assumes a linear charge-field relationship. The energy storage is much higher at a given electric field if the material is ferroelectric or is driven ferroelectric by the field.

Using the data of Fig. 60 one may also attempt to correlate dielectric strength with chemical composition. It is immediately evident that the titanates and zirconates do not fall into distinct classes in this respect. Reference to Figs. 11 through 20 and Tables II and III shows that without exception an additive which improves the volume resistivity of a given base material also improves its dielectric strength and vice versa. Thus Sc^{3+} increases the dielectric strength of $Pb_{.3}Sr_{.7}TiO_3$ and Nb^{5+} increases the dielectric strength of $Pb_{.6}Ba_{.4}ZrO_3$. This may indicate a thermal breakdown mechanism, normaly ascribed to local or general heating (runaway thermal situation) due to conductivity at high electric field.

In view of the effects of additives discussed above one might expect somewhat closer correlation between dielectric strength and volume resistivity than between dielectric strength and permittivity. This is found to be true (Fig. 61), but there are still rather wide variations in overall behavior. Figure 62 shows the correlation of dielectric strength with time constant (product of volume resistivity and permittivity).

Since behavior of zirconates in the degradation studies was markedly better than that of the titanates, and since there was no separation of titanates and zirconates into two distinct classes with respect to dielectric strength, there is no direct correlation between dielectric degradation and dielectric strength. However, as pointed out in Section VII, actual failure during the

FIGURE 61.
DIELECTRIC BREAKDOWN STRENGTH
VS.
RESISTIVITY FOR PEROVSKITE CERAMICS.

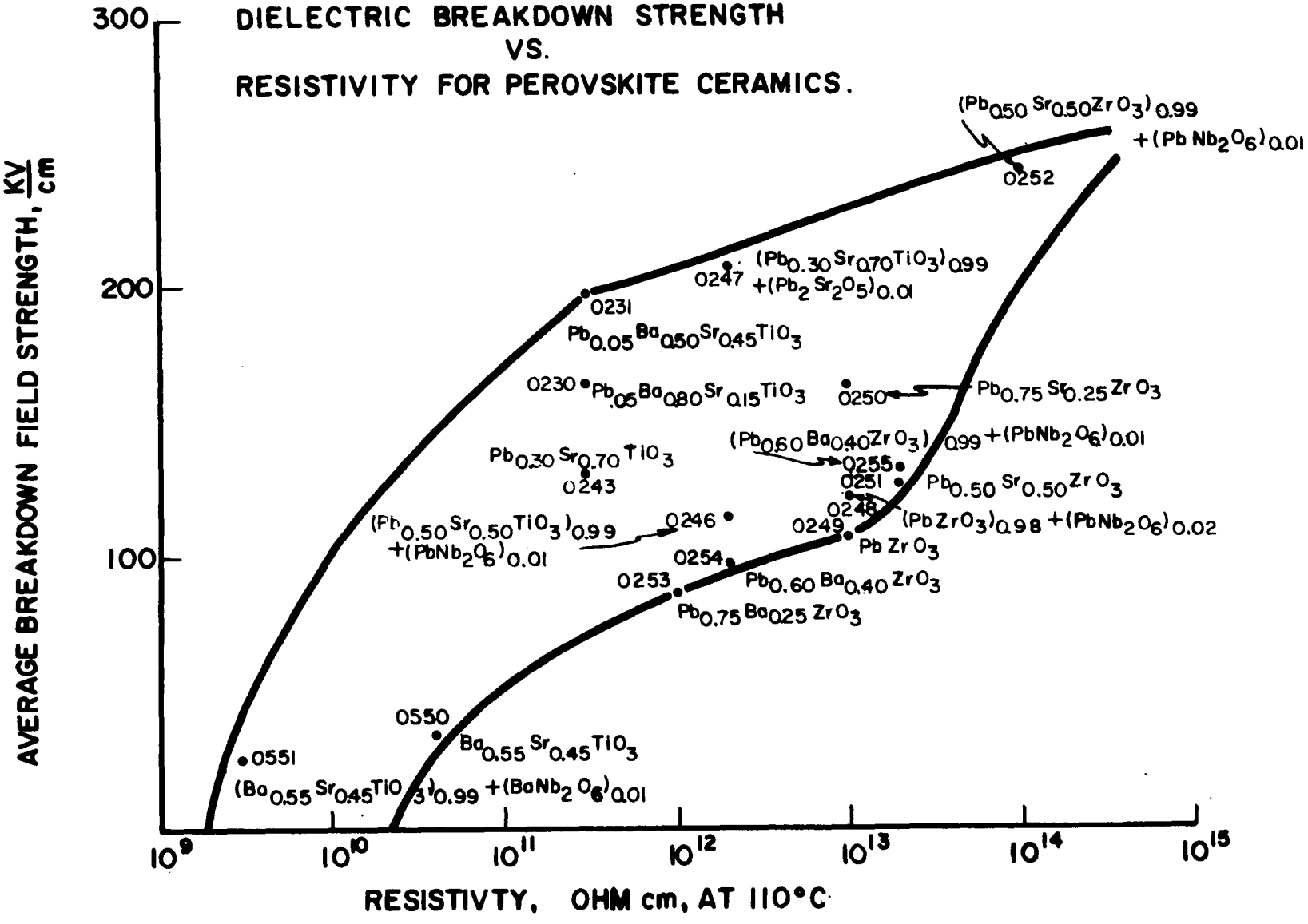

FIGURE 62.
AVERAGE BREAKDOWN FIELD STRENTH
VS.
TIME CONSTANT FOR PEROVSKITE CERAMICS.

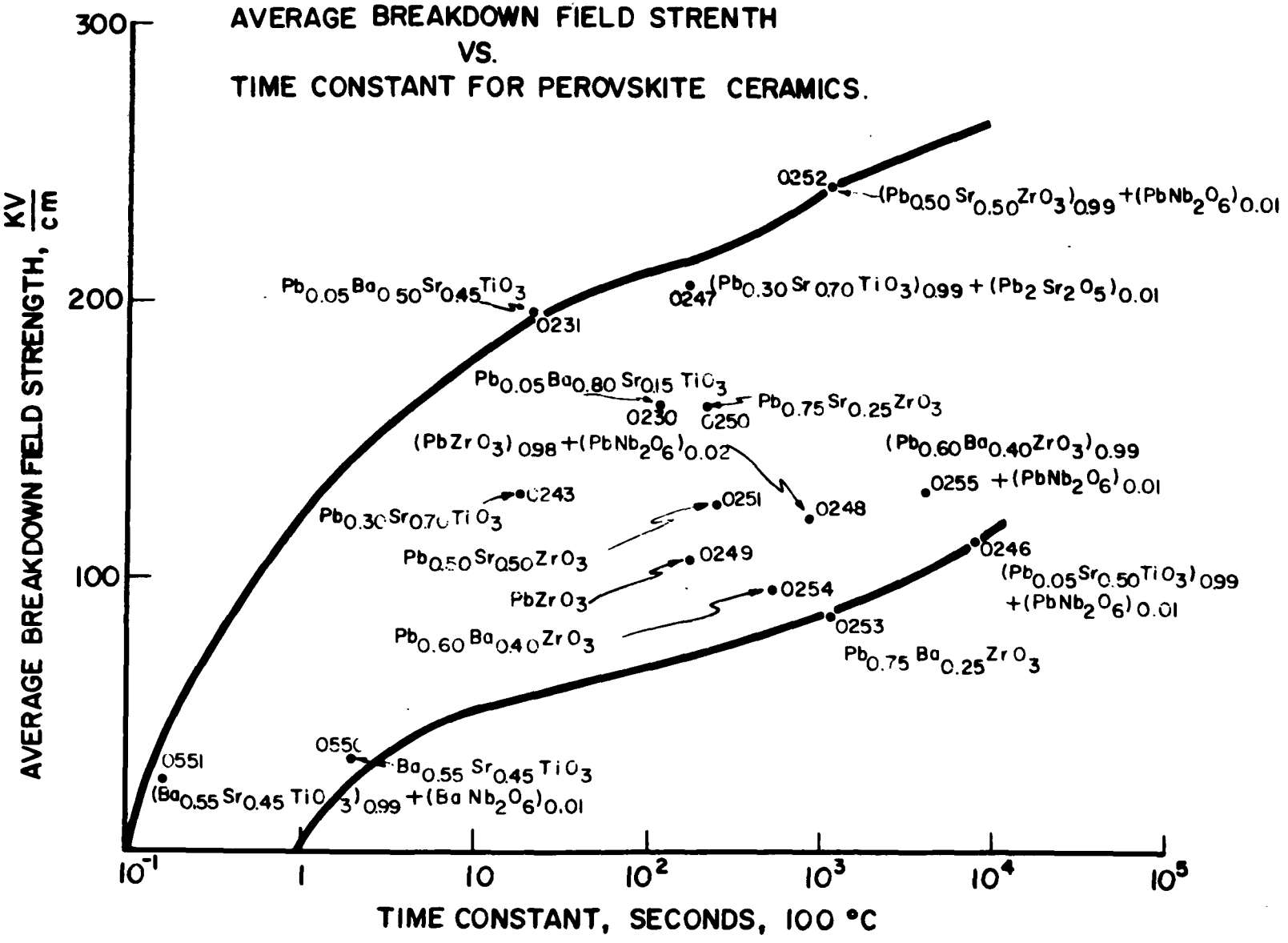

degradation tests was due to dielectric breakdown. This is not reflected in the curves of Figs. 43 through 53 and 56 through 58, since anomalous points due to sudden formation of dielectric breakdown path were eliminated. It is probably fair to say that the dielectric strength for long exposure periods is higher for the zirconates than for the titanates.

Correlation of dielectric degradation with composition is relatively simple. The zirconates are in this respect far superior to the titanates. Dielectric degradation can probably best be ascribed to electrolysis of oxygen. One might expect this to proceed more rapidly with the titanates, since Ti^{4+} is much more readily reduced than is Zr^{4+}.

Since the zirconates have generally higher volume resistivities than the titanates (Fig. 21), and since also the zirconates have better resistance to dielectric degradation, the correlation of dielectric degradation to volume resistivity is good.

Table V lists the range of crystallite sizes for the various compositions prepared in this work. These data were obtained from the photomicrographs of Figs. 22 through 36. It is important to note that a given composition may be subjected to widely different temperature-time schedules during firing, and the grain sizes are generally larger for higher peak temperatures and longer hold at peak temperature. There was no attempt here to obtain a range of grain sizes with a given composition, but since different firing schedules were used for a given composition (Table I), a range of grain sizes was obtained. The behavior in the degradation studies was relatively uniform for high density specimens of a given composition regardless of the firing schedule,

Table V. Range of Crystallite Sizes

in Ceramic Materials Prepared in This Work

Composition	Crystallite size, Microns	Dielectric Strength kV/cm
$PbZrO_3$	< 1 to 2	107
$(PbZrO_3)_{.98}(PbNb_2O_6)_{.02}$	< 1 to 6	121
$Pb_{.5}Sr_{.5}ZrO_3$	3 to 15	126
$(Pb_{.5}Sr_{.5}ZrO_3)_{.99}(PbNb_2O_6)_{.01}$	5 to 20	242
$Pb_{.75}Sr_{.25}ZrO_3$	3 to 10	162
$Pb_{.6}Ba_{.4}ZrO_3$	< 1 to 5	96
$(Pb_{.6}Ba_{.4}ZrO_3)_{.99}(PbNb_2O_6)_{.01}$	3 to 30	131
$Pb_{.75}Ba_{.25}ZrO_3$	1 to 5	86
$Pb_{.3}Sr_{.7}TiO_3$	3 to 15	130
$(Pb_{.3}Sr_{.7}TiO_3)_{.99}(Pb_2Sc_2O_5)_{.01}$	< 1 to 3	206
$(Pb_{.3}Sr_{.7}TiO_3)_{.99}(PbNb_2O_6)_{.01}$	1 to 10	---
$(Pb_{.5}Sr_{.5}TiO_3)_{.99}(PbNb_2O_6)_{.01}$	< 1 to 7	113
$Pb_{.05}Ba_{.8}Sr_{.15}TiO_3$	3 to 20	163
$Pb_{.05}Ba_{.5}Sr_{.45}TiO_3$	3 to 12	196
$Pb_{.5}Sr_{.5}TiO_3$	5 to 25	---

so it may be assumed indepedent of grain size within limits in which high densities may be obtained. In this work it was in effect therefore shown that there is no direct correlation between crystallite size and resistance to degradation.

Table V also lists the dielectric strengths of the various compositions (from Table II), and there again appears to be little correlation with crystallite size.

IX. SUGGESTED FUTURE WORK

In this work it has been established that dielectric failure is less likely in zirconates than in titanates, and that failure is further inhibitedby off-valency additives which raise the volume resistivity of the base material. An off-valency additive which lowers the volume resistivity of the base material has deleterious effects.

It was further demonstrated that failure after long term exposure to high electric fields at elevated temperature is usually due to formation of distinct dielectric breakdown paths rather than high overall current conduction. This occurs at electric fields an order of magnitude lower than the instantaneous dielectric strength.

There are a number of approaches to the problem of dielectric failure in ceramic materials which could be followed in future work. Several are suggested below.

1. It was not possible in this work to correlate crystallite size of ceramic materials with their dielectric strength or resistance to degradation. This could be clarified by preparation of high

density specimens of a range of crystallite sizes and distribution of sizes. This might be done using hot-pressing techniques.

2. In this work many ceramic specimens with 96 to 99% of crystal density were prepared and tested. Even higher densities may be obtained using hot-pressing techniques. This may have an important bearing on dielectric failure.

3. An attempt should be made to correlate failure with the medium surrounding the dielectric. In this work air was used for the degradation studies, transformer oil for the dielectric strength measurements. Failure during the degradation studies was by dielectric breakdown, and this may well be inhibited by a surrounding medium with dielectric strength considerably higher than air. One possibility is molten sulfur.

4. It would be interesting to determine the effects of reversed electric field after a degradation study. For this type of study dielectric breakdown should be completely eliminated either by using an electric field substantially below 10 kv/cm or possibly by using a surrounding medium of much higher dielectric strength than air.

5. Thermal emf measurements could be made after the degradation studies to determine whether a change of conductivity type (n- or p-type) occurred. Here again dielectric breakdown must not have occurred during the degradation study.

6. Electron micrographs could be made before and after a degradation study to determine whether there are any visible effects, such as cracks or obvious electrochemical changes.

7. An attempt to correlate failure with electrode material type might be made.

8. A study of the dependence of failure on capacitor geometry might lead to interesting results. A study could be made of the geometric distribution of electrochemical effects. It is well known that dielectric strength (actual not intrinsic) decreases with increasing thickness, and with imperfect ceramic specimens, at least, the dielectric strength decreases with electrode area increase.

9. Study of other materials with lower permittivyt ($\epsilon/\epsilon_o \sim 30$ to 40) to determine if these are inherently better than the compositions studied in this work. The higher permittivity materials are all relatively close in free energy to a ferroelectric state, and are in this respect quite different from the low permittivity materials previously considered in work at this laboratory.[7] BaZrO with La^{3+} donor additive was the best of the materials studied in that work. With these there were no changes in physical appearance (including no dielectric breakdown) after 1000 hours at 24 kv/cm at 250 or 350°C. This is, of course,

[7] John Koenig, Contract No. NObs-78108, Mdse No. NS-052-036, Final Report dated March 14, 1961.

6. Electron micrographs could be made before and after a degradation study to determine whether there are any visible effects, such as cracks or obvious electrochemical changes.

7. An attempt to correlate failure with electrode material type might be made.

8. A study of the dependence of failure on capacitor geometry might lead to interesting results. A study could be made of the geometric distribution of electrochemical effects. It is well known that dielectric strength (actual not intrinsic) decreases with increasing thickness, and with imperfect ceramic specimens, at least, the dielectric strength decreases with electrode area increase.

9. Study of other materials with lower permittivyt ($\epsilon/\epsilon_o \sim 30$ to 40) to determine if these are inherently better than the compositions studied in this work. The higher permittivity materials are all relatively close in free energy to a ferroelectric state, and are in this respect quite different from the low permittivity materials previously considered in work at this laboratory.[7] BaZrO with La^{3+} donor additive was the best of the materials studied in that work. With these there were no changes in physical appearance (including no dielectric breakdown) after 1000 hours at 24 kv/cm at 250 or 350°C. This is, of course,

[7] John Koenig, Contract No. NObs-78108, Mdse No. NS-052-036, Final Report dated March 14, 1961.

a much more drastic degradation test schedule than the schedules used in this work, but the energy stored ($1/2\ \epsilon E^2$) was about eight times as high during the degradation studies on $(Pb_{.6}Ba_{.4}ZrO_3)_{.99}(PbNb_2O_6)_{.01}$, the best material studied in this work. The time constant of this material at 300°C was about 100 seconds. The dielectric strength of $(Ba_{.97}La_{.02}ZrO_3)$, as shown in reference (7) is about 200 kv/cm at 100°C. Here for $(Pb_{.6}Ba_{.4}ZrO_3)_{.99}(PbNb_2O_6)_{.01}$ the dielectric strength was about 130 kv/cm at 100°C (Table III). On the basis of the degradation studies, however, the long term dielectric strength of the former is better by a much wider margin.

Broadening of these studies to include these lower permittivity materials would permit some conclusions on the possible limitations of an incipient ferroelectric phase. Furthermore, comparison on the basis of equal energy storage (ratio of test electric fields set inversely proportional to the square root of the ratio of permittivities at the respective electric fields) would answer the question as to the desirability of high permittivity materials for energy storage. In the long range this study should be extended to include oil-impregnated paper, mylar, and thin oxide film capacitors as well.

X. ACKNOWLEDGMENTS

The author wishes to thank Dr. Hans Jaffe for his guidance and encouragement. He is indebted to Dr. Robert Gerson, now at the Missouri School of Mines, who directed this work during the first six months. J. Peterson is responsible for most of the electrical measurements, and B. Kost and W. Szczecinski also made contributions. Ceramic specimens were prepared by F. Scholz. W. R. Cook, Jr., is responsible for the x-ray measurements.

XI. INITIAL DISTRIBUTION

Copy No.

1. Electronic Research Division (H. Jaffe)
2. Electronic Research Division (Project Administration)
3. Clevite Patent Department
4-6. Clevite Library
7. Electronic Research Division (Don A. Berlincourt)
8. Electronic Research Division (B. Jaffe)
9. Electronic Research Division (J. Koenig)
10. Electronic Research Division (F. Kulcsar)
11. Electronic Research Division (J. Peterson)
12-110. RADC Distribution List
111-115. Electronic Research Division

DISTRIBUTION LIST FOR CONTRACT REPORTS

Contract No. AF 30(602)-2594

RADC (RASGP, Attn: E. A. Doyle, Jr.) Griffiss Air Force Base, New York	10
RADC (RAAPT) Griffiss Air Force Base, New York	1
RADC (RAALD) Griffiss Air Force Base, New York	1
GEEIA (ROZMCAT) Griffiss Air Force Base, New York	1
U.S. Army Electronics R&D Laboratories Liaison Officer RADC Griffiss Air Force Base, New York	1
AUL (3T) Maxwell Air Force Base, Alabama	1
ASD (ASAPRD Wright-Patterson Air Force Base, Ohio	1
Chief Naval Research Laboratory ATTN: Code 2027 Washington 25, D. C.	1
Commanding Officer U.S. Army Electronics R&D Laboratories ATTN: SELRA/SL-ADT Fort Monmouth, New Jersey	1
DDC (TISIA-2) Arlington Hall Station Arlington 12, Virginia	10
RTD (RTH Bolling Air Force Base 25, D. C.	1
Commandant Armed Forces Staff College (Lib) Norfolk 11, Virginia	1

Director U.S. Army Engineer R&D Laboratories Technical Documents Center Ft. Belvoir, Virginia	1
ESD (ESRL) (ESAT) L. G. Hanscom Field Bedford, Massachusetts	1 1
Commanding Officer & Director U. S. Navy Electronics Laboratory (Lib) San Diego 52, California	1
AFMTC Technical Library (MU-135) Patrick Air Force Base, Florida	1
Sidney J. Stein, Ph. D. Electro-Science Laboratories, Inc. 1133-35 Arch Street Philadelphia 7, Pennsylvania	1
AFSC (SCSE) Andrews Air Force Base Washington 25, D. C.	1
National Aeronautics & Space Administration Langley Research Center Langley Station Hampton, Virginia ATTN: Librarian	1
AFSC (SCFRE) Andrews Air Force Base Washington 25, D. C.	1
Headquarters, USAF (AFCOA) Washington 25, D. C.	1
AFOSR (SRAS/Dr. G. R. Eber) Holloman Air Force Base, New Mexico	1
Commander Naval Missile Center Technical Library (Code No. 3022) Pt. Mugu, California	1

NAFEC Library Building 3 Atlantic City, New Jersey	1
ESD (ESGT) L. G. Hanscom Field Bedford, Massachusetts	2
ESD (ESRDE, Major James W. Van Horn) L. G. Hanscom Field Bedford, Massachusetts	1
ASD (ASRCTE, Mr. E. Miller) Wright-Patterson Air Force Base, Ohio	1
Westinghouse Electric Corporation Air Arm Division (Dr. John Dzimianski) Friendship International Airport P. O. Box 1897 Baltimore 3, Maryland	1
Motorola, Inc. Solid State Integrated Circuits Laboratory ATTN: Mr. J. R. Black 8201 E. McDowell Road Scottsdale, Arizona	1
Hughes Aircraft Company Ground Systems Division ATTN: Mr. F. M. LaFleur Fullerton, California	1
Clevite Research Center Electronic Research Division ATTN: Mr. Don A. Berlincourt Cleveland 8, Ohio	2
Armour Research Foundation of Illinois Institute of Technology Technology Center ATTN: Dr. G. T. Jacobi Chicago 16, Illinois	1
Raytheon Company Research Division ATTN: Dr. P. Nutter Waltham 54, Massachusetts	1

General Telephone and Electric 1
Bayside Laboratories
ATTN: Dr. Thomas Polanyi
Bayside, New York

Syracuse University 1
ATTN: Dr. Glen Glasford
Syracuse, New York

Clevite Corporation 2
Shockley Transistor Division
ATTN: Dr. Hans Queisser
Stanford Industrial Park
Palo Alto, California

Sprague Electric Company 1
ATTN: Dr. Preston Robinson
Director, Consultant
N. Adams, Massachusetts

Frank Brand 1
Chief Microwave Quantum Electronics Branch
SIGRA/SL-PFM
Fort Monmouth, New Jersey

William Spurgeon 1
Bendix Corporation
Research Laboratory Division
Southfield, Michigan

Autonetics Division, North American 1
ATTN: Dr. West
9150 E. Imperial Highway
Downey, California

John G. Landers 1
307 The Great Road
Bedford, Massachusetts

Internation Resistance Company 1
ATTN: Jack Iskind
Project Manager XTL Resistors
401 N. Broad Street
Philadelphia, Pennsylvania

Avco, RAD 1
ATTN: Mr. D. Earles
201 Lowell Street
Wilmington, Massachusetts

Commanding Officer Diamond Ordnance Fuse Laboratories ATTN: Mr. Asaf A. Benderly Washington 25, D. C.	1
Corning Glass Works Electronic Components Division ATTN: Mr. Richard O'Brien Bradford, Pennsylvania	1
Fairchild Semiconductor Corporation ATTN: Mr. Jack Gorry 545 Whisman Road Mountainview, California	1
General Electric Company Semiconductor Products Department ATTN: Mr. Conrad Zierat Electronics Park Syracuse, New York	1
Pacific Semiconductor, Inc. ATTN: Mr. R. A. Campbell Culver City, California	1
Minneapolis Honeywell ATTN: Mr. J. M. Bedrick 1400 Soldiers Field Road Boston, Massachusetts	1
General Telephone & Electronics Laboratories ATTN: Dr. Daniel George Bayside, New York	1
USASRDL (SIGRA/SL-PFS, Mr. N. Korolkoff) Evans Area Fort Monmouth, New Jersey	1
AGED Secretariat Working Group on Low Power Devices 346 Broadway New York 13, New York	3
Texas Instruments, Inc. ATTN: Semiconductor Components Library P. O. Box 5012 Dallas 22, Texas	1

Microwave Associates, Inc. 1
ATTN: Dr. Arthur Uhlir, Jr.
Burlington, Massachusetts

Motorola, Inc. 1
Semiconductor Products Division
ATTN: Dr. Steward S. Flaschen
5005 E. McDowell Road
Phoenix, Arizona

General Electric Company 1
Valley Force Technology Center
ATTN: Mr. T. G. Nicoforo
P. O. Box 8555
Philadelphia 1, Pennsylvania

Dr. Robert Gerson 1
Department of Physics
Missouri School of Mines & Metallurgy
Rolla, Missouri

Department of the Navy 1
Bureau of Ships
Code 6790, Mr. J. Sacks
Washington 25, D. C.

Delco Radio 1
ATTN: Mr. K. Doversberger
Kokomo, Indiana

ARINC 1
ATTN: Dr. H. Jervis
1700 K. Street, N. W.
Washington, D. C.

Commanding Officer 1
U. S. Army Electronics R&D Laboratories
ATTN: SELRA/PEE, Mr. J. Gruol
Fort Monmouth, New Jersey

Battelle Memorial Institute 1
ATTN: Mr. T. Shilladay
Columbus, Ohio

Hughes Aircraft Company 1
Semiconductor Division
ATTN: Library
Post Office Box 1278
Newport Beach, California

International Telephone & Telegraph Corp. Components Division ATTN: Mr. G. G. Perry Post Office Box 412 Clifton, New Jersey	1
National Aeronautics & Space Administration Headquarters ATTN: Mr. Fred Redler Washington, D. C.	1
General Electric Company MSD-VFSTC ATTN: Mr. G. E. Best, Room 2112M Post Office Box 8555 Philadelphia 1, Pennsylvania	1
Dallows Laboratory, Inc. ATTN: Mr. J. T. Cataldo 120 Kansas Street El Segundo, California	1
Sprague Electric Company ATTN: Mr. C. G. Killen North Adams, Massachusetts	1
Commanding Officer U. S. Army Electronics R&D Laboratories ATTN: SIGRA/SL-PEP, Mr. T. S. Gore, Jr. Fort Monmouth, New Jersey	1
Chief, Bureau of Ships Department of the Navy Code 681A2A, Mr. J. M. Kerr, Jr. Room 3327 Washington 25, D. C.	1
Melpar, Inc. ATTN: Dr. Charles Feldman 3000 Arlington Blvd. Falls Church, Virginia	1
ASD (ASRCT-3, Mr. G. Miller) Wright-Patterson Air Force Base, Ohio	1
Goddard Space Flight Center ATTN: Library (for J. W. Adlophsen) Greenbelt, Maryland	1
RADC (RAS, Mr. J. Naresky) Griffiss Air Force Base, New York	1